HEAT AND MASS TRANSFER EFFECTS IN AIR-COOLED VERTICAL TUBE ABSORBERS

by

Rafael A. Pérez Reisler

A thesis submitted in partial fulfillment of the requirements for the degree of

MASTER OF SCIENCE
in
MECHANICAL ENGINEERING

UNIVERSITY OF PUERTO RICO – MAYAGUEZ CAMPUS
2007

Approved by:

_____	_____
Nellore Venkataraman, Ph.D. Member, Graduate Committee	Date
_____	_____
Francisco Rodriguez, Ph.D. Member, Graduate Committee	Date
_____	_____
Jaime Benitez, Ph.D. President, Graduate Committee	Date
_____	_____
Paul A. Sundaram, Ph.D. Chairperson of the Department	Date
_____	_____
Gilberto Villafañe, Ph.D. Representative of Graduate Studies	Date

A mis abuelos Manuel y Rosa. Ellos me enseñaron que las cosas mas importantes en la vida son sencillas. A ellos que tuvieron poco materialmente, pero dieron mucho espiritualmente y dejaron un legado en la familia que siempre los recuerda.

ABSTRACT

Most of the models to predict the heat and mass transfer in vertical absorption chillers underestimate the heat and mass transfer coefficients. Generally the models put too many constraints such as: laminar profile, constant properties, non-absorbable gases are ignored. This investigation attempts to create a more realistic model to estimate the air-cooled absorption process. The model couples the energy and mass balance equations through constraint equations at the interface. Using a method for computing the thermodynamic properties from a Gibbs free energy equation and correlations to estimate the transport properties, a robust MathCad routine was created that computes the solution composition and temperature as functions of the vertical position in the tube. The results from the model show that increasing the air content from 1 to 20% by volume reduces the mass absorption flux by 43%. Furthermore, it suggests that there is a critical tube length that depends on the air concentration at which the absorption process ceases (1.3-m for 1% air).

RESUMEN

La mayoría de los modelos existentes para predecir los efectos de transferencia de calor y masa en procesos de refrigeración por absorción subestiman los efectos de éstos. Generalmente los modelos restringen demasiado el fenómeno con asunciones tales como: flujo laminar, propiedades constantes, no consideran gases no-condensables. Esta investigación intenta crear un modelo más real del fenómeno de absorción enfriado por aire. Usando un método para calcular las propiedades termodinámicas a partir de la energía libre de Gibbs y usando correlaciones para estimar las propiedades de transporte de la solución, se desarrolló un programa robusto en MathCad que calcula la composición y la temperatura de la solución como función de la posición en el tubo vertical. Los resultados del modelo muestran que incrementar el contenido de aire de 1% a 20% por volumen tiene un efecto de reducir el flujo másico de absorción en un 43%. Además, sugieren que existe un largo crítico de tubo que depende de la concentración de aire, al cual el proceso de absorción cesa (1.3-m para 1% de aire).

ACKNOWLEDGEMENTS

I would like to thank all those who in one way or another helped me make this work possible; my advisor Dr. Jaime Benitez for his dedication, and teaching the real meaning of graduate mentorship. His time and patience to help me understand some of the fundamental principles of mass transfer that I applied in this investigation. I would also like to thank the Mechanical Engineering Department, for giving me the opportunity to complete my master in science degree. Special thanks to Zoraida Santiago for her help with all the administrative paper work required.

Thanks to all my family. Without them I would not be here right now. Esther, I met her during my tenure in the graduate program and now is my dear wife. I know she is especially excited that this stage of my career comes to an end, and it would not have been possible without all her continuous support and love. Also thanks to my parents, Rafael and Donna, and all my brothers and sisters, Marisela, Marisa, José, Melisa and George. Finally I would like to thank Adriana Herrera and her husband Ricardo and her son Ricardo Andrés, they are part of our extended family and have provided support and shelter during my final days of this process. Thanks to Denis Barros and Ramon Herrera, part of this success would not have been possible without their continuous prayers.

TABLE OF CONTENTS

LIST OF NOMECLATURE

A – Delmholtz free energy

C_p – Specific heat at constant pressure; KJ/kg-K

C_{ps} – Specific heat of LiBr solution; kJ/kmol-K

C_s – LiBr molar concentration; kmol/m^3

C_v – Gas phase molar concentration; kmol/m^3

D_{Abs} – Diffusivity coefficient of liquid film; m^2/s

D_{ABv} – Diffusivity coefficient of V-phase; m^2/s

F_L – LiBr mass transfer coefficient; kmol/m^2-s

F_V – Gaseous phase mass transfer coefficient; kmol/m^2-s

G – Gibbs free energy; kJ/kmol

G^E – Excess gibbs free energy; kJ/kmol

G^l – Gibbs free energy of liquid phase; kJ/kmol

G_1^∞ – Gibbs free energy of ideal LiBr solution; kJ/kmol

G_2^l – Gibbs free energy of pure water in L-phase; kJ/kmol

H – Enthalpy; kJ/kmol

H_s – Enthalpy of the LiBr solution; kJ/kmol

H_v – Enthalpy of vapor

h_s – Convection heat transfer coefficient; kW/m^2-K

k_s – Thermal conductivity of LiBr solution; kW/m^2-K

L – Molar flow rate water in liquid phase; kmol/s

L_s – Molar flow rate of LiBr in the phase L-phase; kmol/s

M – Molar or specific value, extensive thermodynamic property.

M_i – Molecular weight of species i; kg/kmol

M_{av} – Average molecular rate; kg/kmol

m – Molality of LiBr solution; kg/kmol

m_o – Reference molality; kg/kmol

n – Number of moles

n_i – Number of moles species i

n_j – Number of moles of species j

N_A – Total molar flux of water vapor to liquid film; kmol/m^2-s

P – Pressure, kPa, bar

P_{cM} – Critical pressure of mixture in gaseous phase

p_i – Partial pressure of water at the gas-liquid interface

P_T – Total pressure; kPa

Q – Heat; kJ/kmol

R – Universal gas constant; kPa-m^3/kmol-K

Re_s – Reynolds number of LiBr solution

Re_v – Reynolds number of vapor phase

S – Molar entropy; kJ/kmol-K

S – Surface area; m^2

Sc – Dimensionless Schmidt number

Sh- Dimensionless Sherwood number

St_L- Stanton number for mass transfer

T – Temperature, K

T_{air} – Temperature of cooling air, K

T_{cM} – Critical temperature of mixture, K

T_{Di} – Temperature of inside tube; K

T_s – Bulk temperature of LiBr solution; K

T_{so} – Initial temperature at tube entrance, K

U – Internal energy, kW/kg

U – Overall heat transfer coefficient; W/m^2-K

U* – Dimensionless overall heat transfer coefficient

V – Molar volume, m^3/kmol

V – Molar flow rate of water in gaseous phase; kmol/s

V_s – Molar flow rate of the non-diffusing solvent in V-phase; kmol/s

x_l – Molar fraction of LiBr solution

x_i – Liquid interface molar fraction

x_i – Mole fraction of species i

y – Mole fraction of water in vapor phase

y_l – Mole fraction of air in gaseous phase

Z – Vertical length of absorber; m

Symbols:

γ – Activity coefficient

ξ_M – Reduced inverse viscosity of mixture; $(\mu P)^{-1}$

η – Dimensionless length parameter

κ_s – Mass transfer coefficient in LiBr solution; (m/s)

κ_v – Mass transfer coefficient in gaseous phase; (m/s)

μ_i – Chemical potential of species i

μ_v – Dynamic viscosity in gaseous phase; kg/m-s

ρ – Density; kg/m3

σ_{AB} – Collision diameter, a Leonard Jones parameter °A

υ - Dissociation number (2 for LiBr)

φ – Osmotic coefficient

Δ – Difference operator

Θ –Dimensionless temperature parameter

Ω_D – Diffusion collision integral

LIST OF TABLES

LIST OF FIGURES

1 INTRODUCTION

1.1 Energy and Environment

Improving the quality of life usually implies increasing our individual energy consumption, with the concomitant degradation of the environment. It was not until the latter part of the 20th century that there started to be a worldwide awareness of protecting our planet. Alarming signs, such as the significant depletion of the ozone layer and global warming, stimulated the international community to start creating aggressive policies to protect and preserve our mother earth. A conscience developed that our planet has limits and if we pollute the water, destroy the ozone layer, cut down our forests, and pollute the air indiscriminately the planet would become uninhabitable.

In the mid 90's, heat waves in Chicago caused thousands of deaths in the elderly community. The city of Chicago started a very aggressive green building policy of planting vegetation among the buildings roofs, energy efficient designs and solar energy application in newly constructed projects to mitigate these effects. In addition to mitigating there exists a need to condition buildings and houses which is met by mechanical air conditioning systems.

One of the major areas of energy consumption in the Caribbean is room comfort in residential and commercial sectors. Due to the hot and humid conditions characteristic of the region, room

comfort has become a need instead of a luxury. In Puerto Rico, 25% of the total energy consumption is used for room conditioning (Gonzalez and Khan, 1997). Figure 1.1 shows that in Florida which, similar to Puerto Rico, has a hot and humid environment, 41% of the energy consumed per household is for cooling purposes (Parker et al., 1996). Adding to this the fact that the annual number of new households in Puerto Rico has increased to about 30,000 new units per year (PRPB, 2003), a great need to generate additional electric power is evident.

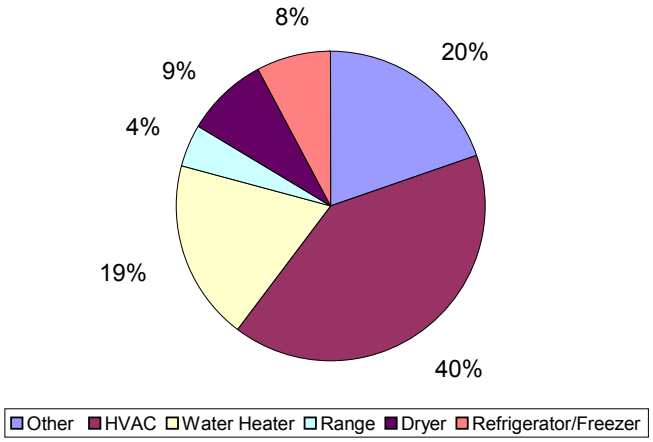

Figure 1.1 Annual electrical breakdown for typical household in Florida (Parker et al., 1996)

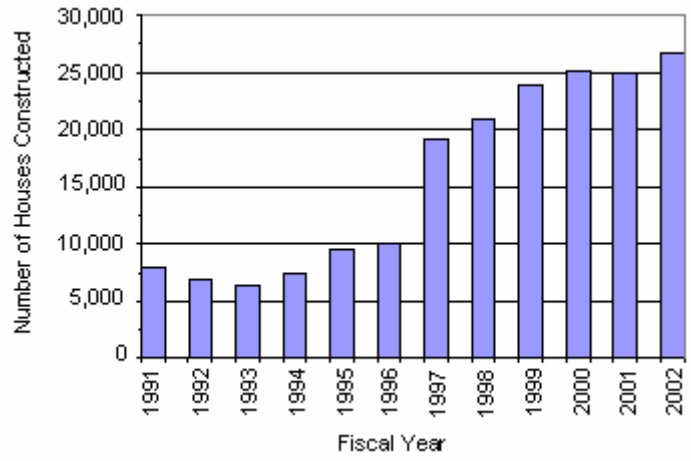

Figure 1.2 Number of households constructed per year in Puerto Rico (PRPB, 2003)

In addition to the great energy consumption, most conventional vapor compression (V-C) refrigeration systems work on chlorofluorocarbons (CFC's) which are environmentally hazardous.

In the early 1980's there was a lot of talk about regulating the use and emissions of CFC's that deplete the ozone layer. Finally, the Montreal Protocol to vanish substances that deplete the ozone layer was signed in 1987 (amended in 1990 and 1992). The Montreal Protocol stipulated that the production and consumption of compounds that deplete ozone in the stratosphere such as: chlorofluorocarbons, halons, carbon tetrachloride, and methyl chloroform, were to be phased out by 2000 (2005 for methyl chloroform). Scientific theory and evidence suggested that, once emitted to the atmosphere, these compounds could significantly deplete the stratospheric ozone layer that shields the planet from damaging UV-B radiation.

1.2 Absorption Cooling Technology

Solar cooling absorption theory has been in existence for years. It is a very attractive concept of using heat instead of work to produce a cooling effect. Such technology could have a large impact for reducing energy consumption while increasing the standard of living. While some isolated efforts have demonstrated the technical feasibility of solar absorption systems, market driven efforts will be required to make the technology commercially feasible.

Puerto Rico, as most tropical regions, has sun available all the year. The insolation in Puerto Rico is high and very steady throughout the year, having peak values reported at over 800 W/m^2

(Lopez and Soderstrom, 1983). This creates very attractive conditions for implementation of solar assisted technology. The use of solar driven absorption machines has been suggested during the last few years to offset the energy consumption in the Caribbean for air conditioning applications (Hernandez et al., 1997). A 35 kW (10 tons) commercial absorption chiller was installed in Cabo Rojo, Puerto Rico, to test the viability of the absorption technology in the region. The experimental results for the 35 kW closed absorption system showed that such systems are technically feasible (Meza et al., 1998) for medium cooling loads.

A thorough study to determine the market size and potential in Puerto Rico was conducted and predicted that the greatest potential for commercializing absorption cooling systems exist in the residential and small business sectors (De Hoyos, 1999). Hence, the effort should be aimed at these markets in which esthetics and space consumption become important issues. Moreover, when referring to typical residences, cooling loads are in the range of 10.5 to 17.5 kW (3-5 tons). Figure 1.3 shows a typical solar assisted absorption system configuration. As seen the components of such a system include: bank of solar panels, thermal storage tank, absorption chiller, auxiliary heater, cooling tower, air handling unit, and various pumps. The system is complex and, although it has been shown to be technically viable, high initial capital investment keeps this technology from becoming conventional everyday use.

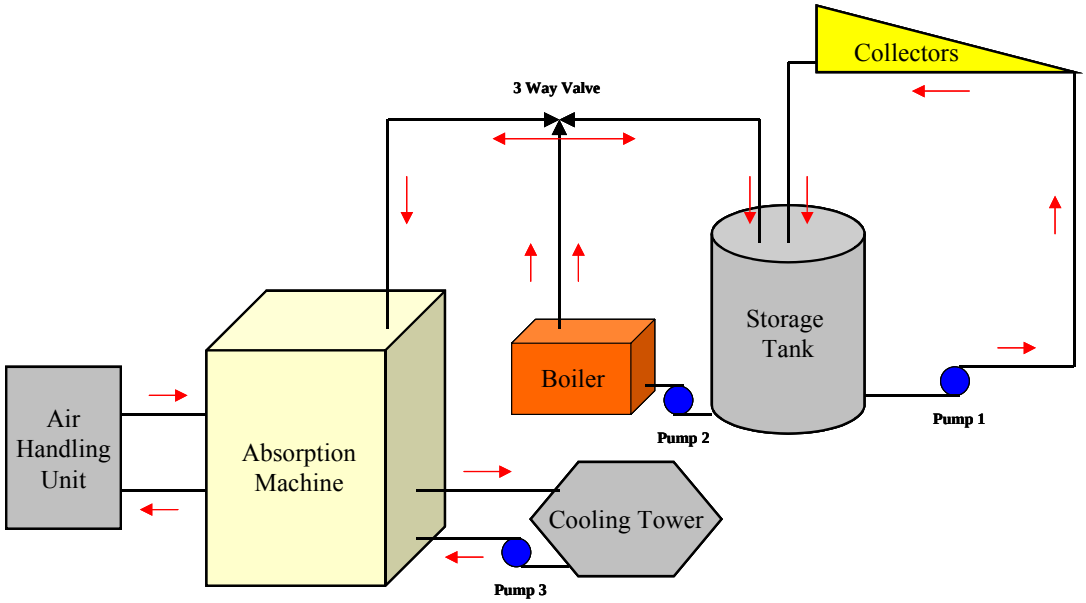

Figure 1.3 Schematic of solar assisted absorption system

For reasons to be explained later, when referring to solar cooling single stage cycles the working pair will always be LiBr/H_2O. Figure 1.4 shows a typical schematic of the components of the absorption cycle that compose a typical absorption machine.

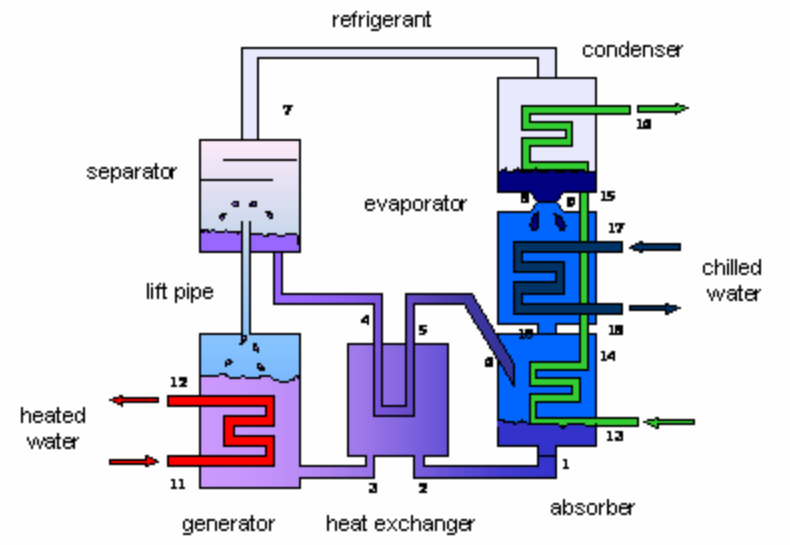

Figure 1.4 Schematic of typical absorption machine

The main components of this cycle are namely: generator, condenser, solution heat exchanger, absorber and evaporator. As shown in Figure 4, the cycle has two water cooled components, the condenser and the absorber. Although a single stage cycle is presented and will be the focus of the work done, double and triple effect chillers also exist, and the main purpose of these cycles is to make a more efficient process and increase the COP by re-using the heat rejected in the condenser and absorber to heat up subsequent effect generators. In the case of more than one stage, heat input is required at temperatures greater than 100 °C, which limits their use to non-solar applications.

Compact air-cooled absorption chillers have been investigated from a thermodynamic standpoint (Alva and Gonzalez, 2002) for use in household applications. It seems to be a good alternative to scale down existing absorption machines. In these air-cooled closed absorption chillers the cooling tower can be eliminated and replaced by fans integrated into the absorption machine design. There have been attempts to prototype these absorption machines, however, they have not been completely successful at operating the cycle at acceptable performance parameters (Castro et al., 2002; Pérez et al., 2004), mostly because of the difficulty of operating the absorber at air cooled conditions. For this reason, it is important to understand the complex transport phenomena dynamics taking place in the absorber to achieve a successful absorption cycle. The purpose of this investigation is to develop a more realistic model of the coupled heat-, mass- and momentum-transfer effects in an air-cooled, falling film absorber that can be used to generate design criteria of this most critical element in a solar-assisted absorption cooling machine. The study will consider: 1. effects of heat and mass transfer coefficients of wavy film flow of the solution inside the tubes, 2. the effect of the presence of non-condensable gases on the heat and

mass transfer calculations, 3. relax the restriction of constant wall temperature, and 4. calculate variations in the thermodynamic and transport properties of LiBr solution as a function of the solution temperature and composition using Gibbs free energy generating functions.

2. LITERATURE REVIEW

2.1 History of Absorption Cooling

Solar absorption cooling has been researched for almost a century. The Einstein refrigerator co-invented in 1926 by Albert Einstein and former student Leó Szilárd is a single pressure absorption refrigerator, similar in design to the gas absorption refrigerator. The refrigeration cycle uses ammonia, butane, and water (Wikipedia, 2007). This is the first reference and eventual patent (1930) of what evolved into the absorption cooling cycle as we know it today. In 1976 a study summarized and reviewed the status of absorption cooling technology (Nash et al., 1976). They reviewed the status of absorption cooling cycle, technological improvements among others. It was concluded that the absorption cycle was the best developed conventional heat actuated technique at that moment. The design constraint of the cycle is due primarily to thermal limitations.

Two years later Auh (1978) reviewed the status of absorption cooling, the main importance focused at improving the efficiency of absorption cooling . He concluded that:

1. For single effect absorption unit using LiBr/H_2O as the working fluid the COP is limited always to less than 1.0.
2. The concentrating type of solar collector is a must to operate the double effect LiBr absorption chiller, in which the COP is no longer limited to 1.0.

3. The COP of a single–effect absorption cycle can theoretically break the 1.0 barrier if the working fluid employed has positive deviations from Raoult's law.

Auh (1978) also reviewed the solar cooling for residential and commercial applications. His recommendations were as follows:

1. Work on system technology is necessary and should focus on system configuration, sub-system options, control strategy and parasitic power requirements by the use of computer and/or hardware simulations.
2. Emphasis should be given to the effective management of the load performance.
3. Emphasis should be given to air-cooled absorption cooling, even if it requires higher heat inputs (>363 K). Search for a new working fluid is an option.

By the later part of the 70's absorption cooling technology was not practical for commercialization. Although the feasibility of the technology was promising, major research and development remained in order to make it a reality. The cost was the major obstacle for the widespread usage of solar cooling. Initial costs were high and service and maintenance unpredictable. At that time the present government policy of subsidizing conventional (non-solar) energy sources was a deterrent to commercialization of solar energy.

2.2 Absorption Chillers Simulations

Muneer and Upal (1985) developed a code to simulate a commercially available Yazaki absorption chiller. Using the climate data for the region of interest they simulated the system performance for different collector types, collector area and storage volume. The results demonstrated that an optimal storage volume to collector area exists. Additionally the system was able to operate at considerably low generator temperatures (between 70-80ºC), thus making it possible to be operated by solar collectors.

In an attempt to increase the COP of the absorption system a simulation of the air conditioning system with a partitioned storage tank in two parts was considered (Sumathy and Li, 2001). The upper part of the tank would start operating in the morning when not much sunshine was available, while the whole tank (top and bottom) would operate in the afternoon. They showed that the stratified tank had a higher collector efficiency and that although partitioned tanks were late morning more efficient, in the early morning the efficiency was low, because the water inlet to the solar collector was from the upper part of the tank and collector efficiency declines as inlet temperature increases.

A model was developed of a solar air conditioning system for space cooling in small residential application in Beirut (Ghaddar et al., 1997). The study showed that for every ton of refrigeration in Beirut a collector area of at least 23.3 m^2 with optimal water storage of 1000 to 1500 liters/m^2 was required for fully solar operation of seven hours. Compared to conventional cooling

systems the solar cooling system could only be considered marginally competitive when combined with domestic water heating.

Hernandez et al. (1997) studied the feasibility of different arrangements of solar assisted absorption air conditioning systems in the Caribbean. A simulation of the performance of a solar powered single effect lithium bromide chiller coupled with dehumidification system was investigated. The research did not consider dynamic thermal building loads. Results from this investigation provided optimization of parameters such as collector's inclination angle, thermal storage to collector area ratio, and amount of collector surface area. An economic analysis for both Puerto Rico and Trinidad estimated costs of $1000 to $1500 per kW. The total payback for this pilot 35 kW was estimated close to ten years.

Atmaca and Yigit (2003) simulated a solar absorption cycle and the effect of different hot water inlet temperature. They studied the effects of the hot water inlet temperatures on the COP and surface area of absorption machine components, and found that increasing the generator inlet temperature increases the COP and decreases both the absorber and solution heat exchanger area. An increase in the storage mass causes the fraction of none purchased energy (FNP) to decrease. As a final recommendation they suggested the use of high performance flat plate collectors for absorption cooling.

Florides et al. (2002) have dedicated more than a decade in solar absorption research. Their work ranges from simulation of solar cooling systems in Cyprus, modeling a domestic size

absorption machine and design and construction of the chiller. The simulations of the system were conducted in TRANSYS (Florides et al., 2002). They considered three different types of collectors, namely Compound Parabolic Concentrator (CPC), flat plate and evacuated tube collectors. These collectors' gains were simulated against the collector slope for Nicosia, Cyprus. Curves were generated for the following parameters; boiler heat vs. storage tank volume, and collector gain vs. storage tank volume and for the boiler heat vs. collector area curves to find the optimal configuration between the collector area and auxiliary heater used. Moreover, system long-term performance was also studied by simulating the Life Cycle saving vs. Collector area. They suggest that, although the system was designed for Cyprus, similar results should be obtained for countries with high solar availability. However, simulations and optimizations as suggested by them should always be performed before deciding the system installation (Florides et al., 2002).

2.3 Experiences in Solar Cooling

In the summer of 1980 an ARKLA SOLAIRE-36 cooling system was installed in the College of Engineering in Riyadh, Saudia Arabia (Sayigh and Saada, 1981). Riyadh is an arid region and during the summer (April to September) the average solar irradiation is about 700 W/m^2. The full system included 28 flat collectors, a storage tank (originally 12 m^3) and a cooling tower. The solar collectors were arranged in two benches of 14 collectors in parallel for a total of 56 m^2 and titled at 15 degrees for maximum solar gain. The original storage of 12 m^3 was doubled to take advantage of the high levels of solar radiation. The system installed had a storage tank heat gain rate of 12ºC per day, and the storage tank was able to operate the system for 15 hours at evaporator outlet temperatures of 17ºC and 24 hours at 21ºC. The average efficiency of the

collectors was 55%, when operating the absorption chiller in the range of 78-90ºC. The parasitic power used in the cooling tower, pumps, and control unit was 1 kW. The electrical power saved using this solar absorption rather than a similar vapor-compression system was 50%.

In 1987, a solar powered air conditioning system was installed and tested at the National University of Singapore. The system components included a 7 kW Yazaki chiller along with 16 Donier heat pipe collectors (2 m^2 each), auxiliary heater, and hot water storage tank, and a 17.5 kW cooling tower (Bong et al., 1987). The system had a controller programmed with three main algorithms: collector to hot water storage tank, storage tank to chiller, and chiller to fan-coil units. The results compare three day performance of the machine based on available solar radiation: a good sunny day (800 to 900 W/m^2), an average day, and a poor day (insolation below 400 W/m^2). The paper discusses how on good days the auxiliary heater is used for early operation and after 17:00, but on poor days the heater is used throughout (the collector pump never turns on). Overall the average cooling capacity provided was reported to be 4 kW with a COP of 0.58 and a solar fraction of 39%.

Another notable solar absorption implementation was a 4.7 kW chiller constructed in the University of Hong Kong (HKU). The system utilized 38.2 m^2 of flat plate collector area, a cooling tower, a fan-coil unit, and an electric auxiliary heater. A controller and Data Acquisition System are used to control and measure the properties of the machine at the different states. The HKU collector efficiency was estimated at 37.5%, with an overall system efficiency of 7.8 to 8.1% and solar fraction of 55% (Yeung et al., 1992).

The performance parameters of an experimental pilot solar assisted system installed in Cabo Rojo, Puerto Rico and operated from October 16, 1997 to December 16, 1997 for forty continuous days were evaluated (Meza, et al., 1998). The system consisted of a 35 kW Yasaki LiBr-H_2O absorption chiller, powered by 113 m^2 of selective surface flat plate collectors, a 5700 liters hot storage tank, a 84 kW cooling tower, a 1800 liters per hour air handling unit, and a 50 kW auxiliary heater. The system was installed to cool a conference room in the National Fish and Wildlife service facilities. Performance parameters such as system COP, time to reach steady state, first and second law efficiencies, latent and sensible load on the chiller, and auxiliary heat requirement were measured and documented in this work. The overall absorption system collector array efficiency was 30.5%. Meza showed experimentally that there exists an optimal collector mass flow rate which for this system was 2.08 kg/s. The nominal cooling capacity was measured at 25 kW with a COP of 0.63 and a 95% solar fraction.

A parallel effort was the development and implementation of a fully automated control system for the pilot solar assisted air conditioning system in Cabo Rojo (Melendez, 2000). Control schemes and algorithms that optimized the energy collection were successfully implemented at the Pilot system at the Cabo Rojo facilities. These algorithms control the flow of water through the solar collectors, the storage tank and auxiliary heater based on radiation available at any given time. The automatic control development and control schemes as means of a fully automated control for solar chillers systems applications effort was further submitted and accepted by the US patent office (Melendez et al., 2003). Their patent for a solar air conditioning system includes an absorption machine coupled to three heat loops. A heat loop of the highly

efficient solar collectors and boiler provide the energy for the absorption machine. A loop through the cooling tower removes the heat from the absorption machine and a chilled water loop which draws heat from room or building. The energy of hot water is taken to a storage tank, the flow through the collectors is regulated to maximize energy collection and storage.

Florides et al. (2003) describe the process of design and construction of a solar absorption machine for residential use. The objective was to evaluate the characteristics and performance of a single stage lithium bromide absorption machine. Heat and mass transfer equations were simulated in a computer code and a sensitivity analysis performed. They studied the tendency of different variables on the COP of the system. Furthermore, they discuss some design strategies for the different components of the absorption machine. A 1 kW prototype was built and experimentally tested, and used to scale the cost of a 10 kW machine. The results and costs analysis for both the prototype and the 10 kW units are documented in the paper.

Hammad (1998) has constructed two different absorption chiller prototypes and tested them in a solar system arrangement in Amman, Jordan. The first experimental prototype and solar collectors were manufactured locally. The solar absorption system was tested for 4 to 5 hours daily during August and September when enough solar radiation was available. The maximum calculated ideal COP for the system was 1.6, while it was experimentally measured at 0.55. In his paper a second generation of absorption machine prototype is discussed. There are two basic improvements the author made when constructing this second generation prototype. The first generation machine used hand made components, while the second prototype used equipment manufactured with new technology commercially available. The other improvement is the increase in machine cooling capacity from an original 0.5 tons to 1.5 tons unit. The result was an

increase in the absorption machine COP from 0.55 (FGU) to 0.75 (SGU). He discusses experimental procedures, sensor placement, monitoring and measurement of performance parameters of this cycle. The main contribution of the paper was that it proved that generation improvement on this type of technology is necessary, and attainable, for improved performance and compactness.

There are many other instances of pilot systems in solar cooling technology; however, the ones mentioned above are considered the cornerstones for the advances in solar cooling technology.

2.4 Air Cooled Absorption Cooling and Absorber Modeling

In the case of air-cooled absorption machines there has been little work done. This is a field that is now starting to be explored. Indeed is has been stated that in order to design and construct an air-cooled absorption chiller the crystallization issue must be seriously addressed (Herold et al., 1996). Since the coefficients of heat and mass transfer are lower in air than for water the operation temperature and pressure of the absorber are slightly higher, hence absorption is less efficient leaving more concentrated solutions.

Alva and González (2002) developed a computer code that simulated an air-cooled absorption machine. In their code, the absorption machine is solar powered and its output is the thermodynamic states of the cycle. They suggest possible arrangements of machine components, namely the condenser, solution heat exchanger, generator and absorber.

Medrano et al. (2002) attempt to quantify the absorption of water vapor in a vertical tube at air-cooled conditions in a falling film configuration. They use water at higher than normal temperatures to simulate air-cooling thermal conditions. The parameters that they considered for performance of absorber were: absorption flux, the outlet solution degree of sub cooling and the falling film heat transfer coefficient.

Castro et al. (2002) did an in depth study of the heat and mass transport phenomena in an air cooled absorption chiller. Their study is based on performance of a 3 kW air cooled absorption prototype. The air cooled elements (condenser and absorber) were numerically modeled in detail to compute the heat and mass transfer coefficients. They developed an absorber test rig in which the absorber is tested at various flow conditions. The heat dissipated of both experimental and calculated runs are plotted at the different mass flow rates. There is very high agreement in the results. Full prototype testing at partial loads yields a significant decrease in COP and cooling capacity in the experimental results compared to the calculated theoretical values. The COP, which was plotted at various generator entry temperatures, was estimated at close to 0.7, but never reached 0.5.

The patent by González and Beauchamp (2003) is for the air-cooled solar assisted single stage absorption machine. The absorption machine uses water as a refrigerant and LiBr as the absorbent carrier. The operation of the compact solar air conditioning system is determined by an optimal control strategy. The field of invention relates to air conditioning system suitable for residential and light commercial applications, and more particularly to solar powered systems for such applications.

Mostafavi and Agnew (1996) investigated the effect of ambient temperature on the surface area of absorption machine components, namely: generator, condenser, evaporator, absorber and solution heat exchanger. The components are all designed and conditions calculated in order to see the effect of the temperature on the surface area. The most important findings of the work are that ambient temperature has no effect on condenser and absorber. The generator and solution heat exchanger surface area will increase slightly as a factor of the ambient temperature.

Kiyota et al. (2003) model absorption in aqueous lithium bromide film falling inside vertical pipes. They model the absorption process in a vertical pipe for a constant heat transfer coefficient on the pipe outer surface. Experimentally, they measured absorption in pipes with inner diameters ranging from 8 to 26 mm, and outer heat transfer coefficient of 2000 and 3300 W/m^2K. The model was found to describe adequately pipes of 13 mm diameters of more. Furthermore, they concluded that the heat transfer area required for the air-cooled condition is three times greater that for the water-cooled condition.

Finally the work of Ileri (1997) is included since it provides standard parameters for measuring performance of solar aided absorption cooling systems. For instance, he introduced the Solar Performance Coefficient (SPC) in order to precisely define the performance of absorption cooling systems. According to him, the Fraction of Non Purchased Energy can be confusing and even misleading when used for cooling applications alone. The SPC can complement and

confirm FNP values obtained. Other standard known parameters are also mentioned, such as: COP, Circulation Ratio (CR) and Second Law Efficiency (Є).

2.5 Modeling of the Absorber

Although a lot of literature has been presented, it should be noticed that the modeling and simulations refer to the absorption machine as a system. However, evidence can be found in all cases of performance of the system is lower than the predicted mainly due to low performance of the absorber. The research that is presented below is a summary of significant analytical and numerical attempts to model the absorption phenomenon in the absorption cooling cycle environment.

In their critical review of coupled heat and mass transfer in falling film absorption, Killion and Garimella (2001) provide a comprehensive review of efforts to mathematically model the heat and mass transfer phenomena that occur during falling film absorption. The review includes details on fundamental equations, boundary conditions, assumptions, and solutions that were used by the different authors. Although, this work excludes all experimental work, important ones, have already been presented in the review above. The paper mentions that most of the work done has been focused on laminar film representation, however because our research interest is wavy film modeling, the laminar review will be omitted.

It is well known that even at low Reynolds numbers (<100) the liquid LiBr film is very unstable and laminar film modeling cannot capture the disturbances by inherent instabilities. Miller

(1998) reviews the hydrodynamics of wavy films and says: “those results imply that natural falling waves are by nature wavy”.

Brauner (1989) proposes a system of wave classification in which he considers two main wave types: capillary waves which he defines as low amplitude, sinusoidal shape, regular frequency, and the wave front is aligned perpendicular to flow direction; and inertial waves which can have higher amplitudes, have a high slope wave front and long wave back. Inertial waves could be modeled with recirculation regions that can really aid in the transport between the film and bulk. These characteristics along with other natural wave properties make wavy film have higher mass flow rates than laminar profiles with equivalent thickness.

Patnaik, et al. (1993) developed an analytical model for estimating the heat and mass transfer coefficients for a vertical tube water cooled absorption chiller. The model is based on the solution of three ordinary differential equations to calculate solution concentration, temperature distribution and coolant temperature. In the paper they present the heat and mass transfer correlations for the wavy film heat and mass transfer coefficients which are used with solution of the fourth order Runge-Kutta scheme for the numerical integration of the parameters mentioned above.

In their model, Patnaik and Perez-Blanco (1996) go back to modeling absorption phenomenon using inertial or roll waves. The hydrodynamics in their work follow the ones described by Brauner (1989) of dividing the waves into four sections and providing expressions for length and

film thickness for each of these sections. They apply Fourier transforms to video images of falling films at Reynolds between 200-300 range in order to determine the frequency, and further show this frequency does agree with experimental data. To solve the transfer coefficients they assume: constant thermodynamic properties, non-linear interface equilibrium, isothermal wall, and no heat transfer to vapor. From this model, the authors show that the non-dimensional mass transfer coefficients are about four times higher for wavy flow than those for laminar flow.

Medrano, et al. (2003) developed a simple model for falling film in the presence of non-absorbable. The model is based on the initial research by Patnaik, et al. (1993) for which the heat and mass transfer correlations are defined, however, this time the presence of non absorbables is considered. The study wants to account for the phenomenon of non-absorbables that have to be periodically removed from the absorption chillers because they hinder the systems performance. The paper shows the effect of inlet non-absorbable air concentration and purge velocity. The model considered consists of three ordinary differential equations solved as initial value problem with constraint equations. The nominal working conditions for this study were Reynolds number of 100, and absorber pressure of 1.3 kPa, a cooling water temperature of 35C and inlet solution concentration of 62% LiBr by weight. The results showed that a minimum purge velocity is required to sweep away the non-absorbable to prevent these from building up and hindering the absorption chiller functionality.

Kim and Ferreira (2006) developed a method for calculating the thermodynamic properties of LiBr aqueous solutions—namely: enthalpy, entropy, specific volume, equilibrium vapor pressure, and specific heat—using a Gibbs free energy equation as a generating function. In the

paper they compared the values estimated by their model to those shown by McNeely (1979) and in the International Critical Tables (ICT, 1928) and show that their model better predicts the experimental results for a broader range of temperatures and pressures. Moreover, the model they developed is applicable for LiBr concentrations ranging from 0 to 70 wt% and for pressures from 74 Pa to 1MPa.

This investigation attempts to create a more realistic model to estimate the air-cooled absorption process. The proposed model couples the energy and mass balance equations through constraint equations at the interface. Using the method developed by Kim and Ferreira (2006) for computing the thermodynamic properties from a Gibbs free energy equation and correlations to estimate the transport properties, and implementing a logarithmic mass transfer driving force relation, a robust MathCad routine was created that computes the solution composition and temperature as functions of the vertical position in the tube.

3. THEORY AND METHODS

Thermodynamics studies the laws that govern the conversion of energy from one form to another, the direction of the heat flow, and the availability of the energy to do work. In principle as shown by Herold, et al (1996) a simple model for describing the absorption cycle can be done from a thermodynamics standpoint. Following this approach, Alva and Gonzalez (2002) developed a computer program that simulated the thermodynamic states of the absorption chiller. The problem with this simple thermodynamic approach is that it is only a starting point to absorption chillers understanding, but has no way of modeling and quantifying the heat and mass transfer effects of the real cycle, hence it is not an acceptable model for real absorption systems. In this chapter, the heat and mass transfer equations to model the absorption process are developed, as well as a method to calculate the $LiBr/H_2O$ thermodynamic and transport properties needed to estimate the heat and mass transfer coefficients.

3.1 Water Lithium Bromide Thermodynamic Properties

The most commonly used refrigerants-absorbent pairs in the market are $H_2O/LiBr$ and NH_3/H_2O. There are a number of other fluid pairs that have been considered such as: $H_2O/NaOH$ and H_2O/SO_3, however NH_3/H_2O and $LiBr/H_2O$ have proven to be the best. The solution properties are very important when choosing the solution pair. Some of these properties are boiling point, specific heat, viscosity and solubility at different temperatures, pressures and concentrations at which they will operate in the absorption cycle. Between NH_3/H_2O and $LiBr/H_2O$, when

considered for solar cooling applications, LiBr/H_2O water is the reasonable choice because of two main reasons: 1) lower working temperatures and pressures 2) for environmental reasons LiBr/ H_2O systems use water as the refrigerant, while in ammonia systems the ammonia-water solution is the refrigerant.

All the basic thermodynamic properties for constant composition phases can be found in the equation describing the internal energy *U* (Smith, et al, 2005).

$$d(nU) = Td(nS) - Pd(nV) \tag{1}$$

In addition to the equation for internal energy *U* other basic thermodynamic relations are:

$$H \equiv U + PV \tag{2}$$

$$A \equiv U - TS \tag{3}$$

$$G \equiv H - TS \tag{4}$$

where *H* is enthalpy, *A* is the Helmholtz free energy, and *G* the Gibbs free energy. These three properties, directly derived from the basic thermodynamic properties, are the building blocks to all thermodynamics relations.

Differentiating equations (2-4) and using Eq. (1) to eliminate internal energy, new relations are obtained as functions of *S, V, T,* and *P*.

$$dU = TdS - PdV \tag{5}$$

$$dH = TdS + VdP \tag{6}$$

$$dA = -PdV - SdT \tag{7}$$

$$dG = VdP - SdT \tag{8}$$

Equations (5-8) are the fundamental thermodynamic relations used to define homogenous fluids of constant composition. Applying to them the criterion for exactness, another set of very useful equations, known as the Maxwell equations, is obtained.

$$\left(\frac{\partial T}{\partial V}\right)_S = -\left(\frac{\partial P}{\partial S}\right)_V \tag{9}$$

$$\left(\frac{\partial T}{\partial P}\right)_S = \left(\frac{\partial V}{\partial S}\right)_P \tag{10}$$

$$\left(\frac{\partial P}{\partial T}\right)_V = \left(\frac{\partial S}{\partial V}\right)_T \tag{11}$$

$$\left(\frac{\partial V}{\partial T}\right)_P = -\left(\frac{\partial S}{\partial P}\right)_T \tag{12}$$

For convenience, enthalpy (H) and entropy (S) are rewritten as functions of T and P as shown below.

$$dH = C_p dT + \left[V - T\left(\frac{\partial V}{\partial T}\right)_P\right] dP \tag{13}$$

$$dS = C_p \frac{dT}{T} - \left(\frac{\partial V}{\partial T}\right)_P dP \tag{14}$$

3.2 Using Gibbs Free Energy to Estimate LiBr/H_2O Thermodynamic properties

Equation (4) defined the Gibbs free energy in a general form, however, extending this definition to a closed system of constant composition:

$$d(nG) = \left[\frac{\partial(nG)}{\partial P}\right]_{T,n} dP + \left[\frac{\partial(nG)}{\partial T}\right]_{P,n} dT \tag{15}$$

Equation (15) can be furthered simplified using equation (8), where

$$\left[\frac{\partial(nG)}{\partial P}\right]_{T,n} = nV \text{ and } \left[\frac{\partial(nG)}{\partial T}\right]_{P,n} = -nS$$

Now, equation (15) can be re-written as:

$$d(nG) = (nV)dP - (nS)dT \tag{16}$$

Extending the applicability of equation (16) to a single phase open system of variable composition:

$$d(nG) = (nV)dP - (nS)dT + \sum_i \left(\frac{\partial(nG)}{\partial n_i}\right)_{P,T,n_j} \tag{17}$$

where, the change in total Gibbs free energy resulting from changes in the number of moles of species *i* at constant temperature and pressure (last term of equation 17) can be defined as the chemical potential μ_i.

$$\mu_i = \left[\frac{\partial(nG)}{\partial n_i}\right]_{P,T,n_j} \tag{18}$$

By substituting (18) into (17),

$$d(nG) = (nV)dP - (nS)dT + \sum_i \mu_i dn_i \tag{19}$$

The definition of chemical potential as shown in equation (18) is an example of the concept of partial molar properties $\overline{M}_i$.

In general,

$$\overline{M}_i = \left[\frac{\partial(nM)}{\partial n_i}\right]_{P,T,n_j} \tag{20}$$

By analogy with equation (18), it can be deduced that chemical potential and the partial molar Gibbs free energy are equivalent.

$$\mu_i \equiv \overline{G}_i \tag{21}$$

The definition of the partial molar properties provides a method for calculating partial properties from solution property data. For any property in general *M*,

$$nM = \text{g}\,(T, P, n1, n2, \ldots)$$

The total differential of *nM* can be expressed as:

$$d(nM) = \left[\frac{\partial(nM)}{\partial P}\right]_{T,n} dP + \left[\frac{\partial(nM)}{\partial T}\right]_{P,n} dT + \sum_i \left(\frac{\partial(nM)}{\partial n_i}\right)_{P,T,n_j} dn_i \tag{22}$$

For constant total moles *n*, equation (22) can be rewritten as,

$$d(nM) = n\left(\frac{\partial M}{\partial P}\right)_{T,x} dP + n\left(\frac{\partial M}{\partial T}\right)_{P,x} dT + \sum_i \bar{M}_i\, dn_i \tag{23}$$

where the subscript *x* represents differentiation at constant composition,

Furthermore,

$$n_i = x_i n \tag{24}$$

Therefore

$$dn_i = x_i dn + n dx_i$$

and

$$n dM + M dn = n\left(\frac{\partial M}{\partial P}\right)_{T,x} dP + n\left(\frac{\partial M}{\partial T}\right)_{P,x} dT + \sum_i \bar{M}_i \left(x_i dn + n dx_i\right) \tag{25}$$

By factoring equation (25) into terms containing *n* and *dn*.

$$n\left[dM - \left(\frac{\partial M}{\partial P}\right)_{T,x} dP - \left(\frac{\partial M}{\partial T}\right)_{P,x} dT - \sum_i \bar{M}_i \, dx_i\right] + dn\left[M - \sum_i \bar{M}_i \, x_i\right] = 0 \tag{26}$$

Then, from equation (26), it follows that:

$$dM = \left(\frac{\partial M}{\partial P}\right)_{T,x} dP + \left(\frac{\partial M}{\partial T}\right)_{P,x} dT + \sum_i \overline{M}_i dx_i \tag{27}$$

$$M = \sum_i x_i \overline{M}_i \tag{28}$$

Multiplying equation (28) by *n*

$$nM = \sum_i n_i \overline{M}_i \tag{29}$$

Equations (28) and (29) allow calculation of mixture properties from the partial properties information. Differentiating equation (28),

$$dM = \sum_i x_i d\overline{M}_i + \sum_i \overline{M}_i dx_i \tag{30}$$

Combining equations (27) and (30) yields the *Gibbs/Duhem equation:*

$$\left(\frac{\partial M}{\partial P}\right)_{T,x} dP - \left(\frac{\partial M}{\partial T}\right)_{P,x} dT - \sum_i x_i d\overline{M}_i = 0 \tag{31}$$

Combining equation (23) with (19),

$$d(nG) = (nV)dP - (nS)dT + \sum_i \bar{G}_i \, dn_i \tag{32}$$

Equation (32) can be used as a generating function for the basic thermodynamic properties: *H*, *S*, *V* and C_p, along with other complementary thermodynamic relations.

From inspection of equation (32),

$$\left(\frac{\partial G}{\partial P}\right)_{T,x} = V \tag{33}$$

$$\left(\frac{\partial G}{\partial T}\right)_{P,x} = -S \tag{34}$$

Using equations (4) and (8) in an expression for *d(G/RT)*,

$$d(G/RT) = \frac{1}{RT}\left[VdP - SdT\right] - \frac{H - TS}{RT^2}dT \tag{35}$$

This is simplified to:

$$d(G/RT) = \frac{V}{RT}dP - \frac{H}{RT^2}dT \tag{36}$$

$$\left[\frac{d(G/RT)}{\partial T}\right]_{P,x} = \frac{H}{RT^2} \tag{37}$$

$$H = -RT^2\left[\frac{\partial (G/RT)}{\partial T}\right]_{P,x} \tag{38}$$

Finally, by combining equation (14) with (32),

$$C_p = -T\left(\frac{\partial^2 G}{\partial T^2}\right)_{P,x} \tag{39}$$

Once a model for the Gibbs free energy as a function of temperature, pressure, and composition is known, equations (33-39) can be used to calculate V, S, H, and C_p.

Kim and Ferreira (2006) presented a model for the Gibbs free energy of LiBr/H_2O solutions:

$$G^l = x_1 G^{\infty}_{1(T,P)} + (1-x_1) G^l_{2(T,P)} + x_1 \upsilon RT\left[\ln\left(\frac{m}{m_o}\right) - 1\right] + G^E_{(T,P,x_1)} \tag{40}$$

In equation (40), the first term is the ideal solution Gibbs energy, the second term is the Gibbs energy of pure water, the third accounts for an ideal mixing process, and the last term is the excess Gibbs energy which accounts for the difference between the real and ideal solution behavior.

The excess Gibbs energy is estimated as,

$$G^E = x_1 \upsilon RT\left[\ln \gamma^{\pm} + (1-\varphi)\right] \tag{41}$$

Here, $\gamma^{\pm}$ and φ are the activity and osmotic coefficients, respectively.

Kim and Ferreira (2006) used experimental solution density and vapor pressure data to propose a model for the osmotic coefficient:

$$\varphi = 1 + \sum_{i=1}^{6}\left(a_i + \frac{ib_i}{2\upsilon}p\right)m^{i/2} \tag{42}$$

And now equation (41) can be restated as,

$$G^E = x_1 \upsilon RT \sum_{i=1}^{6}\left[\frac{2}{i}\left(a_i + \frac{ib_i}{2\upsilon}p\right)\right]m^{i/2} \tag{43}$$

where $a_i = \sum_{j=0}^{2} a_{i,j} T^{-j}$ and $b_i = \sum_{j=0}^{2} b_{i,j} T^{-j}$ where $a_{i,j}$ and $b_{i,j}$ are empirical constants, see Table 3.1.

Another term of equation (40) is the ideal solution Gibbs energy defined as:

$$G_1^{\infty} = H_{1o}^{\infty} - TS_{1o}^{\infty} + \int_{T_o}^{T} C_{p1}^{\infty} dT - T\int_{T_o}^{T} \frac{C_{p1}^{\infty}}{T} dT + V_1^{\infty}(p - p_o^*) \tag{44}$$

Where $C_{p1}^{\infty} = RT^2 \sum_{j=0}^{2} \frac{c_j}{T^j}$, $V_1^{\infty} = RT \sum_{j=0}^{2} \frac{b_{0,i}}{T^j}$

The pure water term can also be simplified to:

$$G_2^{l} = H_{2o}^{l} - TS_{2,o}^{l} + \int_{T_o}^{T} C_{p2}^{l} dT - T\int_{T_o}^{T} \frac{C_{p2}^{l}}{T} dT + V_2^{l}(p - p_o^*) \tag{45}$$

$C_{p2}^{l} = R\sum_{j=0}^{2} d_j T^j$ $V_2^{l} = R\sum_{j=0}^{2} e_j T^j$, where e_j, H_{2o}^{l} and S_{2o}^{l} are empirical constants, see Table 3.1.

Table 3.1 Constants used in equations 42-45 (from Kim and Ferreira, 2006).

i	0	1	2
a_{1j}	-2.19631551E+01	4.93723160E+03	-6.55484060E+05
a_{2j}	-3.81047520E+03	2.61153450E+06	-3.66996910E+08
a_{3j}	1.22808540E+05	-7.71879230E+07	1.03985600E+10
a_{4j}	-1.47167370E+06	9.19528480E+08	-1.18945020E+11
a_{5j}	7.76582130E+06	-4.93756660E+09	6.31755470E+11
a_{6j}	-1.51189220E+07	9.83997440E+09	-1.27378980E+12
b_{0j}	-4.41786540E-05	3.11489920E-02	4.36112260E+00
b_{1j}	3.07939920E-04	-1.86320980E-01	2.73871370E+01
b_{2j}	-4.08079430E-04	2.16079550E-01	-2.51759710E+01
c_j	-9.44013360E+05	-5.84232570E+08	0.00000000E+00
d_j	1.19719330E+01	-1.83055110E-02	2.8709378*10^-5
e_j	2.66299610E-03	-3.86518910E-06	7.46484110E-09
H^{∞}_{10}	-57.1521	H^{l}_{20}	0
S^{∞}_{10}	47.5562	S^{l}_{20}	0
T_o	213.15	p^*_o	0.6108

3.3 Transport Properties

When considering the absorption process, there are two fluids in intimate contact with heat, mass, and momentum transfer; among them: the LiBr aqueous solution and the vapor being absorbed. In order to solve the general heat and mass transfer equations proposed to model the system, both the LiBr solution and the water vapor heat and mass transfer coefficients must be estimated. Transport properties of both fluids must be estimated for that purpose.

3.3.1 Transport Properties of the Water-Lithium Bromide Solution

Thermal Conductivity, k_{sol} (kW/mK)

Using experimental data and extending the information provided by Diguilio, et al (1990) the thermal conductivity of the solution can be estimated from:

$$k_s = \sum_{i=1}^{3}\sum_{j=1}^{4} a_{ij} x^{j-1} T^{i-1} \tag{46}$$

Where a_{ij} are empirical constants and x is the mole fraction of LiBr.

$$a_{ij} = \begin{bmatrix} -0.3863624126 & -0.3122938151 & 17.75694663 & -41.62113683 \\ 0.005245122201 & -0.006413302194 & -0.0800954908 & 0.2130478667 \\ -6.398936707*10^{-6} & 1.013622815*10^{-5} & 0.00010029254 & -0.000281450 \end{bmatrix} \cdot 10^{-3}$$

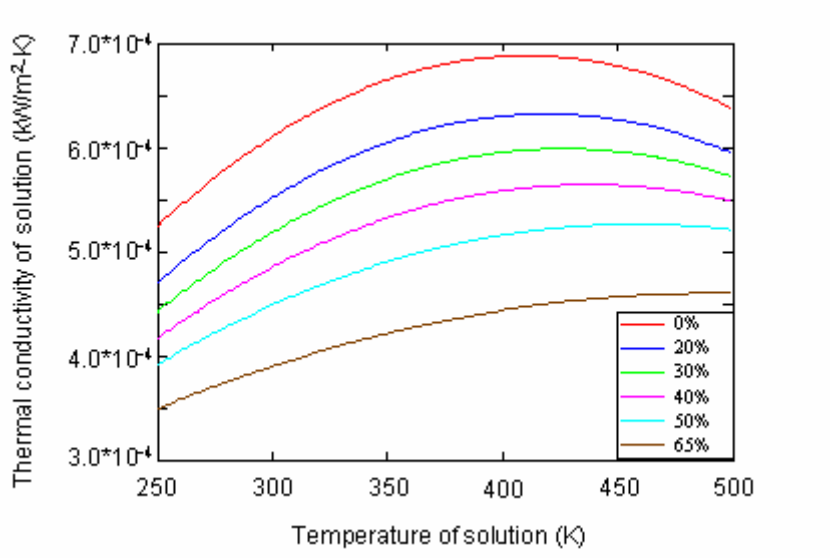

Figure 3.1 LiBr solution thermal conductivity as a function of temperature at various concentrations (%wt of LiBr)

Dynamic Viscosity of LiBr Solution, μ_{sol} (N-s/m^2)

Following a similar approach, Kim and Ferreira (2003) correlated the data from Diguilio, et al (1990) and the dynamic viscosity of the solutions can be estimated from:

$$\ln \mu_s = \sum_{i=1}^{4} \sum_{j=1}^{4} a_{ij} x^{j-1} T^{i-1} \tag{47}$$

Where a_{ij} is defined as,

$$a_{ij} = \begin{bmatrix} 15.4338601 & -1.796143844 & -453.964325 & 1644.664107 \\ -0.1496987184 & 0.08581467986 & 3.186981058 & -11.18992719 \\ 0.0003210580467 & 0.0004050019644 & -0.0006116119513 & 0.02286554179 \\ -2.397708795*10^{-7} & 6.025222928*10^{-7} & 2.699142889*10^{-6} & -1.3359444*10^{-5} \end{bmatrix}$$

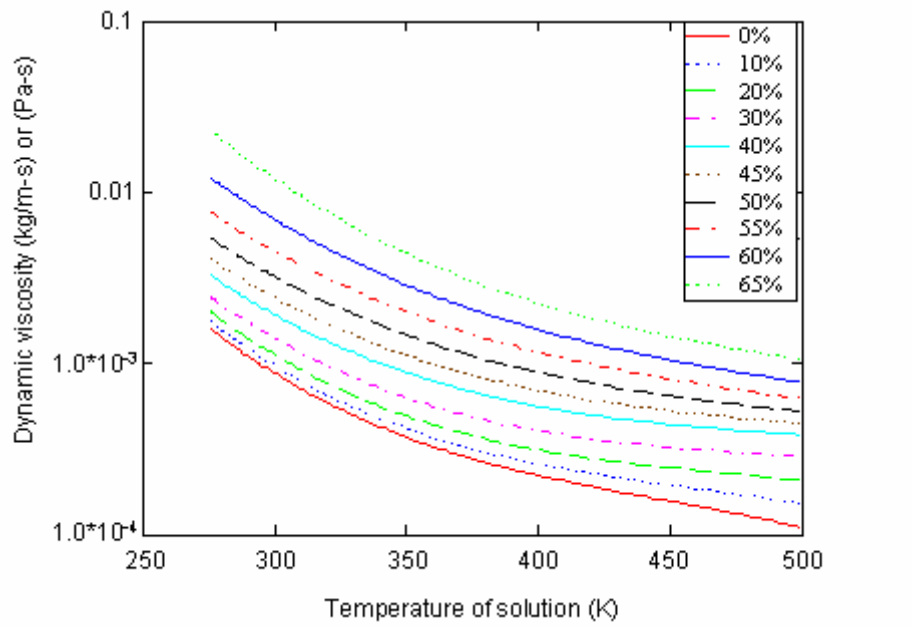

Figure 3.2 Dynamic viscosity of LiBr solution as a function of temperature at various concentrations (%wt of LiBr).

Diffusivity of H_2O-LiBr Solution, (m^2/s)

In this case, the regression model comes from fitting data collected by Gierow and Jernqvist (1993).

$$D_{ABs} = \left(\alpha + \beta x + \gamma x^2\right)\frac{\mu_{sol}(298.15)}{\mu_{sol}(T)} \cdot \frac{T}{298.15} \cdot 10^{-9} \cdot \frac{m^2}{s} \tag{48}$$

Here, α, β, and γ are constants defined as: α=1.271581637, β= 145.271699, γ=-9547.634363.

3.3.2 Transport Properties of Water Vapor and Air Mixture

In the case of the H_2O-air mixture in the absorber the properties of interest are the diffusivity (D_{ABv}), dynamic viscosity (μ_v), and the average density (ρ_v).

Diffusivity of H_2O-Air mixture

In this case and considering this is a binary system that works at very low pressures, the Wilke-Lee equation can be used (Benitez, 2002).

$$D_{ABv} = \frac{10^{-3}\left(3.03 - \frac{0.98}{\sqrt{M_{AB}}}\right)\cdot T_v^{3/2}}{P_{v\_bar}\cdot\sigma_{AB}^2\cdot\Omega_D\cdot\sqrt{M_{AB}}} \tag{49}$$

Here $P_{v,}$ M_A, M_B, $\sigma_{A,}$ σ_B, ε_{Ak}, ε_{Bk} are all constant for a given pair and molar concentration of species A and B. Furthermore, σ_A, σ_B, ε_{Ak}, ε_{Bk} are known as the Lennard-Jones parameters.

Dynamic Viscosity of H_2O-Air mixture,

Using the method proposed by Lucas (Benitez, 2002) for viscosity of gaseous mixtures:

$$\mu_{rM} = \xi_M \mu_v = f(T_{rM}) \tag{50}$$

$$\xi_M = 0.176\left[\frac{T_{cM}}{M_{av}^3 P_{cM}^4}\right]^{\frac{1}{6}} \tag{51}$$

Here, ξ_M, T_{cM}, and P_{cM} are the reduced inverse viscosity($[\mu P]^{-1}$), critical temperature (K) and critical pressure (bars) of the mixture, respectively, and $T_{rM}=T/T_{cM}$

In equation (50), $f(T_{rM})$ can be defined as,

$$f(T_{rM}) = 0.807T_{rM}^{0.618} - 0.357\exp(-0.449T_{rM}) + 0.340\exp(-4.058T_{rM}) + 0.018 \tag{52}$$

The mixture properties are defined as:

$$T_{cM} = \sum_i y_i T_{ci} \tag{53}$$

$$P_{cM} = RT_{cM} \frac{\sum_i y_i Z_{ci}}{\sum_i y_i V_{ci}} \tag{54}$$

$$M_{av} = \sum_i y_i M_i \tag{55}$$

It follows from equations (50-55) that after T_{cM}, M_{av} and P_{cM} are estimated, there is enough information to solve equation (50) for μ_v.

$$\mu_v = \frac{f(T_{rM})}{\xi_M} \tag{56}$$

Density of H_2O-Air mixture (kg/m^3)

The density for the gaseous mixture in this case is estimated using the assumption that the vapor air mixture behaves as an ideal gas. Applying the ideal gas law with the average property data, the density can be estimated as shown in equation (57).

$$\rho_v = \frac{P_v \cdot M_{av}}{R \cdot T_v} \tag{57}$$

3.4 Mass and Energy Balance Equations

In this work, the absorber configuration being considered is a vertical tube arrangement with co-current solution and vapor flows. The steady state mass and energy balance equations will be developed along with the equation which defines the operation line of the absorber.

Consider the co-current flow configuration that is illustrated in Fig. 3.3, where V_1 is the number of moles/s of water vapor plus air entering and L_1 is the moles/s of solution entering.

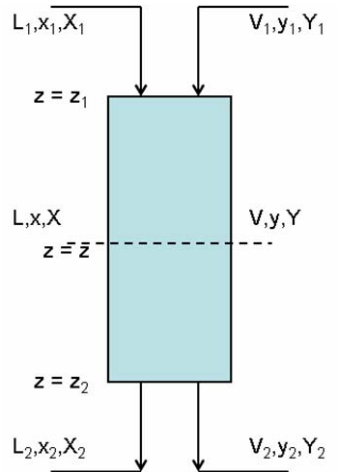

Figure 3.3 Schematic diagram of co-current absorption column.

Concentrations are expressed in terms of y_1 and x_1, the molar fraction of water in V_1 and in L_1, respectively. At the column exit the same parameters are used, but are identified by subscript 2.

Balance of H_2O in the Absorber:

Moles of H_2O entering = moles of H_2O leaving. For the whole column,

$$V_1 y_1 + L_1 x_1 = V_2 y_2 + L_2 x_2 \tag{58}$$

And a balance from the inlet to any point z along the absorber would yield,

$$V_1 y_1 + L_1 x_1 = Vy + Lx \tag{59}$$

As usually happens in absorption problems, there is an inert substance in the gas (air, virtually insoluble in water) and an inert substance in the liquid (LiBr, a nonvolatile salt). To simplify the material balance equations, we define V_s as the molar flow of air, and L_s as the molar flow of

LiBr. We also define the molar ratios *X* (moles of water/mol of LiBr) and *Y* (moles of water/mol of air) respectively as.

$$V_s = V(1-y),\ L_s = L(1-x),\quad Y = \frac{y}{1-y}\ ,\ X = \frac{x}{1-x} \tag{60}$$

Then, equation (59) can be re-written as:

$$V_s Y_1 + L_s X_1 = V_s Y + L_s X \tag{61}$$

And simplifying we get.

$$Y = Y_1 + \frac{L_s}{V_s} X_1 - \frac{L_s}{V_s} X$$

Combining with equation (60) the final form is expressed as:

$$\frac{y}{1-y} = Y_1 + \frac{L_s}{V_s} X_1 - \frac{L_s}{V_s}\left(\frac{x}{1-x}\right) \tag{62}$$

Equation (62) relates the molar fraction of H_2O in both phases at any point along the vertical tube absorber in co-current flow.

Differential Mass Balance of H_2O:

When considering the mass balance of H_2O in a differential tube length (see Fig. 3.4) the rate of mass transfer between the gas phase and the solution (N_A) must be considered.

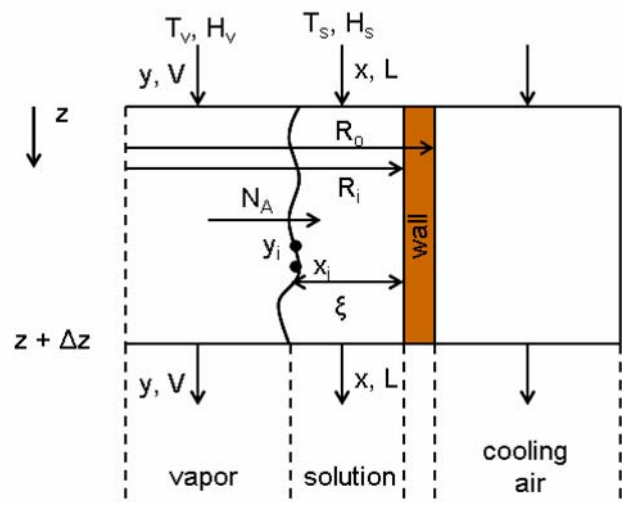

Figure 3.4 Model of co-current vertical tube absorption mass flows.

Vapor Side:

By close inspection of Figure 3.4 we can write the H_2O balance in the liquid phase

$$(xL)|_{z+\Delta z} = (xL)|_z + N_A S \tag{63}$$

Here, $S = \pi D_i \Delta z$ assuming that the liquid film thickness $\xi << R_i$

Rewriting equation (63),

$$xL|_{z+\Delta z} - xL|_z = \pi D_i \Delta z N_A \tag{64}$$

In the limit when Δz tends to zero, equation (64) becomes:

$$\frac{d}{dz}(xL) = \pi D_i N_A \tag{65}$$

Substituting $L = \frac{L_S}{1-x}$ then, equation (65) can be re-written as:

$$\frac{L_S}{(1-x)^2}\frac{dx}{dz} = \pi D_i N_A \tag{66}$$

For the case of diffusion of A through stagnant B, the flux N_A can be expressed as (Benítez, 2002):

$$N_A = F_L \ln\left[\frac{1-x}{1-x_i}\right] \tag{67}$$

Here, x_i is the molar fraction of water at the interface and F_L is the mass transfer coefficient of the liquid phase.

Substituting equation (67) into (66):

$$\frac{L_S}{(1-x)^2}\frac{dx}{dz} = \pi D_i F_L \ln\left[\frac{1-x}{1-x_i}\right] \tag{68}$$

At steady state, the water flux through the gas-liquid interface must be equal to the flux through the gas phase and to the flux through the liquid phase. The flux through the gas phase is given by an expression similar to equation (67),

$$N_A = F_v \ln\left[\frac{1-y_i}{1-y}\right] \tag{69}$$

Here, F_v is the mass transfer coefficient in the gas phase. For steady state operation,

$$F_v \ln\left[\frac{1-y_i}{1-y}\right] = F_L \ln\left[\frac{1-x}{1-x_i}\right]$$

$$\frac{1-y_i}{1-y} = \left[\frac{1-x}{1-x_i}\right]^{F_L/F_v} \tag{70}$$

Since the interfacial concentrations x_i and y_i are in equilibrium,

$$y_i = \frac{p_i}{P_T} \text{ and } p_i = f(x_i, T) \tag{71}$$

Here, p_i is the equilibrium vapor pressure of the solution, a given thermodynamic function of the solution composition and temperature.

Energy Balance

In the case of the energy balance, a control volume on the solution side of the absorption process is used for derivation of the corresponding equations (see Figure 3.5).

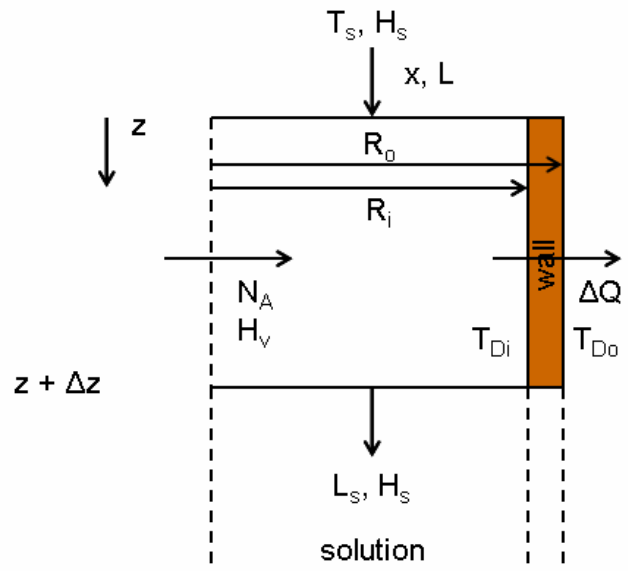

Figure 3.5 Control volume for the energy balance on the LiBr solution.

At steady state, the total energy (E) is conserved, then E_{in} - E_{out} = 0. Based on Figure 3.5, the energy balance becomes,

$$LH_s|_z + N_A S H_v = \Delta Q + LH_s|_{z+\Delta z} \tag{72}$$

By inspection ΔQ can be defined as,

$$\Delta Q = h_s \pi D_i \Delta z \left(T_s - T_{Di}\right) \tag{73}$$

Substituting equation (73) into (72) and simplifying into differential form,

$$LH_s\,|_z + N_A \pi D_i \Delta z H_v = h_s \pi D_i \Delta z \left(T_s - T_{Di}\right) + LH_s\,|_{z+\Delta z}$$

$$\frac{LH_s\,|_{z+\Delta z} - LH_s\,|_z}{\Delta z} = N_A \pi D_i H_v - h_s \pi D_i \left(T_s - T_{Di}\right)$$

$$\frac{d}{dz}\left[LH_s\right] = \left[N_A H_v - h_s\left(T_s - T_{Di}\right)\right]\pi D_i \tag{74}$$

Equation (74) is the differential energy balance in the vertical tube absorption system. In order to write equation (74) in terms of the constant inert molar flow, *Ls*, and liquid molar concentration *x,* a total mass balance will be done on the liquid phase.

Total Liquid Mass Balance:

$$L\,|_z + N_A S = L\,|_{z+\Delta z} \tag{75}$$

$$\frac{dL}{dz} = N_A \pi D_i \tag{76}$$

$$\frac{d}{dz}\left[LH_s\right] = L\frac{dH_s}{dz} + H_s\frac{dL}{dz} \tag{77}$$

And by combining equations (76) and (77)

$$\frac{d}{dz}\left[LH_s\right] = L\frac{dH_s}{dz} + H_s N_A \pi D_i \tag{78}$$

Substituting equation (78) in (74):

$$L\frac{dH_s}{dz} + H_s N_A \pi D_i = \left[N_A H_v - h_s\left(T_s - T_{Di}\right)\right]\pi D_i$$

$$L\frac{dH_s}{dz} = \left[N_A\left(H_v - H_s\right) - h_s\left(T_s - T_{Di}\right)\right]\pi D_i$$

Since $L=L_s/(1-x)$

$$\frac{L_s}{1-x}\frac{dH_s}{dz} = \left[N_A\left(H_v - H_s\right) - h_s\left(T_s - T_{Di}\right)\right]\pi D_i \tag{79}$$

Heat and Mass Transfer Correlations

As proposed by Patnaik, et al. (1993) the heat transfer coefficient for the LiBr solution is estimated using a correlation for fully developed wavy-laminar regime:

$$\frac{h_s\delta}{k_s} = 0.029\cdot(4\,\mathrm{Re}_s)^{0.53}\,\mathrm{Pr}_s^{0.344} \tag{80}$$

For the mass transfer coefficient of the solution, a correlation based on mass transfer mechanism with eddy dissipation at the surface is used:

$$\frac{k_s\delta_r}{D_{AB}} = 1.099*10^{-2}\cdot(4\,\mathrm{Re}_s)^{0.3955}\,Sc_s^{0.5}, \quad \text{for } \mathrm{Re_s} \le 75 \tag{81}$$

$$\frac{k_s\delta_r}{D_{AB}} = 2.995*10^{-2}\cdot(4\,\mathrm{Re}_s)^{0.2134}\cdot Sc_s^{0.5} \quad \text{for } 75<\mathrm{Re_s} \le 400 \tag{82}$$

The left hand side of equations (81) and (82) correspond to the Sherwood number (Sh), and the mass transfer coefficient F_L is implicitly built into these correlations since:

$$F_L = C_s \times k_s \tag{83}$$

Furthermore, Medrano et al. (2003) propose a correlation for the mass transfer coefficient of the vapor based on heat and mass transfer analogy:

$$\frac{k_v \bar{p}_{air} D_i}{D_{AB} p_{Abs} C_v} = 1.62 \times \mathrm{Re}_v^{1/3} Sc_v^{1/3} \left(\frac{D_i}{L} \right)^{1/3} \tag{84}$$

Once these correlations are defined and ready to use in the governing equations, all the equations and dependencies have already been defined analytically before setting the boundary conditions and solving a specific configuration. As mentioned previously, equations (68) and (79) are the governing equations for the mass and energy balance in the vertical tube absorber. These, along with all the thermodynamic property relations to estimate solution and vapor enthalpy, specific heat, entropy, and volume and the heat and mass transfer correlations are the fundamentals for the mathematical model to find solutions for the equations in the air cooled vertical tube absorber. In the next chapter the mathematical model and the method of solution will be presented.

4. MATHEMATICAL MODEL

4.1 Mathematical Modeling

In the previous chapter the theory and methods used to solve the fundamental problem of estimating the heat and mass transfer coefficients in the absorber were introduced. In this chapter the mathematical formulation of the problem to solve the two fundamental differential equations is presented.

Recall the differential mass and energy balances,

$$\frac{L_S}{(1-x)^2}\frac{dx}{dz} = -\pi D_i F_L \ln\left[\frac{1-x}{1-x_i}\right] \tag{68}$$

$$\frac{L_s}{1-x}\frac{dH_s}{dz} = \left[N_A(H_v - H_s) - h_s(T_s - T_{Di})\right]\pi D_i \tag{79}$$

In order to solve numerically these equations, they are first expressed in dimensionless form, and then a numerical method of solution, such as Runge Kutta, can be applied.

Define the dimensionless length, η, as

$$\eta = \frac{z}{Z} \tag{85}$$

And re-rewriting in terms of *z* and *dz*,

$$z = \eta \cdot Z \tag{86}$$

$$dz = Z \cdot d\eta \tag{87}$$

Balance of H_2O in the Liquid Phase:

Equation (68) can be re-written in dimensionless form,

$$\frac{L_S}{(1-x)^2}\frac{dx}{Z \cdot d\eta} = \pi D_i F_L \ln\left[\frac{1-x}{1-x_i}\right] \tag{88}$$

Rearranging

$$\frac{dx}{d\eta} = (1-x)^2 \cdot \frac{Z\pi D_i F_L}{L_S} \cdot \ln\left[\frac{1-x}{1-x_i}\right] \tag{89}$$

Define the Stanton number in the liquid phase, St_L

$$St_L = \frac{Z\pi D_i F_L}{L_S} \tag{90}$$

Equation (89) becomes

$$\frac{dx}{d\eta} = (1-x)^2 \cdot St_L \cdot \ln\left[\frac{1-x}{1-x_i}\right] \tag{91}$$

Energy Balance:

Substituting equation (87) into (79)

$$\frac{L_s}{1-x}\frac{dH_s}{Zd\eta} = \left[N_A(H_v - H_s) - h_s(T_s - T_{Di})\right]\pi D_i \tag{92}$$

Equation (67) gives N_A for substitution into (92). Also, the heat flux term in equation (92) can be rewritten in terms of the overall heat transfer coefficient, U, and the difference between the solution and the cooling air temperatures:

$$\Delta Q = U\pi D_i (T_s - T_{air}) \tag{93}$$

Equation (92) can then be re-written as follows,

$$\frac{L_s}{1-x}\frac{dH_s}{Zd\eta} = \left[F_L (H_v - H_s) \ln\left[\frac{1-x}{1-x_i}\right] - U(T_s - T_{air}) \right] \pi D_i \tag{94}$$

Rearranging,

$$\frac{1}{1-x}\frac{dH_s}{d\eta} = \frac{F_L \pi D_i Z}{L_S}(H_v - H_s) \ln\left[\frac{1-x}{1-x_i}\right] - \frac{UZ\pi D_i}{L_S}(T_s - T_{air}) \tag{95}$$

By substituting equation (90) into (95),

$$\frac{1}{1-x}\frac{dH_s}{d\eta} = St_L (H_v - H_s) \ln\left[\frac{1-x}{1-x_i}\right] - \frac{UZ\pi D_i}{L_S}(T_s - T_{air}) \tag{96}$$

The left-hand side of equation (96) can be expressed in terms of the solution temperature applying the chain rule of differentiation

$$\frac{dH_s}{d\eta} = \frac{dH_s}{dT_s}\frac{dT_s}{d\eta} = Cp_s \frac{dT_s}{d\eta} \tag{97}$$

Substituting (97) into (96)

$$\frac{Cp_s}{1-x}\frac{dT_s}{d\eta} = St_L (H_v - H_s) \ln\left[\frac{1-x}{1-x_i}\right] - \frac{UZ\pi D_i}{L_S}(T_s - T_{air}) \tag{98}$$

Define a dimensionless temperature, Θ

$$\Theta = \frac{T_s - T_{air}}{T_{so} - T_{air}} \tag{99}$$

Then,

$$T_s = (T_{so} - T_{air})\Theta + T_{air} \tag{100}$$

$$\frac{dT_s}{d\eta} = (T_{so} - T_{air})\frac{d\Theta}{d\eta} \tag{101}$$

Substituting in (98),

$$\frac{Cp_s}{1-x}(T_{so} - T_{air})\frac{d\Theta}{d\eta} = St_L(H_v - H_s)\ln\left[\frac{1-x}{1-x_i}\right] - \frac{UZ\pi D_i}{L_S}(T_s - T_{air}) \tag{102}$$

Rearranging,

$$\frac{d\Theta}{d\eta} = \frac{(1-x)}{Cp_s(T_{so} - T_{air})}St_L(H_v - H_s)\ln\left[\frac{1-x}{1-x_i}\right] - \frac{UZ\pi D_i}{Cp_s L_S}\frac{(T_s - T_{air})}{(T_{so} - T_{air})}(1-x) \tag{103}$$

Defining a dimensionless overall heat transfer coefficient, U^*

$$U^* = \frac{UZ\pi D_i}{Cp_s L_S} \tag{104}$$

Equation (104) becomes:

$$\frac{d\Theta}{d\eta} = \frac{(1-x)}{Cp_s(T_{so} - T_{air})}St_L(H_v - H_s)\ln\left[\frac{1-x}{1-x_i}\right] - U^*\Theta(1-x) \tag{105}$$

4.2 Solution to Equations

The dimensionless differential equations must be solved numerically. In the case of equations (91) and (105) the method used for solution is a 4th degree Runge Kutta scheme with algebraic functions correction following each integration step. A step by step methodology that leads to the solution of the equations is presented next.

1. A computer program in MathCAD was written which calculates the thermodynamic and transport properties of the LiBr solution and the water vapor-air mixture as functions of the solution molar fraction ($x1$), solution temperature (T), vapor temperature (Tv) and vapor pressure (Pv). Additionally the interface pressure and concentrations (p_i, x_{ai} and y_{ai}) are computed.

2. Also, the MathCAD program estimates the heat and mass transfer coefficients using the equations (80-84) previously discussed as functions of $x1$, T, Tv and Pv.

3. Furthermore, a function q(u, T, P), defining the two ODE that will be solved simultaneously as functions of u, T and P, is programmed.

$$q(u,T,P) := \begin{bmatrix} -\left[\left(u_0\right)^2 St_L\left(u_0,T\right)\cdot \ln\left(\frac{u_0}{1-C_{int}\left(u_0,T\right)}\right)\right] \\ u_0\cdot\left[St_L\left(u_0,T\right)\frac{H_v - H_s\left(u_0,T,P\right)}{Cp_s\left(u_0,T,P\right)\cdot\left(T_{so}-T_{air}\right)}\cdot\ln\left(\frac{u_0}{1-C_{int}\left(u_0,T\right)}\right) - U_{star}\left(u_0,T,P\right)\cdot u_1\right] \end{bmatrix} \quad (106)$$

The u vector in equation (106) is defined as:

$$u = \begin{pmatrix} u_0 \\ u_1 \end{pmatrix} \tag{107}$$

where u_0 is the LiBr molar fraction in the liquid solution and u_1 the dimensionless solution temperature.

4. Table 4.1 shows the conditions of temperature, pressure and concentration at the tube inlet that are fixed for all the cases analyzed in this work. These conditions are representative of those prevailing in an absorption cooling process.

Table 4.1 – Fixed conditions for absorber tube modeling.

Parameter	Value
LiBr mass fraction in solution, X_{in}	0.62
LiBr molar fraction in solution, x_1	0.253
LiBr solution Reynolds number	100 (wavy-laminar)
Solution inlet mass flow rate	24.5 kg/hr-tube
Cooling air temperature, *Tair*	303.15 K
Cooling air flow rate	0.5 m^3/s-tube
Vapor temperature, T_v	283.15 K
Solution initial temperature, T_{so}	324.15 K
Vapor pressure, P	1.3 kPa
Tube outside diameter[a]	17.2 mm
Flow passage hydraulic diameter[a]	3.48 mm
Fin-flow area/frontal area[a]	0.481
Heat transfer area/total volume[a]	554 m^2/m^3
Fin area/total area[a]	0.95
Staggered arrangement[a] Longitudinal pitch Transverse pitch	44 mm 38 mm
Fin material	Aluminum
Heat transfer area/inside area[a]	17.9
Air Reynolds number	6030
Air heat transfer coefficient[a]	181 W/m^2-K

[a]Properties are for finned circular tubes, surface 7.75-5/8T (Kays and London, p. 270, 1984).

5. RESULTS AND DISCUSSION

5.1 Properties of LiBr Solution

In Chapter 3, the thermodynamic basis used to compute the properties of the LiBr solution as a function of temperature, molar fraction, and pressure was introduced. Furthermore, Chapter 3 also showed that all the necessary thermodynamic properties can be derived directly from the Gibbs free energy equation. This chapter presents the results of some of the most important coefficient and properties of both the solution and water vapor that were computed.

5.1.1 Osmotic and Activity Coefficients.

According to equation (41), both the osmotic and activity coefficients need to be accurately computed in order to estimate the excess Gibbs free energy term. The mathematical formulation for both these coefficients was already developed (Kim and Ferreira, 2006) and will be implemented to compute the Gibbs free energy function. Figures 5.1 and 5.2 show the osmotic and the activity coefficients of LiBr solutions at three different temperatures. These figures were generated using the MathCAD program developed in this work, and they faithfully reproduce the behavior presented by Kim and Ferreira (2006). Figure 5.2 shows the trend of the activity and osmotic coefficients at 298 K. The osmotic coefficient at low molality values is always greater than the activity coefficient until it reaches a cut off value (in Figure 5.2, at $x = 0.1$) where both functions are equal, and from there on the activity coefficient is always greater.

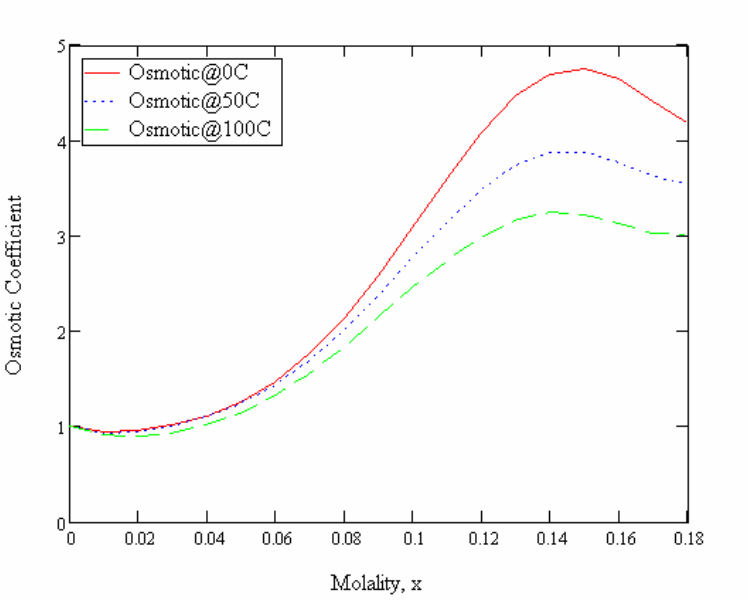

Figure 5.1 Osmotic coefficients of LiBr solutions for various temperatures.

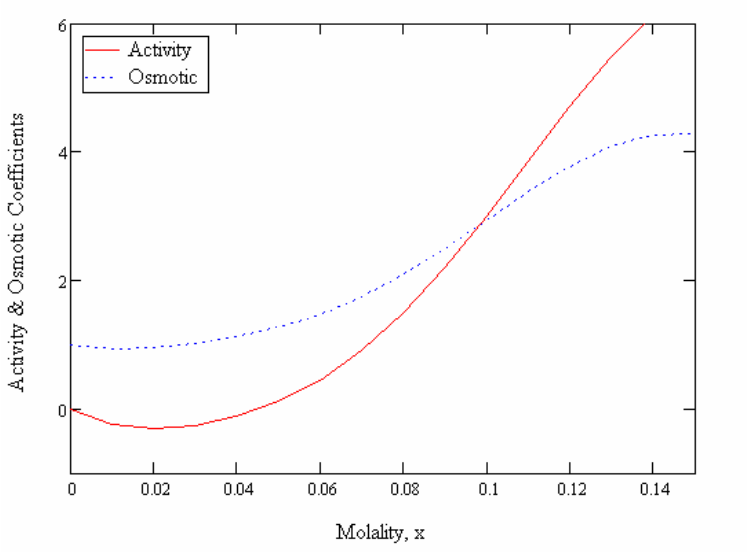

Figure 5.2 Activity and osmotic coefficients of LiBr solutions at 298 K.

5.1.2 Thermodynamic Properties of Solution

Once the osmotic and activity coefficients can be accurately predicted, the next step is to estimate the Gibbs free energy of the solution from equation (40). Figure 5.3 shows the Gibbs free energy of the LiBr solutions as a function of the solution concentration, at various temperatures, and for an absorber pressure of P = 1.3 kPa.

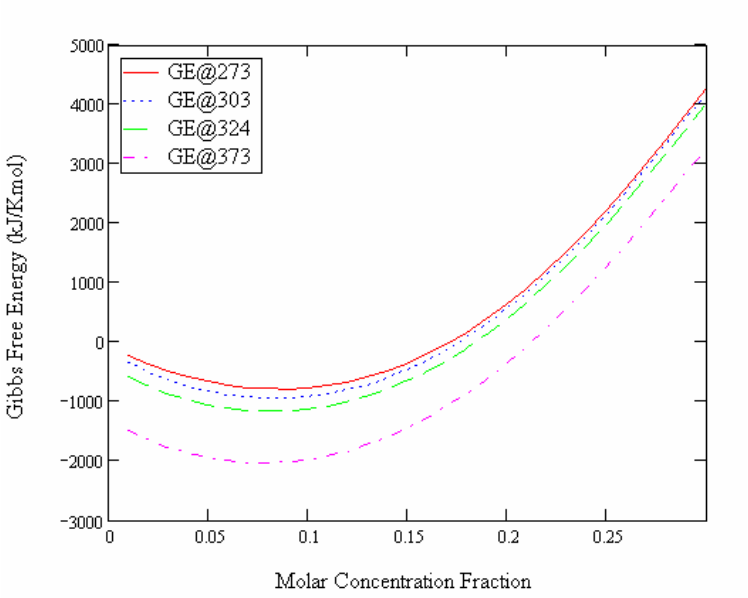

Figure 5.3 Gibbs free energy of the LiBr solution at various temperatures (P = 1.3 kPa).

The Gibbs free energy relationship, as explained in Chapter 3, is the generating function from which the other solution thermodynamic properties of interest are estimated. Applying the necessary mathematical operations (see equations 38 and 39) the enthalpy and specific heat of the solution are calculated. Figures 5.4 and 5.5 show the results at a constant pressure of 1.3 kPa.

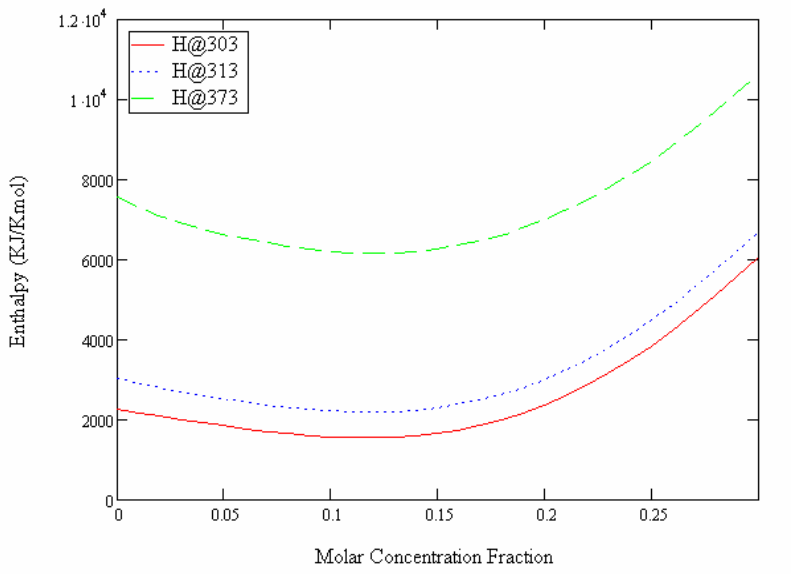

Figure 5.4 Enthalpy of solution vs. molar fraction for various temperatures (P = 1.3 kPa).

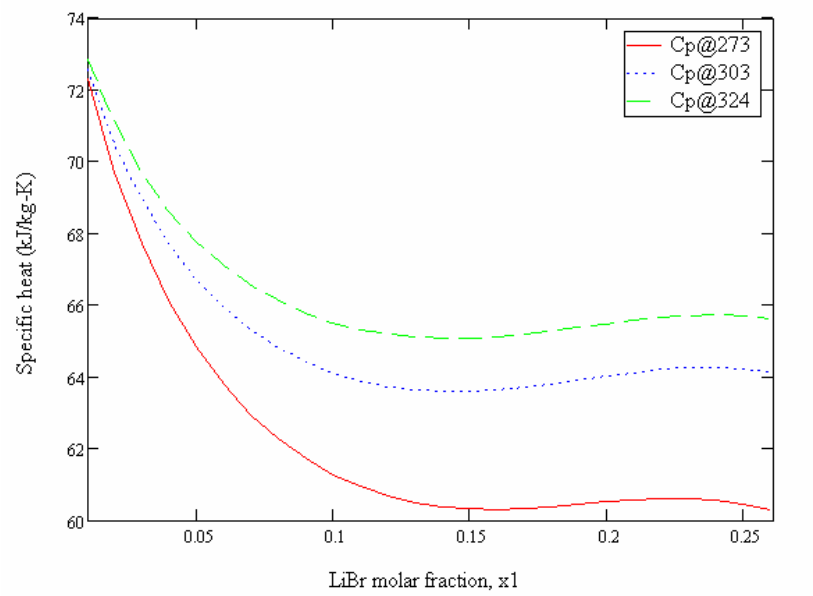

Figure 5.5 Specific heat of LiBr solution vs. molar fraction for various temperatures (P = 1.3 kPa).

5.1.3 LiBr Solution Density and Vapor Pressure

The density of the LiBr solutions can be obtained indirectly by calculating first the solution molar volume from equation (33). The solution density is calculated from this result and the

average molecular weight of the solution. Figure 5.6 shows the results of the density of the LiBr solution as a function of the molar concentration and at two different temperatures. For comparison purposes, Figure 5.6 also includes experimental data published in the International Critical Tables (ICT, 1928). There is an excellent agreement between the values predicted from the Gibbs free energy equation and the experimental data.

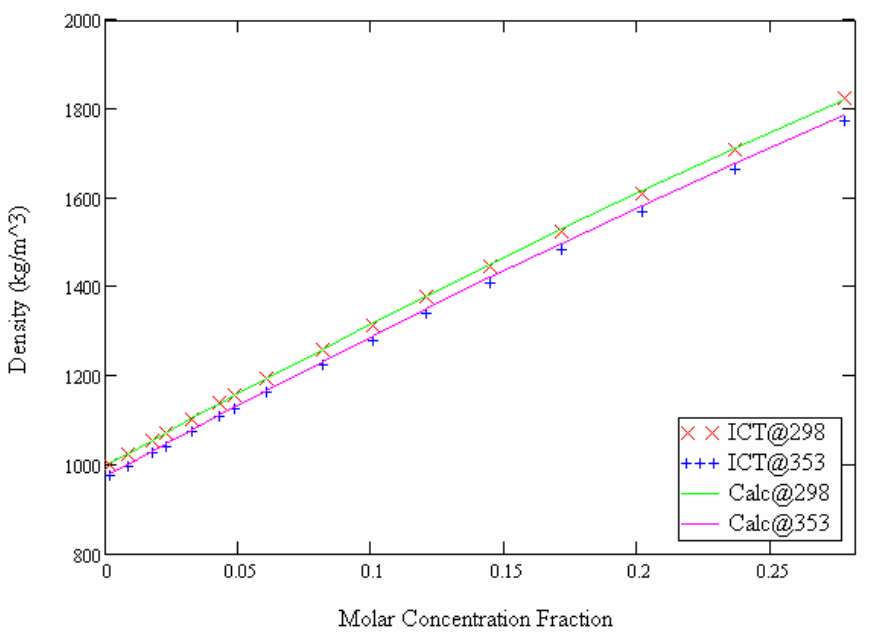

Figure 5.6 Density of LiBr solutions vs. molar fraction for two temperatures.

Another thermodynamic property of great significance is the equilibrium vapor pressure of the LiBr solution. Figure 5.7 shows the vapor pressure of the solution as a function of composition and temperature. Experimental values of the LiBr vapor pressure (ICT, 1928) are included in the plot to show the excellent agreement between the model predictions and actual data.

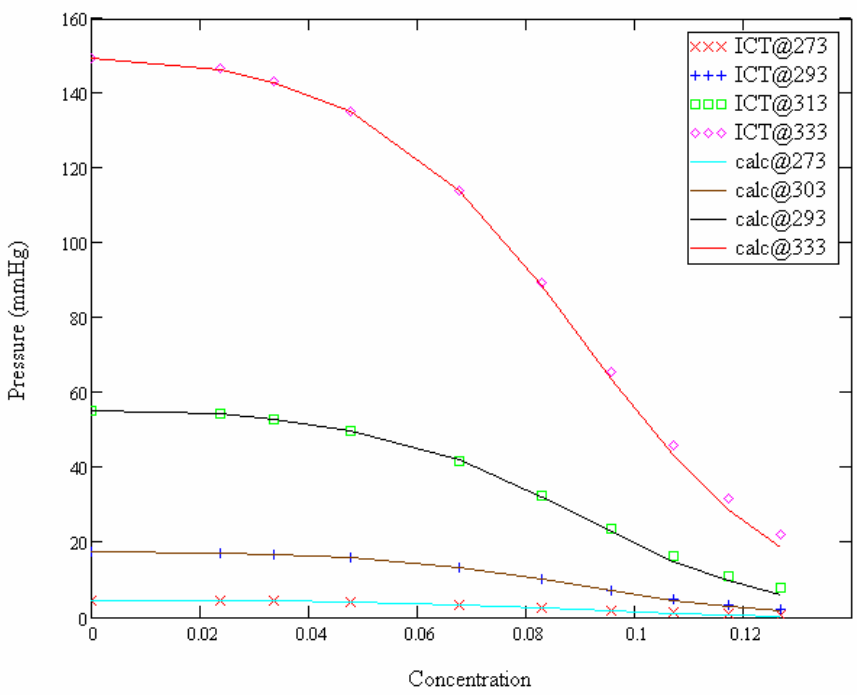

Figure 5.7 Vapor pressure of LiBr solutions for different concentrations and temperatures.

5.2 Results of Vertical Tube Absorption

The results of the absorption in a vertical tube at air cooled conditions will now be discussed. To present these results and for convenience they will be divided into three different sections, namely: the effect of non-absorbables (air) in the absorption process, the effect of water vapor inlet flow rate, and the effect of tube length. In order to properly assess the effects of these variables on the absorption process, some base values must be established. For the case of tube length and inlet air concentration, they are 1 meter and 5% by volume, respectively. The water vapor inlet base flow rate requires some explanation.

As shown in Table 4.1, the inlet solution flow rate is fixed at 24.5 kg/hr per tube corresponding to a solution Reynolds number of 100, in the wavy-laminar flow regime. According to the work

of Medrano, et al. (2003) and Patnaik, et al. (1993), the maximum concentration change that can be achieved in a vertical tube absorber, in the presence of non-adsorbables, and under air-cooling conditions is from 62% to 60% LiBr by weight. If all the water vapor entering the tube were absorbed, this change in concentration would require a vapor flow rate of 0.65 kg/hr per tube. This was taken as the minimum water vapor flow rate. The effect of the vapor flow rate on the absorption process was assessed by considering multiples of this minimum flow rate. The base condition was taken as 111% of the minimum.

5.2.1 Effect of air concentration in the absorption process

The information presented shows the percent of water vapor in the gas mixture instead of the percent of air. In this section the only parameter that is changing with respect to the base conditions is the percent of water vapor present in the gaseous phase; all the other conditions remain constant. Figures 5.8 and 5.9 show the effect of the air concentration at the inlet on the temperature and concentration of the solution as a function of the position along the tube. Figure 5.8 shows that the solution temperature decreases as the concentration of non-absorbables increases. However, the difference in the outlet temperature between case 1 (1% air) and case 5 (20% air) is only 2.8˚K. In all the cases, the solution temperature decreases rapidly near the tube entrance, changing gradually into a gentler slope for the last two thirds of the tube length.

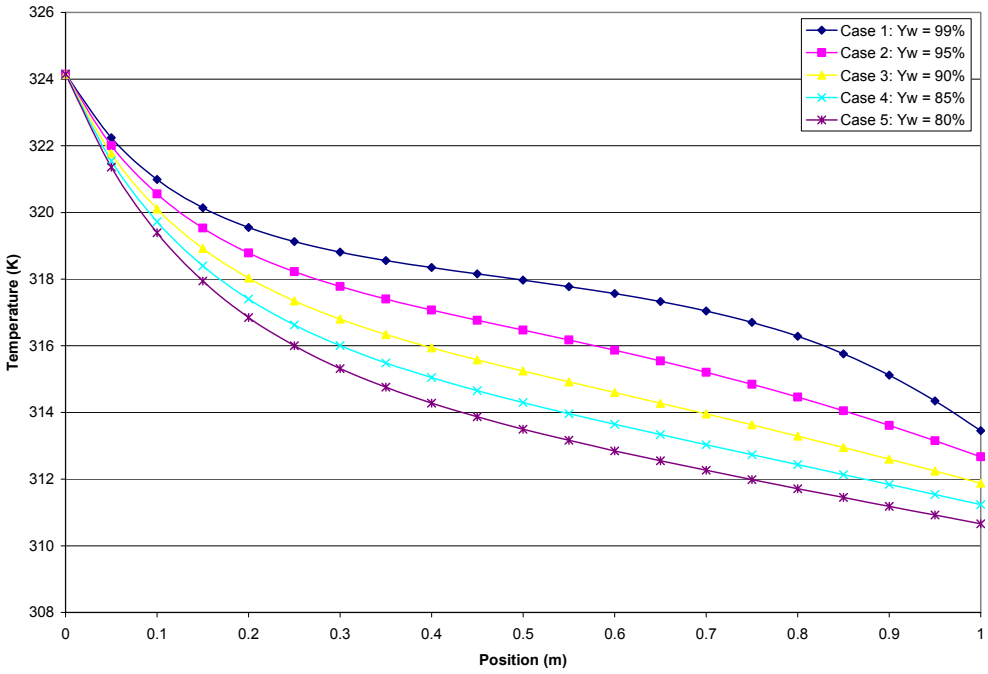

Figure 5.8 Solution temperatures as a function of position and non-adsorbable concentrations.

In the case of the solution concentration, Figure 5.9 shows the opposite behavior. As the air concentration increases in the vapor phase, there is less of a change in the LiBr solution concentration. This is evidence that the presence of non-absorbables reduces the amount of water vapor absorbed by the solution. This would also explain the temperature behavior observed in Figure 5.8 since the absorption of the water vapor releases the latent heat of condensation which has to be removed by the cooling air. Therefore, as the rate of water vapor absorption is reduced by the presence of air, the rate of cooling of the solution increases.

Figure 5.10 shows the gas phase velocity inside the tube as a function of position and air concentration. It shows that as the amount of air increases at the tube inlet so does the gas velocity along the tube. Hence increasing the amount of air at the inlet increases the gas velocity

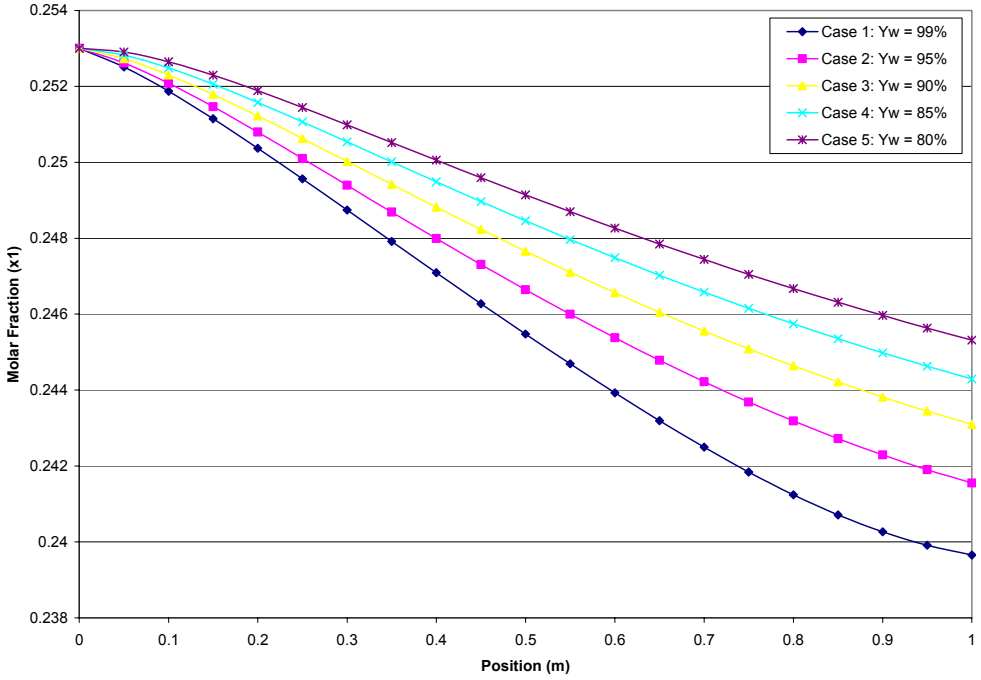

Figure 5.9 LiBr concentration as function of position and non-absorbables concentration.

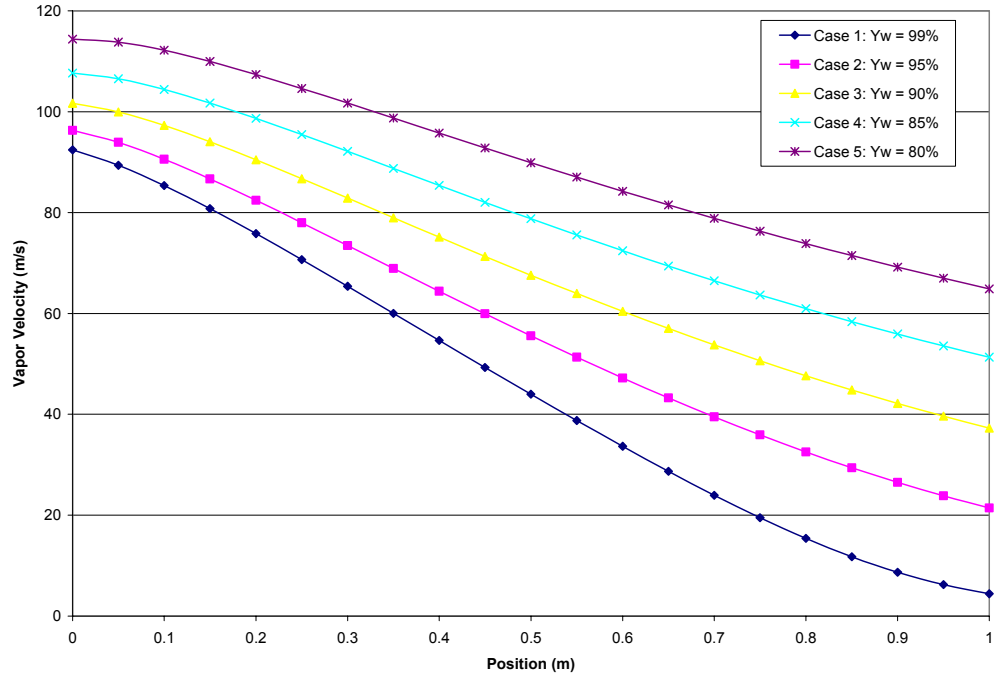

Figure 5.10 Gas velocities as a function of position and non-absorbables concentration.

at the tube outlet. In Figure 5.10 for instance, at an inlet water vapor concentration of 99% the tube outlet velocity is about 4.4 m/s versus 64.9 m/s tube outlet velocity for the case of 80% water vapor inlet concentration. When there are non-absorbables present in the system, they must be purged continuously to avoid excessive accumulation. The purge velocity is obtained from these plots. The purge velocity is the gas velocity at the tube outlet.

Figure 5.11 shows the changes in water vapor fraction of the gas as it moves downward in the vertical tube. From the results already shown, it seems reasonable that at the higher water vapor fractions better absorption would occur, and a larger water vapor fraction gradient would occur. In Figure 5.11, for the case of an initial water vapor fraction of 99%, a gradient of 20.8% in the water vapor fractions is seen from entrance to exit, while the gradient at an initial concentration of 80 % is only 15.2%.

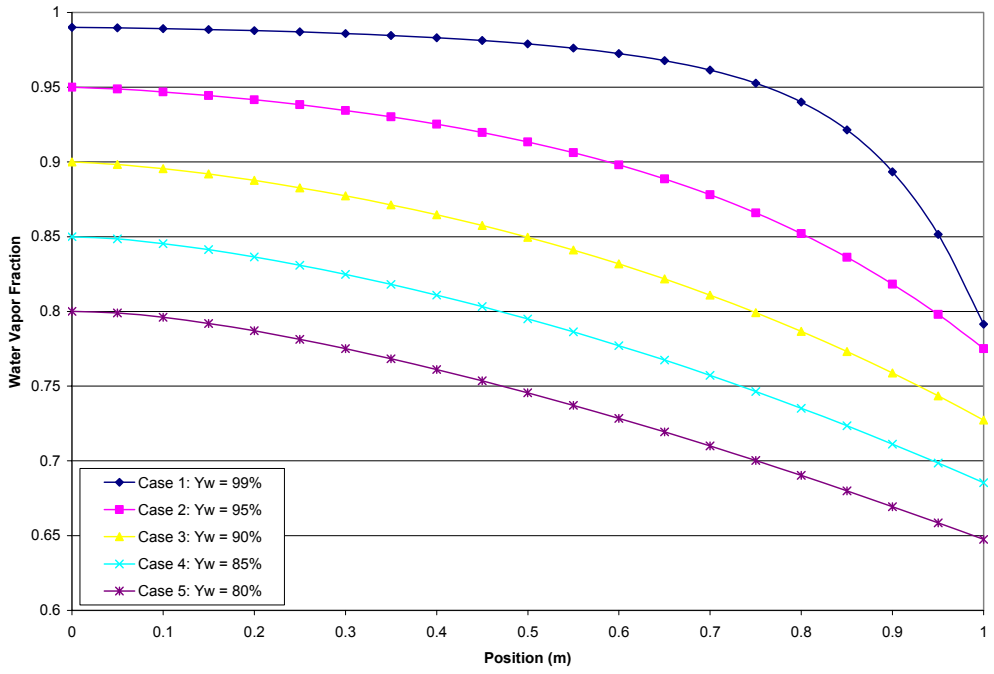

Figure 5.11 Water vapor fractions as a function of position and initial concentration in the gas.

Figure 5.12 shows the mass absorption flux along the tube for different initial concentrations of air. According to these results, the mass absorption flux follows a parabolic trend. It starts increasing from the tube inlet and reaches a maximum at a distance of about 0.3m. In case 1 the maximum might be shifted slightly to the right at about 0.35m. Looking at case 1 in greater detail, notice that in this case the mass absorption flux decreases faster than in all the other cases. Towards the end of the tube, it decreases to values that are smaller than those for the other four cases. This suggests that the driving force for mass transfer in the case 1 is decreasing at a faster rate than for the other four cases.

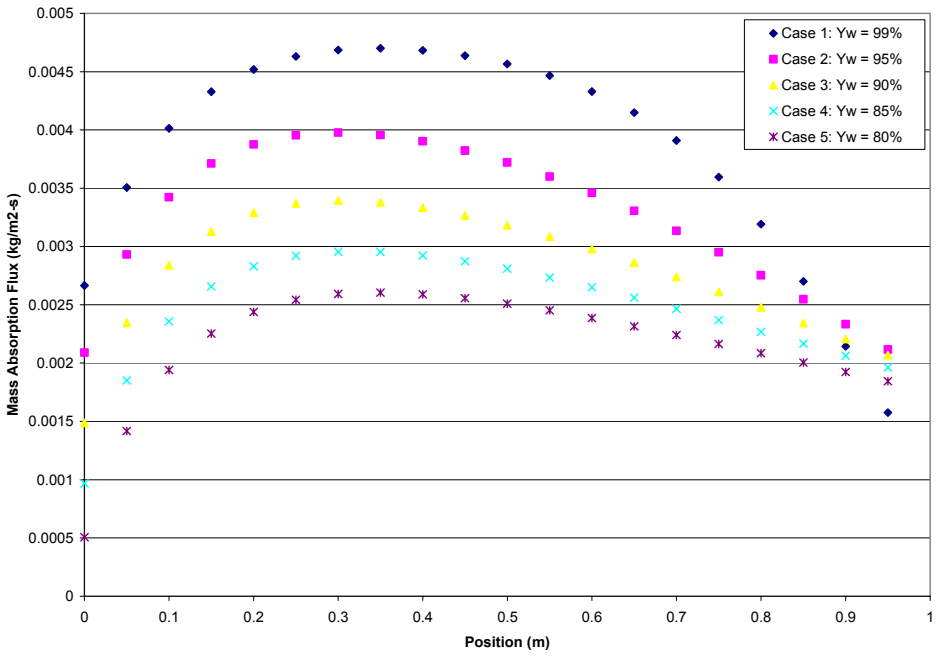

Figure 5.12 Mass absorption flux as a function of position and initial water vapor concentration.

Figure 5.13 shows how the driving force for mass transfer from the gas to the liquid film changes along the tube for different initial concentrations of air. The plot illustrates, for each case, the partial pressure of water vapor in the gaseous phase and the corresponding LiBr solution

equilibrium vapor pressure, as they change along the tube. It is very important to observe these curves because the difference between the partial pressure of the vapor and the vapor pressure of the solution is to mass transfer what the temperature difference is to heat transfer, hence as this difference diminishes the absorption process is reduced.

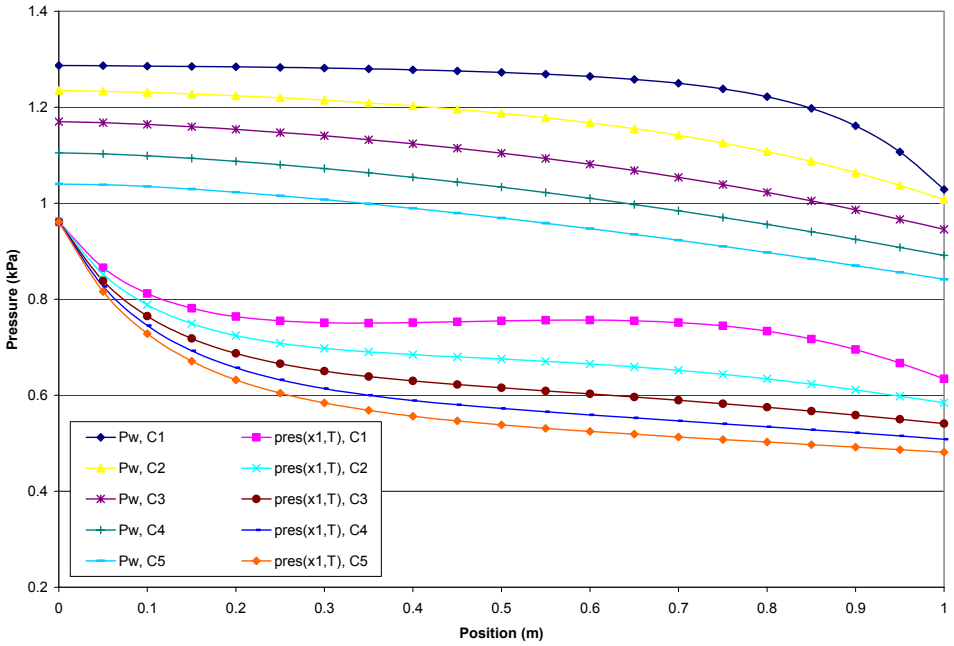

Figure 5.13 Solution vapor pressure and water vapor partial pressure in the gas along the tube.

As seen in Figure 5.12, the mass absorption flux for case 1 decreases faster than for all other four cases and becomes the smallest at the tube end. This is consistent with the behavior observed in Figure 5.13 where the partial pressure of the vapor for case 1 decreases rapidly towards the end of the tube, with the result of the lowest driving force for mass transfer at the tube exit.

5.2.2 Effect of increasing the water vapor flow rate at the tube inlet

This section will present plots similar to those presented in the previous section, however, now all parameters of the base case will be held constant except for the water vapor mass flow rate at the inlet of tube. The different cases considered for this part will correspond to increasing multiples of the minimum amount of vapor flow needed to complete the absorption process. Figures 5.14 and 5.15, respectively, show the temperature and concentration of the solution as a function of position for different inlet vapor flow rates.

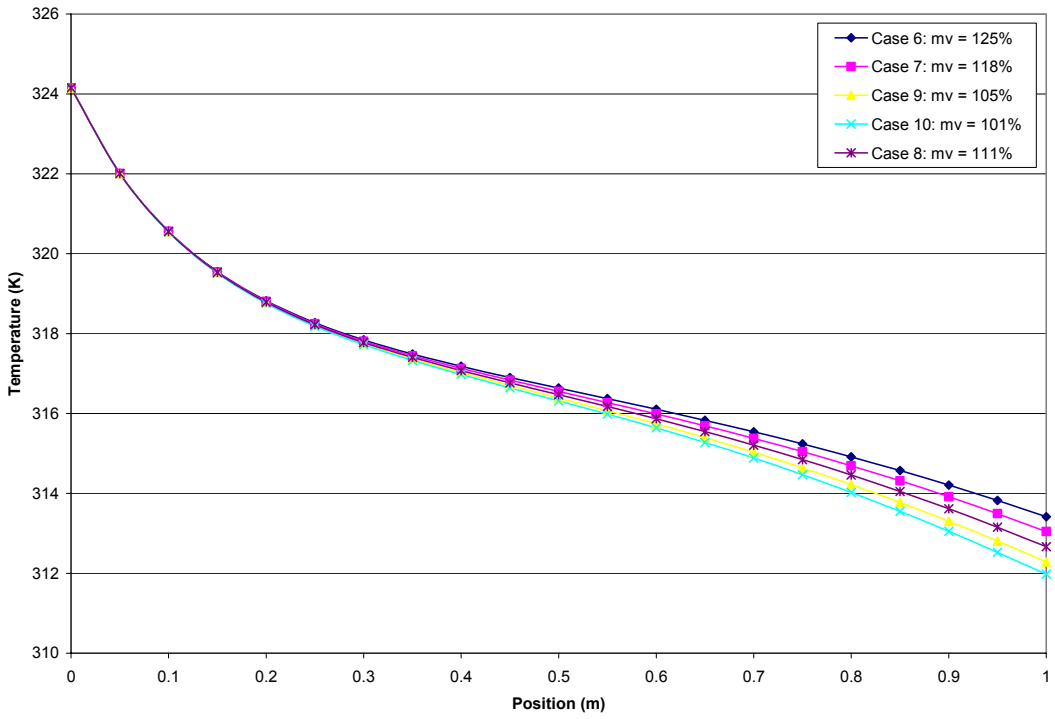

Figure 5.14 Solution temperatures as a function of position and initial water vapor flow rate.

In both cases the behavior is very similar. For the first half of the tube length, there is virtually no difference in solution temperature or concentration due to the different water vapor flow rates

considered. However, towards the end of the tube higher water vapor flow rates produced higher solution temperatures and lower solution LiBr concentrations, evidence of increased absorption rates.

Figure 5.16 shows the velocity of the vapor with respect to the position in the tube for different initial vapor flow rates. Let us take a look at the two extreme cases. For case 6, corresponding to 125% of the minimum flow, the inlet vapor velocity is 108.4 m/s and the vapor exits the tube at 29.5 m/s, for a total reduction of 72.8% of the velocity in the tube length. For 101% of the minimum flow rate, the vapor enters at 87.6 m/s and exits at 16.3 m/s, for a reduction of 81.34% in vapor velocity from inlet to outlet.

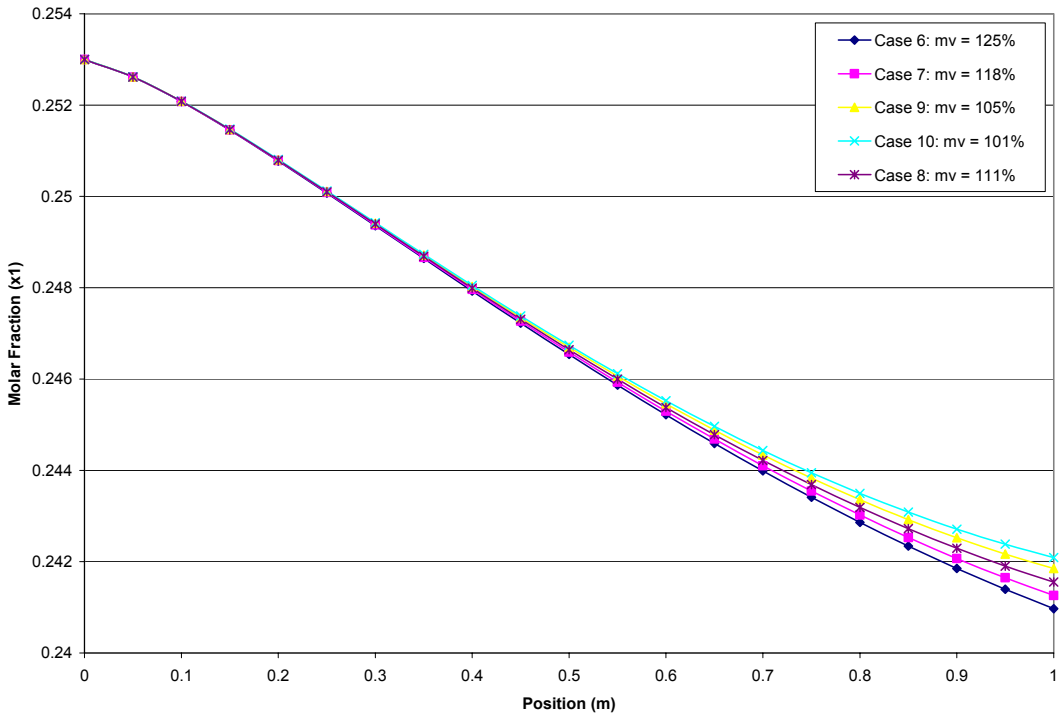

Figure 5.15 Solution LiBr fractions as a function of position and initial water vapor flow rate.

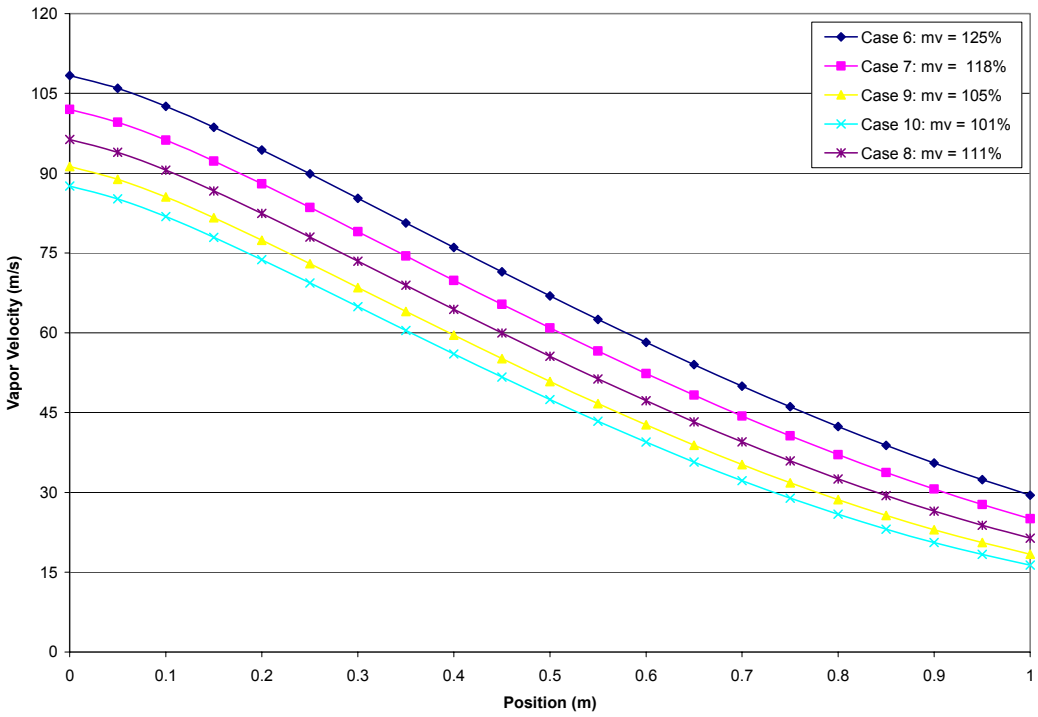

Figure 5.16 Gas velocities as a function of position and initial water vapor flow rate.

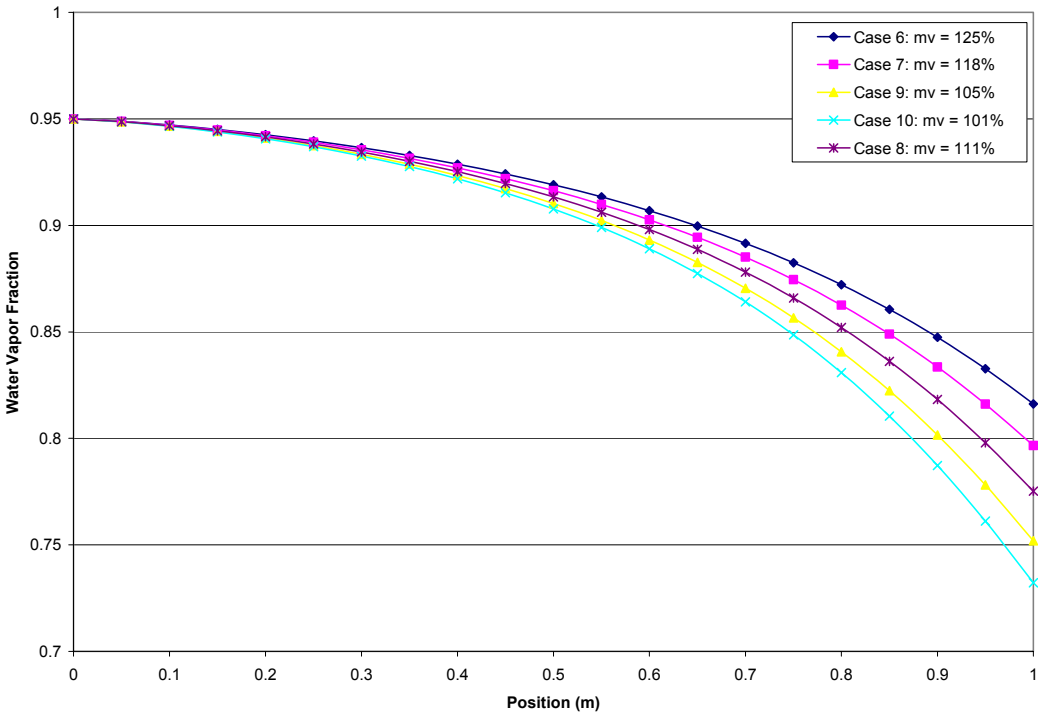

Figure 5.17 Gas compositions as a function of position and initial water vapor flow rate.

Figure 5.17 shows the effect of the vapor mass flow rate on the water concentration of the gaseous phase. For case 6, at 125% of the minimum vapor flow required, the inlet water concentration is 95%, dropping to 81.6% at the tube outlet. For case 10, at 101% of the minimum, it goes from 95% to 73.2%

To further explore the importance and effect of the water vapor mass flow rate on the absorption process, Figure 5.18 shows the mass absorption flux as a function of position and inlet vapor flow rate. It shows that as the inlet water vapor flow rate increases, the mass absorption flux also increases. This is consistent with the results observed in Figures 5.14 and 5.15, where the solution temperature increased and its LiBr concentration decreased with increasing vapor flow rates.

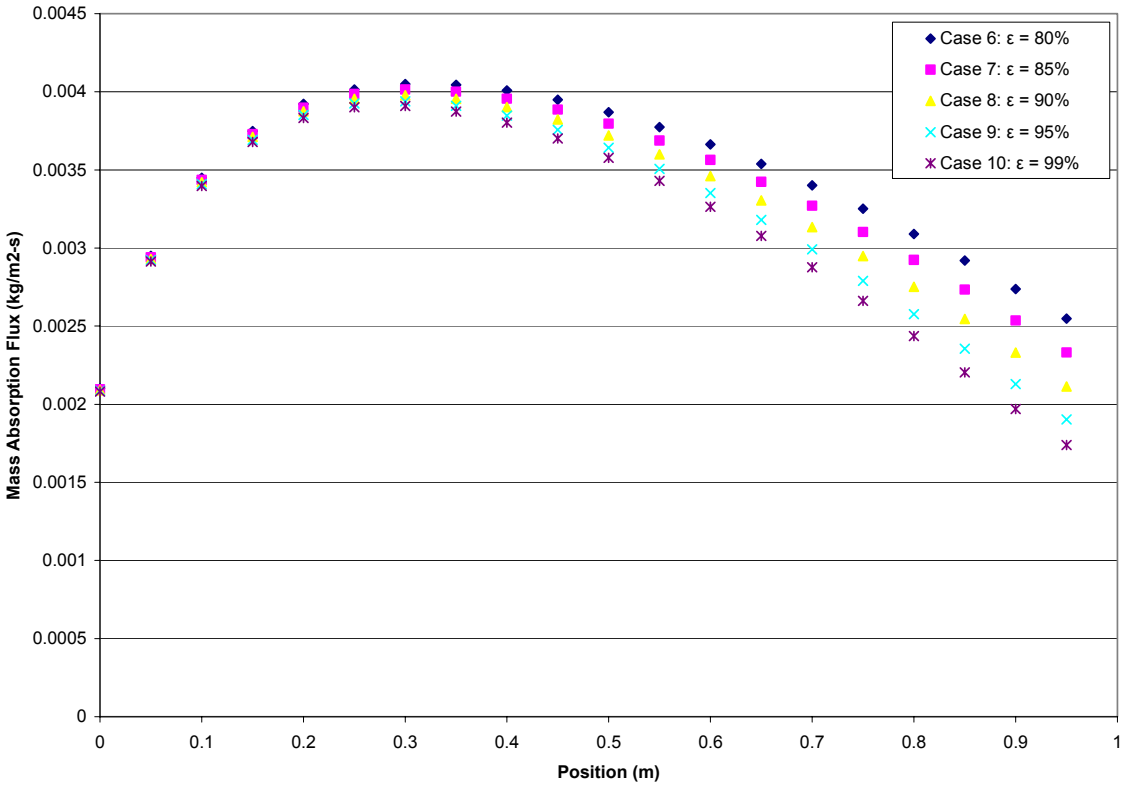

Figure 5.18 Absorption flux as a function of position and initial water vapor flow rate.

5.2.3 Effect of Increasing the Tube Length

This section considers the effect on the absorption process of increasing the tube length beyond the base length of 1 m considered in all the previous cases. The results in this section will be shown at a tube length of 2 meters. The model was verified at different lengths from 1 to 3 meters; however, a length of more than 2 meters in a vertical tube absorber would be highly impractical. Also, since this study is limited to co-current flow of vapor and solution, the results obtained for a 1-meter tube are similar to the results obtained for a longer tube at the 1-meter position, and similarly for any given length.

Figure 5.19 shows the solution temperature versus position for different inlet non-absorbables molar fractions for a tube length of 2 meters. For the portion of tube from the inlet to the 1-meter position, the trends have been previously discussed in Section 5.2.1. However, after the 1-meter position, some new trends are observed. For instance, the temperature for case 16 (1% air), rapidly decreasing at the 1-m position, equals that for case 17 (5% air) at about 1.25 meters. From this point on, the temperature continues decreasing and at 1.40 meters the temperature of case 16 becomes the lowest of all the cases considered.

Moreover, the plot for case 16 can be divided into 3 stages, namely: the entrance region, the absorption region, and the heat exchanger region. The entrance region would go from the inlet to the 0.35-m position where both heat and mass transfer are taking place. The absorption region would extend from the 0.35-m to the 1.3-m position. In this region, the mass transfer process is dominant starting at the maximum absorption flux value (0.00414 kg/m^2-s) and declining to a low mass absorption flux value (0.00022 kg/m^2-s), a reduction by a factor of almost 19 times. From the 1.3-m position on, the tube becomes a heat exchanger cooling the solution, while the mass absorption flux in this region tends to zero. For case 17 (5% air) the behavior is similar, but the absorption region is longer, up to about the 1.6-m position. For cases 18, 19, and 20 (10%, 15%, and 20% air, respectively), the absorption region extends all the way to the end of the 2-m tube.

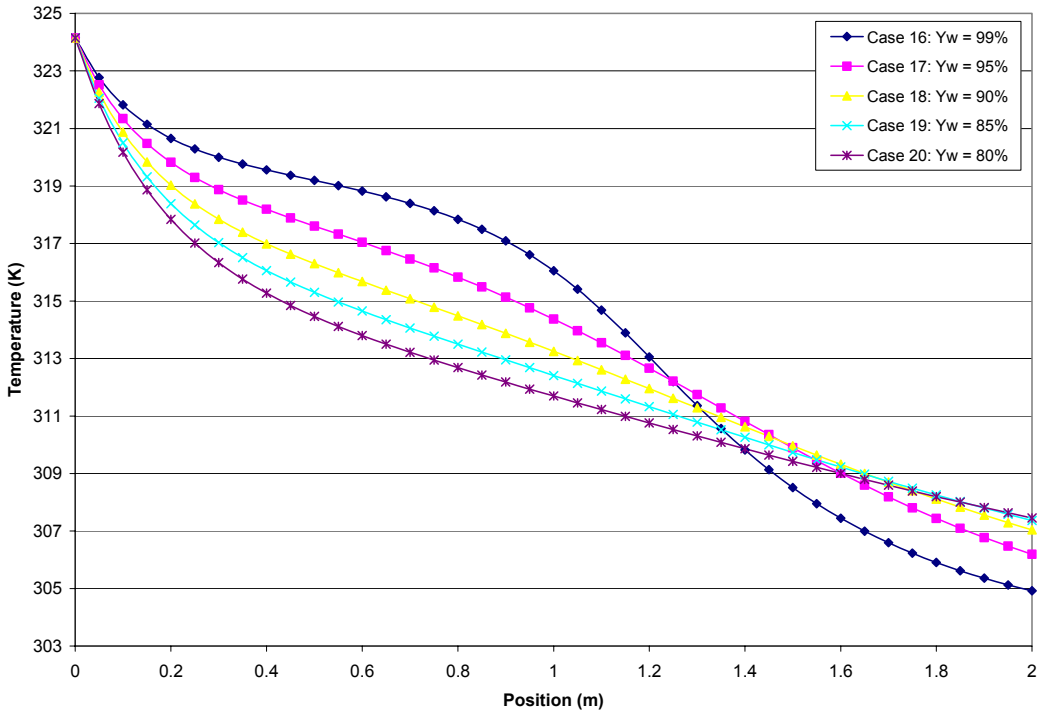

Figure 5.19 Solution temperatures as a function of position and non-absorbables concentration for a tube length of 2 meters.

Figure 5.20 presents the solution LiBr concentration as a function of position and non-absorbables concentration for a tube length of 2 meters. This figure validates the results discussed above for Figure 5.19. It is evident from this plot that there is a critical tube length beyond which no more absorption takes place. This critical length depends on the concentration of non-absorbables present in the inlet vapor. For 1% air, the critical length is about 1.3 m, while for 5% air it is about 1.6 m. For the higher non-absorbables concentrations studied (10%, 15%, and 20%) the critical length would be beyond 2 m.

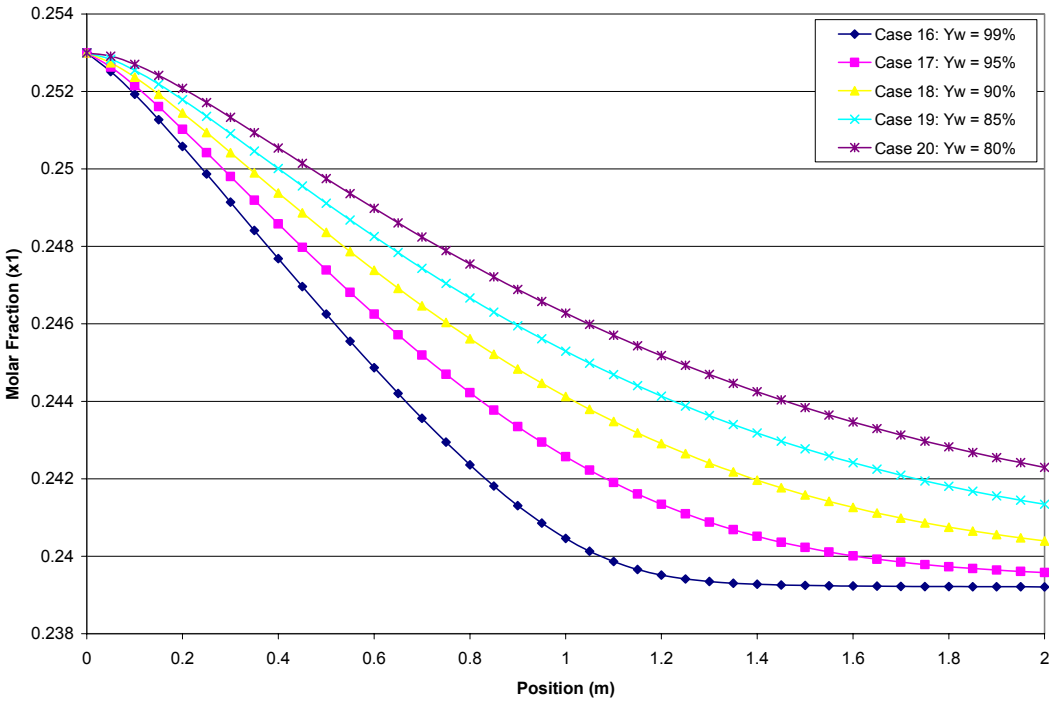

Figure 5.20 Solution LiBr concentration as a function of position and non-absorbables concentration for a tube length of 2 meters.

Figure 5.21 shows the gas velocity as a function of position and non-absorbables concentration for a tube length of 2 meters. Notice that Figures 5.20 and 5.21 reveal exactly identical trends, except for the fact that the inlet concentration of the LiBr solution was fixed for all the model runs, therefore the starting point for all plots in Figure 5.20 is the same. All the discussion presented with respect to Figure 5.20 also applies to Figure 5.21.

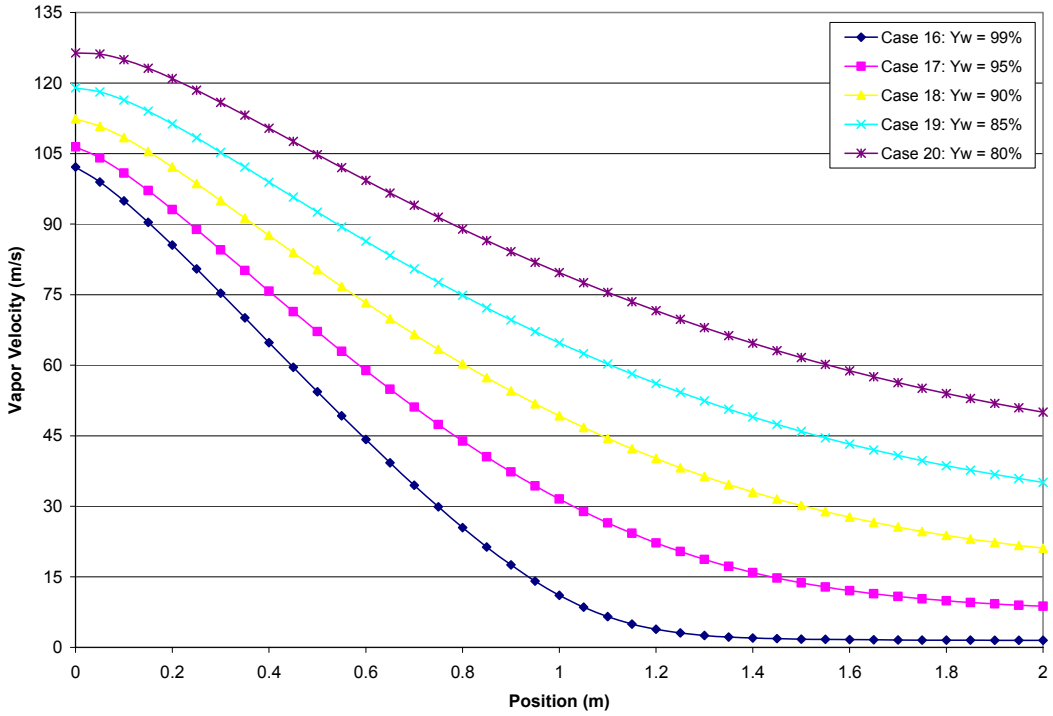

Figure 5.21 Gas velocity as a function of position and non-absorbables concentration for a tube length of 2 meters.

Figure 5.22 shows the mass absorption flux as a function of position and non-absorbables concentration for a tube length of 2 meters. As was mentioned before, the maximum absorption fluxes for all the cases are observed at the 0.35-m position. Subsequently from the 0.35-m to the 1.3-m positions, the mass transfer process is completely consumed (for case 16). The behavior of case 16 is close to the ideal behavior of the vertical tube with no non-absorbables present. All other cases (17-20) will also follow the same patterns and can be divided into the same three regions, however the presence in each of more air hinders the absorption process, especially after the entrance region, and instead of the absorption process being consumed rapidly it takes longer.

The maximum mass absorption flux for case 16 is 0.00414 kg/m^2-s and for case 20 is 0.00022 kg/m^2-s. Comparing the maximum absorption fluxes to that of case 16, the relative values for cases 17-20 are 83.58%, 70.56%, 61.18%, and 53.45%, respectively.

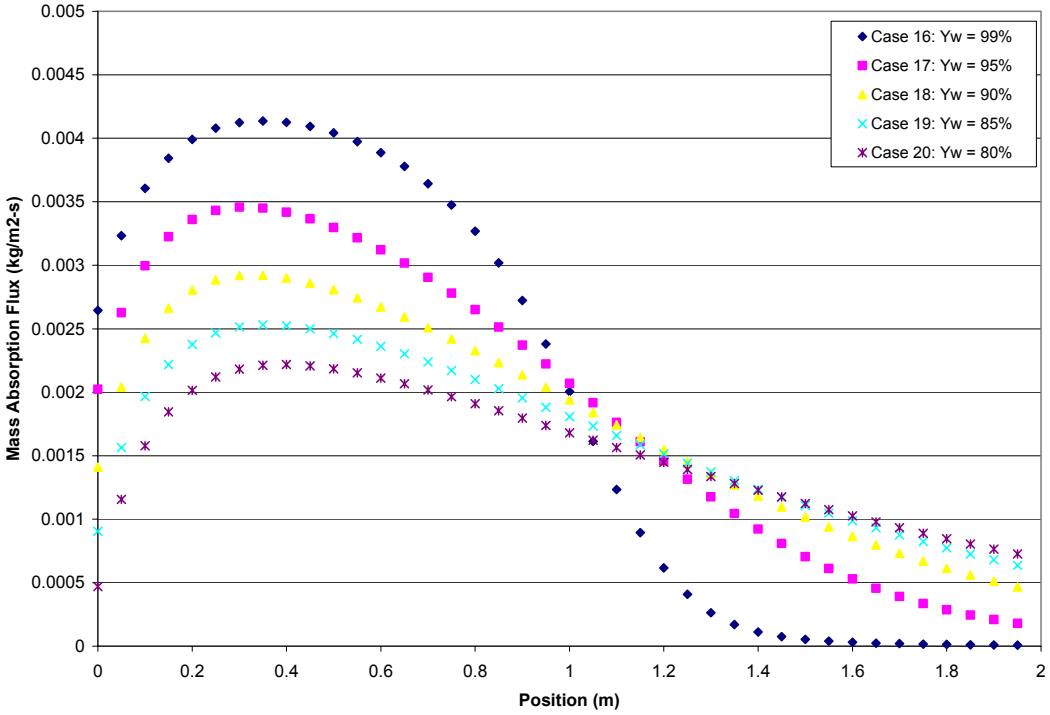

Figure 5.22 Mass absorption flux as a function of position and non-absorbables concentration for a tube length of 2 meters.

Figure 5.23 shows the water vapor molar fraction in the gas as a function of position and non-absorbables concentration for a 2-m tube. Notice that the outlet water vapor concentration changes drastically. For case 16, the inlet water vapor molar fraction is 99% while the exit value is about 29.5% for a reduction of 69.5%. For the case with the greatest percent of air (case 20) the vapor fraction at the inlet is 80% and 48.6% at the exit for a 31.4% reduction.

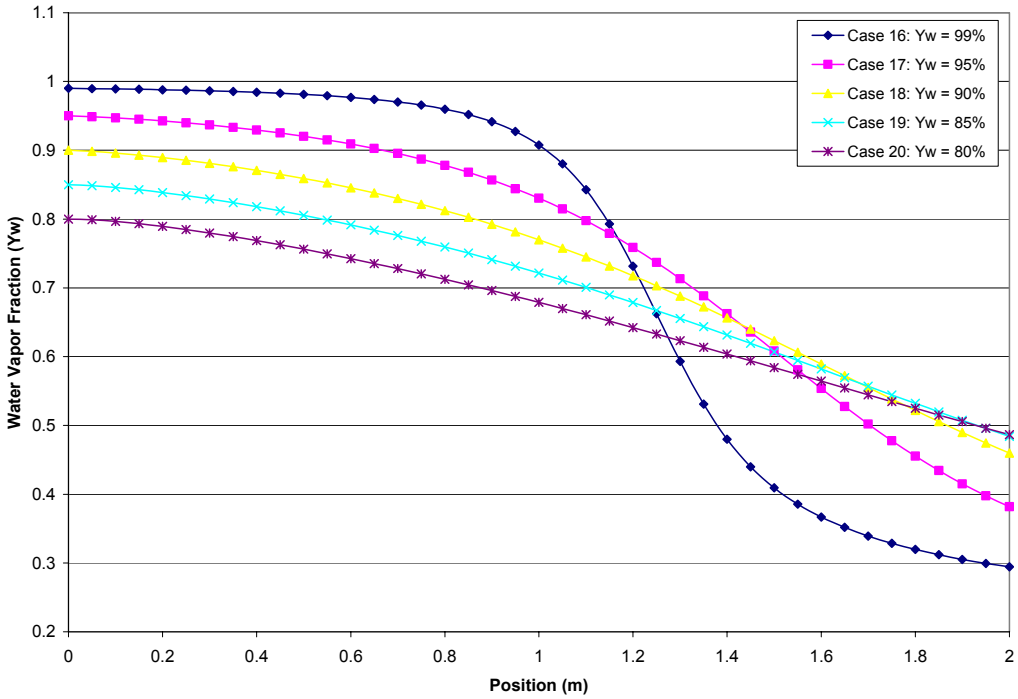

Figure 5.23 Water vapor molar fraction in the gas as a function of position and initial non-absorbables concentration for a tube length of 2 meters.

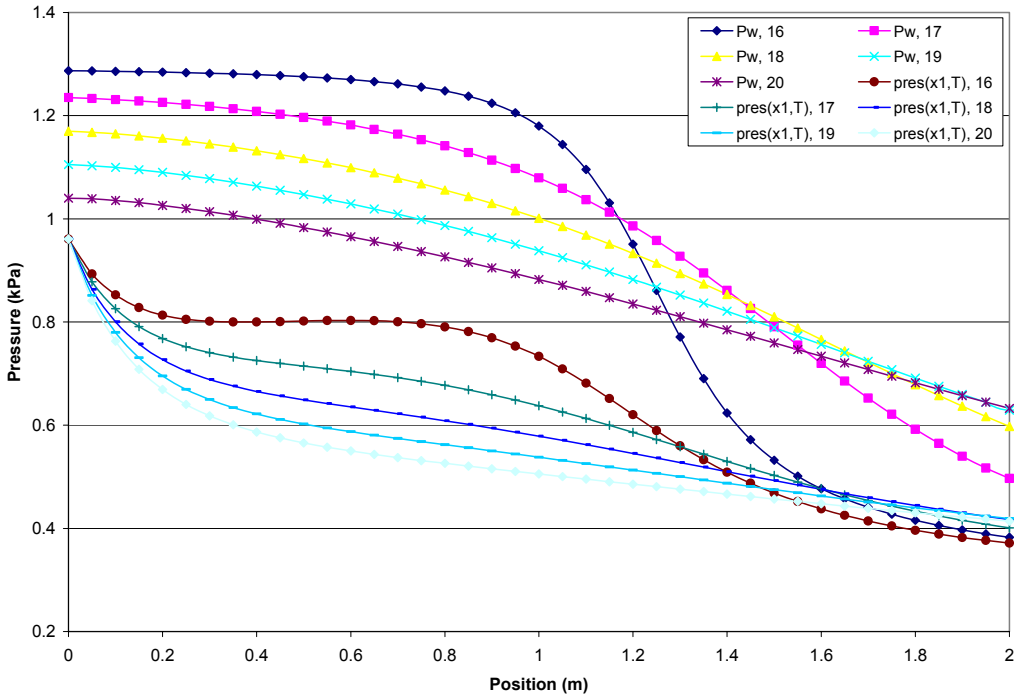

Figure 5.24 Driving force for absorption as a function of position and non-absorbables concentration for a tube length of 2 meters.

Figure 5.24 shows the differences that exist between the water vapor partial pressure and the solution vapor pressure. To support the results that already presented, observe that for the case of 99% vapor after the 2.0-meter position the pressures are equal, hence the mass transfer process is completely canceled. For the case of 95% vapor the mass transfer process is almost completely consumed, however for cases below 95% vapor fraction the mass transfer process is still in progress at the tube end.

5.3 Comparison of Results

The results for the model developed in this investigation has been previously presented in this chapter, however, in order to develop a yardstick for comparison of this model against other models and experiments conducted a summary of results and comparison to known results will be shown.

Table 5.1 shows the results of mass absorption flux and water vapor tube outlet velocity of a previous modeling effort (Medrano et al, 2003) in which a vertical tube absorber is considered operating at higher than normal cooling water temperatures to simulate air cooling. The model builds on an experimental setup in which data for vertical tube absorption were collected (Medrano et. al, 2002) and are presented in Table 5.3.

Table 5.1 – Results of mass absorption flux for various cases of non-absorbables concentrations (X_{in}=62 %wt, P=1.3 kPa, T_{cw}=35C, Re=100, Z=1.5m, Medrano et al.)

% of air	Mass Absorption Flux (kg/m2-s)	Tube Outlet Velocity (m/s)
1	0.00210	30
5	0.00195	30
10	0.00165	30
20	0.00120	30

Table 5.2 – Results of present model (X_{in}=62 %wt, P=1.3 kPa, T_{air}=30C, Re=100)

Case No.	U (kW/m^2-s)	F_L ($kmol/m^2$-s)	F_V ($kmol/m^2$-s)	V_f (m/s)	Re #	ρ_s (kg/m^3)	δ_s (m)	Mabs (kg/m2-s)	Heat Load (kW/m^2)
Case 16: Yw = 99%	0.587	0.002018	0.000116	1.47	95.48	1717.15	0.000423	0.001992	18.39
Case 17: Yw = 95%	0.583	0.001961	0.000148	8.74	93.33	1720.32	0.000425	0.001937	18.05
Case 18: Yw = 90%	0.578	0.001898	0.000168	21.09	90.96	1723.60	0.000428	0.001814	17.59
Case 19: Yw = 85%	0.574	0.001844	0.000182	35.09	88.88	1726.41	0.000430	0.001672	17.16
Case 20: Yw = 80%	0.570	0.001796	0.000194	50.00	87.03	1728.90	0.000432	0.001530	16.76

The results presented in Table 5.1 validate the present model predictions of the absorption mass flux estimated at various air concentrations, summarized in Table 5.2. There is good agreement between both models at low concentrations of air. However at high air concentrations their model under predicts the mass absorption flux. For case 16 through 20 (air % of 1,5,10 and 20) the present model predicts 94.86%, 99.33%, 110% and 127% of the result as presented in Table 5.1. The greatest % difference would be 27% at the highest concentration of air. Their model under-predicts the mass absorption flux at high air concentrations because they erroneously use a linear mass transfer driving force which, at high concentrations, has the effect of ignoring the bulk flow contribution to the total flux term.

Results have been extracted by an experimental setup (Medrano et al., 2002) in which they do an experimental setup to measure various effects such as: solution flow rate, cooling water temperature, and absorption pressure on the heat and mass transfer. Furthermore they run test at higher than normal cooling water temperatures to model air cooling conditions. For this experiment the presence of non-condensables is not considered. Table 5.3 documents the experimental results they measured.

Table 5.3 – Data from experimental results collected from Figs. 7, 8, and 9 in reference (Medrano et al. 2002).

LiBr flow rate, (kg/hr)	% wt	Pressure	Tcw	Z	Mass Absorption Flux, (kg/m-s)	U (kW/m2-s)	Re #
26	57.9	1.3	35	1.5	0.0015		100
26	57.9	1.3	40	1.5	0.0005		100
26	57.9	1.3	35	1.5	--	0.35-0.50	100
26	57.9	1.3	40	1.5	--	0.20-0.35	100
26	57.9	1.3	35	1.5	0.0015	--	90
26	57.9	1.3	35	1.5	0.0025	--	90
26	57.9	1.3	30	1.5	0.002	--	90
26	57.9	1.3	30	1.5	0.00325	--	90

From the experimental results it is clearly observed that the present model results correlate very well with the measurements they make for mass absorption flux at 35°C at constant Reynolds of 100. Notice that they obtain 0.0015 kg/m^2-s and values presented in Table 5.2 are all in this range of 0.0015-0.0020 kg/m^2-s. Furthermore, from the other available results it is observed that in their experiment increasing the cooling water temperature to 40°C was highly detrimental, while decreasing the temperature to 30°C had the effect of increasing by 100% the mass absorption flux. Moreover, it is important to comment that these experimental results are at a solution inlet concentration of 57.9 %wt and the percent of non-absorbables is not documented.

6. Conclusions and Recommendations

6.1 Conclusions

The main objective of this investigation was to be able to develop a more realistic model of an air cooled absorber than those available in the literature. The basis for developing the model was an in depth study of the heat and mass transfer coupled phenomena and a relaxation of some of the typically assumed constraints.

A very important tool developed in this work was the use of a Gibbs free energy equation as a generating function to estimate the thermodynamic properties (enthalpy, specific heat, density, and equilibrium vapor pressure) of aqueous LiBr solutions in terms of the solution composition, temperature and pressure. This analytical model is easily programmable for computer application eliminating the need to use tabulated or graphical thermodynamic data to describe changes in the solution properties as it flows down the vertical tube absorber.

The model was developed and the results were presented and discussed in the previous chapter. Three different factors affecting the absorption process were studied which are: concentration of non-absorbables in the vapor, water vapor inlet mass flow rate, and length of the tube. The results of the variation of these factors is documented, however, the most important of these findings are listed below.

1) Increasing the non-absorbables inlet concentration from 1% to 20% causes a decrease of the water vapor mass absorption flux by 43.7%. In an inverse effect relation, the tube outlet gas velocity, known as the purge velocity, increases from 4.43 m/s at 1% non-absorbables to 64.88 m/s at 20%.

2) In the case of increasing the inlet water vapor flow rate from 101% to 125% of the minimum, the water vapor mass absorption flux increased by 10%.

3) For co-current flow of the vapor and LiBr solution, there is a critical tube length beyond which no more absorption takes place. This critical length depends on the concentration of non-absorbables present in the inlet vapor. For the set of operating conditions considered in this work and 1% air, the critical length is about 1.3 m, while for 5% air it is about 1.6 m. For the higher non-absorbables concentrations studied (10%, 15%, and 20%) the critical length would be beyond 2 m.

4) The use of an extended heat transfer surface consisting of finned circular tubes such as described in this work would allow operating the absorber using air for cooling with an overall heat transfer coefficient of the same order of magnitude as those achieved in water cooled bare tubes.

6.2 Recommendations

The present investigation takes a step forward towards modeling a vertical tube in air cooled absorption conditions. The results are encouraging and show good agreement with previous literature results. However there are still some improvements to this model that should be considered. A first consideration would be to study the effect of heat transfer from the liquid solution to the gas. In this work, like all others previous models, this effect is considered negligible. Another improvement of the model could be the possibility of analyzing countercurrent flow of the gas and liquid solution. A very important contribution would be validating the model results with experimental data under actual thermal loading.

REFERENCES

Alva, L.H. and González, J.E., "Simulation of an Air Cooled Solar Assisted Absorption Air Conditioning System", Journal of Solar Energy Engineering, v.124, pp.276-282, 2002.

Atmaca, I. and Yigit, A., "Simulation of Solar-Powered Absorption Cooling System", Renewable Energy, vol., pp. 1277-1293, 2003.

Auh, P.C. "Solar Cooling Research and Development Overview." Paper presented in the Third Annual Solar Heating and Cooling RandD Contractors, Meeting. Sept. 1978.

Benítez, J. Principles and Modern Applications of Mass Transfer Operations, John Wiley and Sons, NY, 2002.

Bong, T. Y., Ng, K. C., and Tay, A. O., "Performance study of a solar powered air conditioning system", Solar Energy, Vol. 39 No. 3 pp. 173-182, 1987.

Brauner, N. "Modeling of wavy flow in turbulent free falling films." Int. J. Multiphase Flow, 15(4):505-20, 1989.

Carey, V.P., 1992, "Liquid-Vapor Phase-Change Phenomena: An Introduction to the Thermophysics of Vaporization and Condensation Processes in Heat Transfer Equipment", Taylor and Francis.

Castro, J., Leal, L., Pozo, P., Segarra, C., 2002, "Development and performance air-cooled Water LiBr absorption cooling machine". Proceedings of International Forum on Renewable Energy, January 2002.

De Hoyos, M., "A Method to Assess the Potential Market and Economic Feasibility of a Renewable Energy Product: The Solar Air Conditioning System Case", MBA Thesis, University of Puerto Rico, Mayagüez, PR. 1999.

DiGuilio, R. M., Lee, R. J., Meter, S. M., and Teja, A. S. "Properties of lithium bromide-water solutions at high temperatures and concentrations." ASHRAE Transactions, 96:702-708, 1990.

Florides, G., Kalogirou, S., Tassou, S., and Wrobel, L., "Modeling and Simulation of an Absorption Solar Cooling System for Cyprus", Solar Energy, vol. 72, pp. 43-51, 2002.

Florides, G., Kalogirou, S., Tassou, S., and Wrobel, L., "Modelling Simulation and Warming Impact Assessment of a Domestic Size Absorption Solar Cooling System", Applied Thermal Engineering, vol. 22, pp 1313-1325. , 2002.

Florides, G., Kalogirou, S., Tassou, S., and Wrobel, L., "Design and Construction of a LiBr-Water Absorption Machine", Energy Conversion and Management, vol. 44, 15, pp. 2483-2508, 2003.

Ghaddar, N.K., Shihab, M., and Bdeir, F., "Modeling and simulation of solar absorption system performance in Beirut.", Renewable Energy, vol. 10, No. 4, pp. 539-558, 1997.

Gierow, M. and A. Jernqvist, "Measurement of mass diffusivity with holographic interferometry for H_2O/NaOH and H_2O/LiBr working pairs." International Absorption Heat Pump Conference Proceedings, Book No. 100361, 1993.

González, J.E. and Khan, A. Y., "Solar-Assisted Air Conditioning System for Applications in Puerto Rico," Report # 96-311 of the Urban Consortium Energy Task Force, 1997.

González, J.E. and Beauchamp, G., "Compact Solar-Powered Air Conditioning Systems," U. S. Patent 6,539,738, awarded April 1, 2003, assigned to University of Puerto Rico

Hammad, M. and Zurigat, Y., "Performance of a Second Generation Solar Cooling Unit", Solar Energy, vol. 62, No. 2 pp. 79-84, 1998.

Hernandez, H.R., González, J.E., and Khan A.Y., "A Parametric Study of Solar-Assisted Air Conditioning and Dehumidification Systems Operating in the Caribbean Region", Proceedings of the ASME Solar Energy Division, pp.327-334, 1997.

Herold, K.E., Radermacher, R., and Klein, S.A., 1996, "Absorption Chillers and Heat Pumps", CRC Press, New York, NY.

ICT, 1928. International Critical Tables, McGraw-Hill, New York.

Ileri, A., "Discussion of performance parameters for solar-aided absorption Cooling Systems", Renewable Energy, vol. 10(4), pp. 617-624, 1997.

Incropera, F.P., and Dewitt, D.P., 1996, "Fundamentals of Heat and Mass Transfer", John Wiley and Sons, Inc. NewYork, NY.

Kakac, S., Hongtan, L., 2002, "Heat Exchangers: Selection, Rating and Thermal Design", 2nd Edition, CRC Press, New York, NY.

Kays, W.M., and London, A.L., "Compact Heat Exchangers", 3rd Edition, 1984.

Killion, J., and Garimella, S., "A critical review of models of coupled heat and mass transfer in falling film absorption.", International Journal of Refrigeration, vol. 24, pp. 755-797, 2001.

Kim, D.S. and Ferreira, C.A., "A Gibbs energy Equation for LiBr aqueous solutions", International Journal of Refrigeration, vol. 29, pp.36-46, 2006.

Kim, D.S. and Ferreira, C.A., "Solar absorption cooling, first progress report", Delft University of Technology, 2003.

Kiyota, M., Morioka, I., and Matsuyama, T., "Steam absorption into aqueous lithium bromide solution films falling inside vertical pipes.", Heat Transfer-Asian Research, vol 32, No. 8, pp. 740-752, 2003.

Lopez, A. M., and Soderstrom, K.G., 1983, "Insolation in Puerto Rico", ASME Solar Engineering, pp. 70-75.

McNeely, L. A. "Thermodynamic properties of aqueous solutions of lithium bromide." ASHRAE Transactions, 85:413-434, 1979.

Medrano, M., Bourouis, M., and Coronas, A., "Absorption of Water Vapor in the Falling Film of Water-LiBr Inside a Vertical Tube at Air-Cooling Thermal Conditions", International Journal of Thermal Sciences, vol. 41, pp. 891-898, 2002.

Medrano, M., Bourouis, M., Pérez-Blanco, H., and Coronas, A., "A simple model for falling film absorption on vertical tubes in the presence of non-absorbables", International Journal of Refrigeration, vol. 26: 108-116, 2003.

Melendez, L.V., "Automation and Control of Solar Air Conditioning System", M.S. Thesis, University of Puerto Rico, Mayagüez, PR, 2000.

Meléndez, L.V., González, J.E., and Beauchamp, G., "Automation and Control of Solar Air Conditioning Systems", U. S. Patent 6,536,677, awarded March 25, 2003, assigned to University of Puerto Rico.

Meza, J.I., González, J.E., and Khan, A.Y. "Experimental Assessment of a Solar Assisted Air Conditioning System for Applications in Puerto Rico," ASME Proceedings of Solar Energy Division, pp.149-154, 1998.

Miller, W. A., "The experimental analysis of aqueous lithium bromide vertical falling film absorption." Dissertation, University of Tennessee, Knoxville, 1998.

Mostafavi, M., and Agnew, B., "The effect of ambient temperature on the surface area of components of an air-cooled lithium bromide/water absorption unit.", Applied Thermal Engineering, vol. 16, No. 4, pp. 313-319, 1996.

Muneer, T., and Uppal, A.H., "Modeling and simulation of a solar absorption cooling system.", Applied Energy, vol. 19, pp. 209-229, 1985.

Nash, J.M. and Harstad, A.J., "Application of Solar Energy to Air Conditioning Systems." Report prepared for the US Department of Energy under contract, NAS 8-32036, Nov. 1976.

Parker, D.S., Mazzara, M.D., and Sherwin, J.R., "Monitored Energy Use Patterns in Low-Income Housing in a Hot and Humid Climate," Tenth Symposium on Improving Building Systems in Hot Humid Climates, p. 316, Ft Worth, TX, 1996

Patnaik V., and Perez-Blanco, H. "A study of absorption enhancement by wavy film flows." Int. J. of Heat and Fluid Flow, 17(1):71-7, 1996.

Patnaik, V., Pérez-Blanco, H., and Ryan, W. A. "A simple analytical model for the design of vertical tube absorbers." ASHRAE Transactions:69-80, 1993.

Pérez, R.A., Sanchez, H.M., Gonzalez, J.E., Alva, L.H., "Design and Construction of a compact air-cooled absorption machine for solar energy applications", International Solar Energy Conference, pp.361-367, 2004.

PRPB, "Selected statistics of the construction industry in Puerto Rico," Puerto Rico Planning Board, Program for Economic and Social Planification, Economic Analysis Subprogram, p.15, 2003.

Sayigh, A.A.M., and Saada, M.K., "A three and a half ton solar air conditioner's performance in Riyadh, Saudi Arabia." Proceedings of the International Solar Energy Society Congress, Brighton, vol. 1, pp. 537-543, 1981.

Smith, J. M., Van Ness, H. C., and Abbott, M. M. Introduction to Chemical Engineering Thermodynamics, 7th ed. McGraw-Hill, NY, 2005.

Sumathy, K., and Li, Z.K., "Simulation of a solar absorption air conditioning system.", Energy Conversion and Management, vol. 42, pp. 313-327, 2001.

Wark, K., and Richards, D.E., 1999, "Thermodynamics: Sixth Edition", McGraw Hill Company, Inc., New York, NY.

Wikipedia, 2007, Ëinstein Refrigerator". Available on the web at: http://en.wikipedia.org/wiki/Einstein_refirgerator.

Yeung, M. R., Yuen, P. K., Dunn, A., and Cornish, L. S., "Performance of a solar powered air conditioning system in Hong Kong", Solar Energy, vol. 48 No. 5, pp. 309-319, 1992.

APPENDIX A

This is a program to Calculate the Heat & Mass Transport Coefficients of the LiBr Solution and Water + Air Mixture in the Absorber.

Properties of LiBr Solution:
The following sections calculate the transport properties of LiBr solution which will later be used to estimate the heat and mass transfer coefficients.

Molar & Mass Fraction Calculations:
In this Section we define the molarity of m as a function of both the molar concentration and the mass concentration. For convenience we will express molarity (m) in terms of molar concentration x_1.

$\upsilon := 2 \qquad R := 8.314 \qquad M_1 := 86.84 \qquad M_2 := 18.015 \qquad ORIGIN := 1$

$$mol(x1) := \frac{x1}{(1 - x1)\cdot M_2}$$

$$x(x1) := \sqrt{\frac{x1}{(1 - x1)\cdot M_2}}$$

$x(0) = 0 \qquad x(.261) = 0.14$

$$Xw(x1w) := \sqrt{\frac{x1w}{(1 - x1w)\cdot M_1}}$$

$Xw(0) = 0 \qquad Xw(0.556) = 0.12$

1.0 Thermal Conductivity:

$$a\_k := \begin{pmatrix} -0.3863624126 & -0.3122938151 & 17.75694663 & -41.62113683 \\ 0.005245122201 & -0.006413302194 & -0.08009549080 & 0.2130478667 \\ -6.398936707\cdot 10^{-6} & 1.013622815\cdot 10^{-5} & 0.00010029254 & -0.000281450 \end{pmatrix} \cdot 10^{-3}$$

$$k_{sol}(x1, T) := \left[\sum_{i=1}^{3} \sum_{j=1}^{4} \left[a\_k_{i,j} \cdot x1^{j-1} \cdot \left(\frac{T}{K} \right)^{i-1} \right] \right] \cdot \frac{kW}{m\cdot K}$$

$$k_{sol}(0.153, 298K) = 4.602 \times 10^{-4} \frac{kW}{m\cdot K}$$

2.0 Dynamic Viscocity of the Solution:

$$a\_mu := \begin{pmatrix} 15.4338601 & -1.796143844 & -453.964325 & 1644.664107 \\ -0.1496987184 & 0.08581467986 & 3.186981058 & -11.18992719 \\ 0.0003210580467 & -0.0004050019644 & -0.006116119513 & 0.02286554179 \\ -2.397708795\cdot 10^{-7} & 6.025222928\cdot 10^{-7} & 2.699142889\cdot 10^{-6} & -1.335944410^{-5} \end{pmatrix}$$

$$\ln\mu_{sol}(x1,T) := \sum_{i=1}^{4}\sum_{j=1}^{4}\left[a\_mu_{i,j}\cdot x1^{j-1}\cdot\left(\frac{T}{K}\right)^{i-1}\right] \qquad \ln\mu_{sol}(0,298K) = -7.01$$

$$\mu_{sol}(x1,T) := e^{\ln\mu_{sol}(x1,T)}\cdot\frac{kg}{m\cdot s}$$

$$\mu_{sol}(0,298K) = 9.025\times 10^{-4}\,\frac{kg}{m\cdot s} \qquad \mu_{sol}(0.237,313K) = 5.276\times 10^{-3}\,\frac{kg}{m\cdot s}$$

Here we define the film thickness (δ) as a function of a parameter we call wetted surface (Γ). Furthermore, the reynolds No. can be expressed as function of Γ, in which for wavy film profile we fix the Re=100.

Hence the Mass Flow Rate can be defined as...

$D_i := 0.0167m$ **where Di is he inside tube diameter.** $Re_s := 100$

$$m_s(x1,T) := Re_s\cdot\frac{\pi}{4}\cdot D_i\cdot\mu_{sol}(x1,T)$$

$$m_s(0.1074,293K) = 2.55\times 10^{-3}\,\frac{kg}{s} \qquad m_s(0.202,313K) = 4.576\times 10^{-3}\,\frac{kg}{s}$$

3.0 Diffusivity of the LiBr Solution:

$\alpha := 1.271581637$ $\beta := 145.271699$ $\gamma := -9547.634363$

$$D_{ABs}(x1,T) := \left(\alpha + \beta\cdot mol(x1) + \gamma\cdot mol(x1)^2\right)\cdot\left(\frac{\mu_{sol}(x1,298.15K)}{\mu_{sol}(x1,T)}\right)\cdot\left(\frac{T}{298.15K}\right)\cdot 10^{-9}\cdot\frac{m^2}{s}$$

$$D_{ABs}(0.14,298K) = 1.799\times 10^{-9}\,\frac{m^2}{s}$$

4.0 Volume & Density of LiBr Solution:

$$b := \begin{pmatrix} -4.417865410^{-5} & 3.114899210^{-2} & -4.36112261^{0} \\ 3.07939921^{-4} & -1.86320981^{-1} & 2.73871371^{1} \\ -4.08079431^{-4} & 2.16079551^{-1} & -2.51759711^{1} \\ 0 & 0 & 0 \\ 0 & 0 & 0 \\ 0 & 0 & 0 \end{pmatrix}$$

$i := 1..6$

$$bb(i,T) := \sum_{q=1}^{3} \left[b_{i,q} \cdot \left(\frac{T}{K} \right)^{-q+1} \right]$$

$$ee := \begin{pmatrix} 2.66299611^{-3} \\ -3.86518911^{-6} \\ 7.46484111^{-9} \end{pmatrix} \qquad kmol := 1000mole$$

$$V_{1inf}(T) := R \cdot \frac{T}{K} \cdot bb(1,T) \cdot \frac{m^3}{kmol}$$

$$V_{2L}(T) := R \cdot \left[ee_1 + ee_2 \cdot \frac{T}{K} + ee_3 \cdot \left(\frac{T}{K} \right)^2 \right] \cdot \frac{m^3}{kmol}$$

$$V_E(x1,T) := x1 \cdot R \cdot \frac{T}{K} \cdot \left(bb(2,T) \cdot x(x1) + bb(3,T) \cdot x(x1)^2 \right) \cdot \frac{m^3}{kmol}$$

$$V_L(x1,T) := x1 \cdot V_{1inf}(T) + (1 - x1) \cdot V_{2L}(T) + V_E(x1,T)$$

$$D_L(x1,T) := \frac{1}{V_L(x1,T)} \qquad DF := \frac{kg}{kmol}$$

$$\rho_s(x1,T) := D_L(x1,T) \cdot \left[x1 \cdot M_1 + (1 - x1) \cdot M_2 \right] \cdot DF$$

$$\rho_s(0,273.15K) = 1.001 \times 10^3 \frac{kg}{m^3} \qquad \rho_s(0.202,313K) = 1.605 \times 10^3 \frac{kg}{m^3}$$

5.0 Mass Flow Rate per Wetted Perimeter & Film Thickness:

$$\Gamma(x1,T) := \frac{m_s(x1,T)}{\pi \cdot D_i} \qquad \Gamma(0.253,323K) = 0.132\frac{kg}{m\cdot s} \qquad G := 9.8\cdot\frac{m}{s^2}$$

$$\delta(x1,T) := \left(\frac{3\cdot\mu_{sol}(x1,T)\cdot\Gamma(x1,T)}{\rho_s(x1,T)^2\cdot G}\right)^{\frac{1}{3}} \qquad \delta(0.202,313K) = 3.306\times 10^{-4}\,m$$

Vapor + Air Mass Transfer Calculations:
(laminar vapor profile)

$$R_u := 8.314\frac{kPa\cdot m^3}{kmol\cdot K} \qquad kPa := 1000Pa$$

6.0 Calculating Absorber Mass Flow Rates & Breakdowns:

6.1 Absorption Inlet & Outlet Flows:
This is given we already calculated the solution m.f.r. and we can now set the inlet and outlet solution weight concentrations in order to compute the LiBr and vapor mfr.

Inlet Flows:

$$X_{s\_in} := 0.62 \qquad X_{s\_out} := 0.604 \qquad m_s(0.253,323K) = 6.934\times 10^{-3}\frac{kg}{s}$$

$$m_{LiBr\_in}(x1,T) := m_s(x1,T)\cdot X_{s\_in} \qquad m_{LiBr\_in}(0.253,323K) = 4.299\times 10^{-3}\frac{kg}{s}$$

$$m_{H2O\_in}(x1,T) := m_s(x1,T)\cdot\left(1 - X_{s\_in}\right) \qquad m_{H2O\_in}(0.253,323K) = 2.635\times 10^{-3}\frac{kg}{s}$$

Also we know the LiBr is not created or destroyed so the same amount present in the inlet is present in the outlet...hence,

Outlet Flows:

$$m_{LiBr\_out}(x1,T) := m_{LiBr\_in}(x1,T)$$

$$m_{s\_out}(x1,T) := \frac{m_{LiBr\_out}(x1,T)}{X_{s\_out}}$$

$$m_{H2O\_out}(x1,T) := m_{s\_out}(x1,T) - m_{LiBr\_out}(x1,T)$$

$$m_{s}(0.202,313K) = 4.576\times 10^{-3}\,\frac{kg}{s}$$

$$m_{s\_out}(0.202,313K) = 4.697\times 10^{-3}\,\frac{kg}{s}$$

$$m_{H2O\_out}(0.253,313K) = 3.421\times 10^{-3}\,\frac{kg}{s}$$

6.2 Calculating the Absorption Mass Flow Rate:

Using the calculated inlet and outlet flows for the H2O we can now estimate the absorption mass flow rate.

$$m_{abs\_i}(x1,T) := m_{H2O\_out}(x1,T) - m_{H2O\_in}(x1,T)$$

$$m_{abs\_i}(0.202,313K) = 1.212\times 10^{-4}\,\frac{kg}{s}$$

The eta term used here is too increase the minimum flow of vapor to see the effect this has on the absorption.

$$\eta_{abs} := 0.90$$

$$m_{abs}(x1,T) := \frac{m_{abs\_i}(x1,T)}{\eta_{abs}}$$

$$m_{abs}(0.253,324.15K) = 1.99766\times 10^{-4}\,\frac{kg}{s}$$

Now we know the m.f.r. of the water vapor and we now the gaseous mixture has a 5% molar concentration of Air, hence...

$$y_{H2O} := 1.0 \qquad T_v := 283K \qquad P_v := 1.3\cdot 10^{-2}bar$$

$$SF := \frac{kg}{kmol}$$ species factor for Molecular weight

$$N_{H2O\_in}(x1,T) := \frac{m_{abs}(x1,T)}{M_2\cdot SF}$$

$$N_{H2O\_in}(0.202,313K) = 7.476\times 10^{-6}\,\frac{kmol}{s}$$

$$N_{IG\_in}(x1,T) := \frac{N_{H2O\_in}(x1,T)}{y_{H2O}}$$

$$N_{IG\_in}(0.202,313K) = 7.476\times 10^{-6}\,\frac{kmol}{s}$$

7.0 Creating the Absorber Operation Curve

In this section the equations that correlates the bulk concetration of the liquid side with the gaseous side and vise versa.

Liquid Side:

Properties of solution phase entering the absorber:

$P := 1.30\,kPa$ $T_{so} := (51 + 273.15)K$ $X_{s\_in} := 0.62$ LiBr weight fraction $T_v := 283$

$$x1 := \frac{\frac{X_{s\_in}}{M_1}}{\frac{X_{s\_in}}{M_1} + \frac{1 - 1X_{s\_in}}{M_2}} \qquad x1 = 0.253$$ LiBr mole fraction

$x_W(x1) := 1 - x1$ $x_W(x1) = 0.747$ Bulk water mole fraction

$$X_{W1}(x1) := \frac{x_W(x1)}{1 - x_W(x1)} \qquad X_{W1}(x1) = 2.954$$ Water to LiBr mole ratio

$m_{so}(x1, T_{so}) := m_s(x1, T_{so})$ initial flow rate of solution.

$m_{so}(x1, T_{so}) = 6.778 \times 10^{-3}\ \frac{kg}{s}$ $m_{LiBr\_in}(x1, T_{so}) = 4.202 \times 10^{-3}\ \frac{kg}{s}$

$$L_S := \frac{m_{LiBr\_in}(x1, T_{so})}{\frac{M_1 \cdot kg}{kmol}} \qquad L_S = 4.839 \times 10^{-5}\ \frac{kmol}{s}$$ LiBr molar flow rate

Vapor Side:

Properties of gas phase entering the absorber:

$y_{H2O} := 0.80$ $y_W := y_{H2O}$ $y_W = 0.8$ $T_{sv} := 283K$ saturation temperature of H2O at 1.3 kPa

$kJ := 1000J$

$N_{abs}(x1, T) := N_{IG\_in}(x1, T)$ Total vapor molar flow rate at the entrance

$N_{abs}(x1, T_{so}) = 1.107 \times 10^{-5} \frac{kmol}{s}$

$V_S := (1 - y_W) \cdot N_{abs}(x1, T_{so})$ Air molar flow rate

$V_S = 2.215 \times 10^{-6} \frac{kmol}{s}$

$Y_{W1} := \frac{y_W}{1 - y_W}$ $Y_{W1} = 4$ Water vapor to Air molar ratio.

$r_1 := \frac{L_S}{V_S}$ $r_1 = 21.849$

$H_v := 2520 \frac{kJ}{kg} \cdot \frac{M_2 \cdot kg}{kmol}$ $H_v = 4.54 \times 10^4 \frac{kJ}{kmol}$ Enthalpy of the saturated vapor, from Steam Tables

This is the line of operation of the absorber, and the derivation shows that in this the Yw1 and Xw1 are both intlet conditions and are fixed.

$RHS(x1) := Y_{W1} + r_1 \cdot X_{W1}(0.253) - r_1 \cdot \left(\frac{1 - x1}{x1}\right)$

$y_W(x1) := \frac{RHS(x1)}{1 + RHS(x1)}$ Operating line

$y_W(0.253) = 0.8$ Check with the inlet concentrations

$y1(x1) := 1 - y_W(x1)$ $y1(x1) = 0.202$

$P_W(x1) := y_W(x1) \cdot P$ $P_W(x1) = 1.038kPa$ partial pressure of water in gaseous mixture at the entrance

Properties of H2O + Air Gaseous Mixture:
The following are the physical estimation of the diffusivity, density, and dynamic viscosity of the Gaseous mixture coming into the absorber.

8.0 Wilke-Lee Equation for Vapor + Air Diffusivity Estimation:
Using the Wilke-Lee Equation and the Leonnard-Jones Parameters the values for the Diffusivity of Water Vapor to air is estimated.

$$\sigma_{AB}(\sigma_A,\sigma_B) := \frac{\sigma_A + \sigma_B}{2}$$

$$\varepsilon_{ABk}(\varepsilon_{Ak},\varepsilon_{Bk}) := \sqrt{\varepsilon_{Ak}\cdot\varepsilon_{Bk}}$$

$$ax := 1.06036 \quad bx := 0.15610 \quad cx := 0.19300 \quad dx := 0.47635$$

$$ex := 1.03587 \quad fx := 1.52996 \quad gx := 1.76474 \quad hx := 3.89411$$

$$xx(T_v,\varepsilon_{Ak},\varepsilon_{Bk}) := \frac{\frac{T_v}{K}}{\varepsilon_{ABk}(\varepsilon_{Ak},\varepsilon_{Bk})}$$

$$M_{AB}(M_A,M_B) := 2\cdot\left(\frac{1}{M_A}+\frac{1}{M_B}\right)^{-1}$$

$$\Omega(T_v,\varepsilon_{Ak},\varepsilon_{Bk}) := \frac{ax}{xx(T_v,\varepsilon_{Ak},\varepsilon_{Bk})^{bx}} + \frac{cx}{e^{dx\cdot xx(T_v,\varepsilon_{Ak},\varepsilon_{Bk})}} + \frac{ex}{e^{fx\cdot xx(T_v,\varepsilon_{Ak},\varepsilon_{Bk})}} + \frac{gx}{e^{hx\cdot xx(T_v,\varepsilon_{Ak},\varepsilon_{Bk})}}$$

$$D_{AB}(T_v,P_v,M_A,M_B,\sigma_A,\sigma_B,\varepsilon_{Ak},\varepsilon_{Bk}) := \frac{10^{-3}\cdot\left(3.03-\frac{0.98}{\sqrt{M_{AB}(M_A,M_B)}}\right)\cdot\left(\frac{T_v}{K}\right)^{\frac{3}{2}}}{\frac{P_v}{bar}\cdot\sigma_{AB}(\sigma_A,\sigma_B)^2\cdot\Omega(T_v,\varepsilon_{Ak},\varepsilon_{Bk})\cdot\sqrt{M_{AB}(M_A,M_B)}}\cdot 10^{-4}\cdot\frac{m^2}{s}$$

Applying this Model to H_2O & Air...

Lennard-Jones Constants

	Collision Diameter	Energy of interaction	Molecular Weight	
				Water Parameters
	$\sigma_A := 2.641$	$\varepsilon_{Ak} := 809.1$	$M_A := 18$	
				Air Parameters
	$\sigma_B := 3.62$	$\varepsilon_{Bk} := 97$	$M_B := 29$	

$$D_{AB}(273K, 0.0\,1bar, 18, 29, 2.641, 3.62, 809.1, 97) = 1.889\times 10^{-3}\,\frac{m^2}{s}$$

$$D_{ABV}(T_v,P_v) := D_{AB}(T_v,P_v,18,29,2.641,3.62,809.1,97) \qquad D_{ABV}(273K, 0.0\,1bar) = 1.889\times 10^{-3}\,\frac{m^2}{s}$$

9.0 Estimation of Average Viscocity using Lucas Method:

This method was proposed by Lucas (1980) for the use in non-polar gases, and now we extend it for the application of air and water vapor. For vectors the values will be O_2,N_2 and H_2O will be tabulated following this order.

$$y(x1) := \begin{pmatrix} y1(x1) \\ 1 - y1(x1) \end{pmatrix} \quad Tc := \begin{pmatrix} 132.2 \\ 647.3 \end{pmatrix} \quad Pc := \begin{pmatrix} 37.45 \\ 220.9 \end{pmatrix} \quad M := \begin{pmatrix} 29 \\ 18 \end{pmatrix} \quad Vc := \begin{pmatrix} 0.0848 \\ 0.0568 \end{pmatrix} \quad Zc := \begin{pmatrix} 0.289 \\ 0.229 \end{pmatrix}$$

Calculating Critical mixture properties:

$ORIGIN := 1$ $\qquad T_v := 283K$ **The average temperature is the water vapor temperature in the absorber.**

$i := 1..2$ $\qquad R := 8.314$

$$T_{cm}(x1) := \sum_i \left(y(x1)_i \cdot Tc_i\right) \qquad T_{cm}(0.01) = 647.546$$

$$P_{cm}(x1) := R \cdot T_{cm}(x1) \cdot 10^{-2} \cdot \frac{\sum_i \left(y(x1)_i \cdot Zc_i\right)}{\sum_i \left(y(x1)_i \cdot Vc_i\right)}$$

10^-3 to convert to bars b/c correlation uses bars

$P_{cm}(0.01) = 217.078$

$$M_{v\_av}(x1) := \left[\sum_i \left(y(x1)_i \cdot M_i\right)\right] \qquad T_{rM}(x1, T_v) := \frac{\frac{T_v}{K}}{T_{cm}(x1)}$$

$$f(x1, T_v) := 0.807 \cdot T_{rM}(x1, T_v)^{0.618} - 0.357 \cdot e^{-0.449 \cdot T_{rM}(x1, T_v)} + 0.340 \cdot e^{-4.058 \cdot T_{rM}(x1, T_v)} + 0.018$$

$$\xi_M(x1) := 0.176 \left(\frac{T_{cm}(x1)}{M_{v\_av}(x1)^3 \cdot P_{cm}(x1)^4}\right)^{\frac{1}{6}}$$

$$\mu(x1, T_v) := \frac{f(x1, T_v)}{\xi_M(x1)} \cdot 10^{-6} \cdot \frac{g}{cm \cdot s}$$

the 10^-6 factor is to put the result in unit of g/cm-s

$\mu(0.01, 283K) = 7.878 \times 10^{-5} \frac{g}{cm \cdot s}$ $\qquad VF := 10^{-1} \cdot \frac{kg \cdot cm}{g \cdot m}$

$$\mu_v(x1, T_v) := \mu(x1, T_v) \cdot VF$$

this is dividing by 1000 and multiplying by 100 to get result in kg/m-s

$\mu_v(0.01, T_v) = 7.878 \times 10^{-6} \frac{kg}{m \cdot s}$ $\qquad \mu_v(1.0, T_v) = 7.939 \times 10^{-6} \frac{kg}{m \cdot s}$

10.0 Density of H2O + Air mixture:

$$\rho_v(x1, T_v, P_v) := \frac{P_v \cdot M_{v\_av}(x1)}{R_u \cdot T_v} \cdot \frac{kg}{kmol}$$

$$\rho_v(0.01, T_v, P_v) = 9.942 \times 10^{-3} \frac{kg}{m^3}$$

11.0 Vapor Volumetric & Mass Flow Rates and Velocity:

$$Q_{gas\_in}(x1, T, T_v, P_v) := \frac{N_{IG\_in}(x1, T) \cdot R_u \cdot T_v}{P_v} \qquad VF := \frac{kPa \cdot m^3}{kmol \cdot K \cdot kPa} \cdot K$$

$$Q_{gas\_in}(0.202, 313K, T_v, P_v) = 0.014 \frac{m^3}{s}$$

$$V_{gas}(x1, T, T_v, P_v) := \frac{Q_{gas\_in}(x1, T, T_v, P_v)}{\frac{\pi}{4} \cdot (D_i - 2 \cdot \delta(x1, T))^2}$$

$$V_{gas}(0.253, 323K, T_v, P_v) = 103.616 \frac{m}{s}$$

$$m_{gas}(x1, T, T_v, P_v) := Q_{gas\_in}(x1, T, T_v, P_v) \cdot \rho_v(x1, T_v, P_v)$$

$$m_{gas}(0.202, 313K, T_v, P_v) = 1.297 \times 10^{-4} \frac{kg}{s} \qquad m_{gas}(0.237, 313K, T_v, P_v) = 5.371 \times 10^{-5} \frac{kg}{s}$$

12.0 Calculating the Mass Transfer for Gaseous Phase:
Now that we know the mass flow rate of the vapor we can go on to calculating the dimentionless parameters Re & Sc

$$Re_V(x1, T, T_V, P_V) := \frac{4 \cdot m_{gas}(x1, T, T_V, P_V)}{\mu_V(x1, T_V) \cdot \pi \cdot (D_i - 2 \cdot \delta(x1, T))}$$

$$Re_V(0.202, 313K, T_V, P_V) = 1.346 \times 10^3$$

Before we can calculate the Schmidt No. we need to estimate the average density (rho) of the water vapor and ir mixture...and the molar concentration.

$$C_V(T_V, P_V) := \frac{P_V}{R_u \cdot T_V} \qquad C_V(T_V, P_V) = 0.553 \frac{mol}{m^3}$$

And the Schmidt No. follows...

$$Sc_V(x1, T_V, P_V) := \frac{\mu_V(x1, T_V)}{\rho_V(x1, T_V, P_V) \cdot D_{ABV}(T_V, P_V)} \qquad Sc_V(x1, T_V, P_V) = 0.506$$

Using Medrano et al. Eq. (5) we see by comparison of L.H.S. with solution of R.H.S. and knowing everthing ion the R.H.S. except for the Fv mass transfer coefficient, where Fv=kv*pair/pair

$Z := 2.0m$ **Change Z here!**

$$RHS_V(x1, T, T_V, P_V) := 1.62 Re_V(x1, T, T_V, P_V)^{\frac{1}{3}} \cdot Sc_V(x1, T_V, P_V)^{\frac{1}{3}} \cdot \left(\frac{D_i}{Z}\right)^{\frac{1}{3}}$$

$$RHS_V(x1, 313K, T_V, P_V) = 3.574$$

$$F_V(x1, T, T_V, P_V) := \frac{C_V(T_V, P_V) \cdot D_{ABV}(T_V, P_V)}{D_i} \cdot RHS_V(x1, T, T_V, P_V)$$

$$F_V(0.253, 323K, T_V, P_V) = 1.727 \times 10^{-4} \frac{kmol}{m^2 \cdot s}$$

13.0 Estimating the Dimentionless Parameter for the LiBr solution:
Once all the LiBr transport properties were calculated as shown abouve we can follow a similar procedure for the Fv estimation to estimate the FL mass transfer coefficient.

For convenience and b/c the correlations for FL and Hs in the Perez-Blanco use reduced thickness δr and kinematic viscosity ν, we will define these here for future use.

$$\nu_S(x1,T) := \frac{\mu_{sol}(x1,T)}{\rho_S(x1,T)} \qquad \nu_S(0.202,313K) = 2.173\times 10^{-6}\,\frac{m^2}{s}$$

and the reduced film thickness...

$$\delta(0.253,323K) = 4.136\times 10^{-4}\,m \qquad \delta(0.202,313K) = 3.306\times 10^{-4}\,m$$

$$\delta_r(x1,T) := \left(\frac{\nu_S(x1,T)^2}{G}\right)^{\frac{1}{3}} \qquad \delta_r(0.253,323K) = 9.808\times 10^{-5}\,m$$

Although we assumed a Re=100 above in order to estimate the film thickness...now we compute the value.

$$V_S(x1,T) := \frac{m_S(x1,T)}{\rho_S(x1,T)\cdot\pi\cdot D_i\cdot\delta(x1,T)}$$

$$V_S(0.202,313K) = 0.164\,\frac{m}{s} \qquad V_S(0.237,323K) = 0.174\,\frac{m}{s}$$

$$Re_{S\_calc}(x1,T) := \frac{\rho_S(x1,T)\cdot V_S(x1,T)\cdot 4\,\delta(x1,T)}{\mu_{sol}(x1,T)}$$

$$Re_{S\_calc}(0.202,313K) = 100 \qquad Re_{S\_calc}(0.237,313K) = 100$$

Solution Schmidt No.:

$$Sc_S(x1,T) := \frac{\mu_{sol}(x1,T)}{\rho_S(x1,T)\cdot D_{ABS}(x1,T)} \qquad Sc_S(0.202,313K) = 1.098\times 10^{3}$$

Solution Average Molecular Weight:

$$M_{S\_av}(x1) := \left[x1\cdot M_1 + (1-x1)\cdot M_2\right]\cdot\frac{kg}{kmol} \qquad M_{S\_av}(x1) = 35.419\,\frac{kg}{kmol}$$

14.0 Estimating the Mass Transfer Coeffiecient of the Solution, FL:

Here we estimate the Ks and FL mass transfer coeficients to be used in mass balance for differential equation

$$RHS_S(x1,T) := 1.09910^{-2}\cdot Re_{S\_calc}(x1,T)^{0.3955}\cdot Sc_S(x1,T)^{0.5}$$

$$RHS_S(0.253,323K) = 3.52$$

$$\kappa_S(x1,T) := \frac{D_{ABs}(x1,T)}{\delta_r(x1,T)}\cdot RHS_S(x1,T) \qquad \kappa_S(.253,323K) = 4.063\times 10^{-5}\,\frac{m}{s}$$

By comparing page 79 Eq. from Benitez to correlation for Ks mass transfer coefficient...but first we define the Cs or concentration in kmol/m^3 of solution.

$$C_S(x1,T) := \frac{\rho_S(x1,T)}{M_{S\_av}(x1)} \qquad C_S(0.202,313K) = 50.29\frac{kmol}{m^3}$$

$$F_L(x1,T) := C_S(x1,T)\cdot\kappa_S(x1,T) \qquad F_L(0.253,313K) = 1.732\times 10^{-3}\,\frac{kmol}{m^2\cdot s}$$

15.0 Osmotic Coefficient, Equilibrium Pressure and Saturated H2O pressure:

Thermal and equilibrium properties from Kim

$$kJ := 1000J$$

$$a := \begin{pmatrix} -2.19631554\,10^{1} & 4.937231610^{3} & -6.55484061\,0^{5} \\ -3.81047521\,0^{3} & 2.61153451\,0^{6} & -3.66996911\,0^{8} \\ 1.22808541\,0^{5} & -7.71879231\,0^{7} & 1.03985601\,0^{10} \\ -1.47167371\,0^{6} & 9.19528481\,0^{8} & -1.18945021\,0^{11} \\ 7.76582131\,0^{6} & -4.93756661\,0^{9} & 6.31755471\,0^{11} \\ -1.51189221\,0^{7} & 9.83997441\,0^{9} & -1.27378981\,0^{12} \end{pmatrix}$$

$$aa(p,T) := \sum_{q=1}^{3}\left[a_{p,q}\cdot\left(\frac{T}{K}\right)^{-q+1}\right]$$

$$\alpha(T) := 11.375 - 3.859\cdot10^{3}\cdot\left(\frac{T}{K}\right)^{-1} + 5.132\cdot10^{5}\cdot\left(\frac{T}{K}\right)^{-2}$$

$$\beta(T) := 0.86 - 1.958\cdot10^{2}\cdot\left(\frac{T}{K}\right)^{-1} + 2.314\cdot10^{4}\cdot\left(\frac{T}{K}\right)^{-2}$$

This is to calculate the saturated pressure to use in the θθ equation show below.

$$ps(T) := 10^{7.05 - \frac{1603.54}{\frac{T}{K}} - \frac{104095.5}{\left(\frac{T}{K}\right)^{2}}}\ kPa$$

$$\phi\phi2(x1,T) := 1 + \sum_{j=1}^{6}\left[(aa(j,T))\cdot x(x1)^{j}\right]$$

$$\theta\theta(x1,T) := \cosh\left(\alpha(T) - \beta(T)\cdot\ln\left(\frac{ps(T)}{kPa}\right)\right)\cdot\exp\left(\phi\phi2(x1,T)\cdot\upsilon\cdot x(x1)^{2}\cdot M_2\cdot\beta(T)\right)$$

$$pres(x1,T) := \exp\left[\beta(T)^{-1}\cdot\left(\alpha(T) - \ln\left(\theta\theta(x1,T) + \sqrt{\theta\theta(x1,T)^{2} - 1}\right)\right)\right]\cdot kPa$$

$$pres(0.21,298K) = 0.41\,kPa$$

16.0 Enthalpy of the Solution:

16.1 Contribution of Water in Enthalpy Function:

$$dd := \begin{pmatrix} 11.971933 \\ -1.830551\cdot10^{-2} \\ 2.870937\cdot10^{-5} \end{pmatrix} \qquad H_{20} := 0$$

$$T := 298 \qquad po := 0.6108$$

$$To := 273.15$$

$$H_{2L}(P,T) := H_{20}\cdot\frac{kJ}{kmol} + \left[R\cdot\left[dd_1\cdot\left(\frac{T}{K} - To\right) + \left(\frac{dd_2}{2}\right)\cdot\left[\left(\frac{T}{K}\right)^{2} - To^{2}\right] + \left(\frac{dd_3}{3}\right)\cdot\left[\left(\frac{T}{K}\right)^{3} - To^{3}\right]\right]\cdot\frac{kJ}{kmol}\right. \ldots$$
$$\left. + R\cdot\left[ee_1 + ee_2\cdot\frac{T}{K} + ee_3\cdot\left(\frac{T}{K}\right)^{2}\right]\cdot\left(\frac{P}{kPa} - po\right)\cdot\frac{kJ}{kmol} - R\cdot\left[ee_1\cdot\frac{T}{K} + 2\cdot ee_2\cdot\left(\frac{T}{K}\right)^{2}\right]\cdot\left(\frac{P}{kPa} - po\right)\cdot\frac{kJ}{kmol}\right.$$

$$H_{2L}(101.3kPa, 298K) = 1.79\times10^{3}\ \frac{kJ}{kmol} \qquad \frac{H_{2L}(12.34kPa, 323.15K)}{M_2\cdot\frac{kg}{kmol}} = 209.066\frac{kJ}{kg}$$

16.2 Estimating the Excess Enthalpy Term:
Using the Kim & Ferreira Eq. #28 to compute HE

$z := 1..6$ $e := 1..3$

$$daa(z,T) := \sum_{j=1}^{3}\left[(-j+1)\cdot\left[a_{z,j}\cdot\left(\frac{T}{K}\right)^{-j}\right]\right]$$

$$dbb(e,T) := \sum_{j=1}^{3}\left[(-j+1)\left[b_{e,j}\cdot\left(\frac{T}{K}\right)^{-j}\right]\right]$$

$$H_E(x1,T,P) := -x1\cdot\upsilon\cdot R\cdot\left(\frac{T}{K}\right)^{2}\cdot\left[\sum_{j=1}^{6}\left[\left[\left(\frac{2}{j}\right)\cdot daa(j,T)\right]\cdot x(x1)^{j}\right] + \sum_{j=1}^{3}\left[2\cdot\left(\frac{dbb(j,T)\cdot\frac{P}{kPa}}{2\cdot\upsilon}\right)\cdot x(x1)^{j}\right]\right]\cdot\frac{kJ}{kmol}$$

$$H_E(0.2, 298K, 1.3kPa) = 2.053\times 10^{3}\ \frac{kJ}{kmol}$$

16.3 Ideal Enthalpy value for LiBr:

$$H_{10} := -57.1521\frac{kJ}{kmol} \qquad cc := \begin{pmatrix} -9.440133610^{5} \\ -5.842325710^{8} \\ 0 \end{pmatrix}$$

$$H_{Linf}(P,T) := H_{10} + R\cdot\left[cc_{1,1}\cdot\left[To^{-1} - \left(\frac{T}{K}\right)^{-1}\right] + \frac{cc_{2,1}}{2}\cdot\left[To^{-2} - \left(\frac{T}{K}\right)^{-2}\right] + \frac{cc_{3,1}}{3}\cdot\left[To^{-3} - \left(\frac{T}{K}\right)^{-3}\right]\right]\frac{kJ}{kmol} \ldots$$
$$+\left[R\cdot\left[b_{1,1}\cdot\frac{T}{K} + b_{1,2} + b_{1,3}\cdot\left(\frac{T}{K}\right)^{-1}\right] - R\cdot\left[b_{1,1}\cdot\frac{T}{K} - b_{1,3}\cdot\left(\frac{T}{K}\right)^{-1}\right]\right]\cdot\left(\frac{P}{kPa} - po\right)\frac{kJ}{kmol}$$

$$H_{Linf}(101.3kPa, 298K) = -7.654\times 10^{3}\ \frac{kJ}{kmol} \qquad H_{Linf}(5kPa, 298K) = -7.656\times 10^{3}\ \frac{kJ}{kmol}$$

16.4 Total Enthalpy of Solution:
After computing the quantity of the components that correspond to the Enthalpy Function, it follows from Eq. 25 that can be used to estimate the total Enthalpy.

$$Hl(x1,T,P) := x1\cdot H_{Linf}(P,T) + (1-x1)\cdot H_{2L}(P,T) + H_E(x1,T,P)$$

$$Hl(0.152,298.15K,3kPa) = 1.343\times 10^{3}\ \frac{kJ}{kmol}$$

17.0 Total Enthalpy of Solution:
Using the derived relationship between Cp and H we can calculate the Specific Heat, Cps, of Solution.

$$Cp(x1,T,P) := \frac{d}{dT}Hl(x1,T,P)$$

$$Cp_S(x1,T,P) := Cp(x1,T,P)$$

$$Cp_S(0.237,298.15K,2kPa) = 63.839\ \frac{kJ}{kmol\cdot K}$$

19.0 Solution HTC and Overall HTC:

$$Pr_S(x1,T,P) := \frac{Cp_S(x1,T,P)\cdot \mu_{sol}(x1,T)}{k_{sol}(x1,T)\cdot M_{s\_av}(x1)} \qquad Pr_S(0.202,313K,1kPa) = 16.011$$

$$h_{sd}(x1,T,P) := \frac{k_{sol}(x1,T)}{\delta(x1,T)}\cdot 0.029\left(Re_{s\_calc}(x1,T)^{0.53}\cdot Pr_S(x1,T,P)^{0.344}\right)$$

$$h_{sd}(0.2,298K,1.3kPa) = 1.042\ \frac{kW}{m^2\cdot K}$$

Estimate heat transfer coefficient for the cooling air

Use finned circular tubes surface 7.75-5/8T (p. 270, Kays and London)
Assume air average temperature of 300K
Information of per Tube (Outside)

$Vdot_{air} := 0.5\frac{m^3}{s}$ $Vdot_{air} = 1.059\times 10^{3}\ \frac{ft^3}{min}$

$A_{fr} := 1.5in\cdot Z$ $A_{fr} = 0.076m^2$

$u_{air} := \frac{Vdot_{air}}{A_{fr}}$ $u_{air} = 6.562\frac{m}{s}$

$Vol_{tube} := 1.75in\cdot 1.5in\cdot Z$ $Vol_{tube} = 3.387\times 10^{-3}\ m^3$

$A_{HT} := 554\frac{m^2}{m^3}\cdot Vol_{tube}$ $A_{HT} = 1.876m^2$

$A_{Inside} := \pi\cdot D_i\cdot Z$ $A_{Inside} = 0.105m^2$

$\frac{A_{HT}}{A_{Inside}} = 17.883$

$\rho_{air} := 1.1766\frac{kg}{m^3}$ $mdot_{air} := Vdot_{air}\cdot\rho_{air}$ $mdot_{air} = 0.588\frac{kg}{s}$

Free flow area/frontal area: $\sigma := 0.481$

$A_c := A_{fr}\cdot\sigma$ $A_c = 0.037m^2$

$G := \frac{mdot_{air}}{A_c}$ $G = 16.051\frac{kg}{m^2\cdot s}$ $\mu_{air} := 1.853\cdot 10^{-5}Pa\cdot s$

Flow passage hydraulic diameter: $D_h := 3.48mm$

$Re_{air} := \frac{D_h\cdot G}{\mu_{air}}$ $Re_{air} = 3.014\times 10^{3}$ $Pr_{air} := 0.711$

From Figure 10-92 Kays and London

$St_{air} := \frac{0.0045}{Pr_{air}^{0.667}}$ $St_{air} = 5.65 \times 10^{-3}$ $Cp_{air} := 1 \frac{kJ}{kg \cdot K}$

$h_{air} := St_{air} \cdot G \cdot Cp_{air}$ $h_{air} = 90.681 \frac{W}{m^2 \cdot K}$

Assume that the fins are made of aluminum:

$k_{fin} := 170 \frac{W}{m \cdot K}$ $\delta_{fin} := 0.016 in$

Fin length: $l_{fin} := \frac{1.5 - 0.676}{2} in$ $l_{fin} = 0.01 m$

Calculate fin effectiveness:

$m_{fin} := \sqrt{\frac{2 \cdot h_{air}}{k_{fin} \cdot \delta_{fin}}}$ $m_{fin} = 51.235 \frac{1}{m}$ $m_{fin} \cdot l_{fin} = 0.536$

$\eta_{fin} := \frac{\tanh(m_{fin} \cdot l_{fin})}{m_{fin} \cdot l_{fin}}$ $\eta_{fin} = 0.914$

Overall surface effectiveness:

Fin area/total area = 0.95 $\eta_O := 1 - 0.95 \cdot (1 - \eta_{fin})$ $\eta_O = 0.918$

$$U(x1, T, P) := \left(\frac{1}{h_{sd}(x1, T, P)} + \frac{1}{\eta_O \cdot \frac{A_{HT}}{A_{Inside}} \cdot h_{air}} \right)^{-1}$$

$U(0.2, 298K, 1.3kPa) = 0.613 \frac{kW}{m^2 \cdot K}$

APPENDIX B

Absorber Design

Reference:C:\Documents and Settings\Rafael\Desktop\Archivos_Finales_Tesis\Math_Cad\Properties_RAP6.mcd

In the program of properties the interface gas mole fraction is defined as shown in equation below using x1, T and P as the parameters, however, this is would be true is this was the bulk fraction in the gaseous phase. In order to estimate the interface mole fraction the xi, T and P must be known, and obviously both xi and yi are not easily measured, hence they are found by iteration using a solve block.

Interface Concentrations:

$T_{so} = 324.15K$ $\quad ORIGIN := 0$

$T := T_{so}$

$r2(x1, T, T_v, P_v) := \dfrac{F_L(x1, T)}{F_v(x1, T, T_v, P_v)}$

$x_{ai} := 0.796$

Given

$$\frac{1 - \dfrac{pres(1 - x_{ai}, T)}{P}}{1 - y_W(x1)} = \left(\frac{1 - x_W(x1)}{1 - x_{ai}}\right)^{r2(x1, T, T_v, P_v)}$$

$C_{int}(x1, T) := Find(x_{ai})$

$C_{int}(x1, T) = 0.76$

$y_{ai}(x1, T) := \dfrac{pres(1 - C_{int}(x1, T), T)}{P}$ $\quad y_{ai}(x1, T) = 0.917$

$T_{air} := (30 + 273.15)K$

$St_L(x1, T_s) := \dfrac{\pi D_i \cdot F_L(x1, T) \cdot Z}{L_S}$ $\quad St_L(x1, T) = 2.2004$

$H_s(x1, T, P) := Hl(x1, T, P)$

For the Solution Side:

$$m_{sRK}(x1) := \frac{L_S}{x1} \cdot M_{s\_av}(x1) \qquad G := 9.8\frac{m}{s^2}$$

where, $M_{s\_av}(x1) = 35.4194\frac{kg}{kmol}$

$$\Gamma_{RK}(x1) := \frac{m_{sRK}(x1)}{\pi \cdot D_i}$$

$$\delta_{RK}(x1,T) := \left(\frac{3 \cdot \mu_{sol}(x1,T) \cdot \Gamma_{RK}(x1)}{\rho_s(x1,T)^2 \cdot G} \right)^{\frac{1}{3}}$$

$$Ve_{sRK}(x1,T) := \frac{m_{sRK}(x1)}{\rho_s(x1,T) \cdot \pi \cdot D_i \cdot \delta_{RK}(x1,T)}$$

$$Re_{sRK}(x1,T) := \frac{\rho_s(x1,T) \cdot Ve_{sRK}(x1,T) \cdot 4\delta_{RK}(x1,T)}{\mu_{sol}(x1,T)}$$

$$RHS_{sRK}(x1,T) := 1.099 \cdot 10^{-2} \cdot Re_{sRK}(x1,T)^{0.3955} \cdot Sc_s(x1,T)^{0.5}$$

$$\kappa_{sRK}(x1,T) := \frac{D_{ABs}(x1,T)}{\delta_r(x1,T)} \cdot RHS_{sRK}(x1,T)$$

$$F_{LRK}(x1,T) := C_s(x1,T) \cdot \kappa_{sRK}(x1,T)$$

$$St_{LRK}(x1,T) := \frac{\pi D_i \cdot F_{LRK}(x1,T) \cdot Z}{L_S}$$

Overall HTC Coefficient:

$$h_{sRK}(x1,T) := \frac{k_{sol}(x1,T)}{\delta_{RK}(x1,T)} \cdot 0.029 \cdot \left(Re_{sRK}(x1,T)^{0.53} \cdot Pr_s(x1,T,P)^{0.344} \right) \qquad h_{sRK}(x1,T) = 1.0074 \frac{kW}{m^2 K}$$

$$U_{RK}(x1,T) := \left(\frac{1}{h_{sRK}(x1,T)} + \frac{1}{\eta_O \cdot \frac{A_{HT}}{A_{Inside}} \cdot h_{air}} \right)^{-1} \qquad U_{RK}(x1,T) = 0.7382 \frac{kW}{m^2 K}$$

$$\Theta(T) := \frac{T - T_{air}}{T_{so} - T_{air}}$$

$$U_{star}(x1,T,P) := \frac{U_{RK}(x1,T) \cdot \pi \cdot D_i \cdot Z}{L_S \cdot Cp_s(x1,T,P)}$$

For the gas Side:

$$m_{vRK}(x1) := \frac{V_S}{y1(x1)} \cdot M_{v\_av}(x1) \cdot SF \qquad m_{vRK}(x1) = 1.9492 \times 10^{-4} \frac{kg}{s}$$

$$Re_{vRK}(x1,T,T_v) := \frac{4 \cdot m_{vRK}(x1)}{\mu_v(x1,T_v) \cdot \pi \cdot (D_i - 2 \cdot \delta_{RK}(x1,T))}$$

$$Sc_v(x1,T_v,P_v) := \frac{\mu_v(x1,T_v)}{\rho_v(x1,T_v,P_v) \cdot D_{ABV}(T_v,P_v)}$$

$$RHS_{vRK}(x1,T_v,P_v) := 1.62 \cdot Re_{vRK}(x1,T,T_v)^{\frac{1}{3}} \cdot Sc_v(x1,T_v,P_v)^{\frac{1}{3}} \cdot \left(\frac{D_i}{Z} \right)^{\frac{1}{3}}$$

$$F_{vRK}(x1,T) := \frac{C_v(T_v,P_v) \cdot D_{ABV}(T,P)}{D_i} \cdot RHS_{vRK}(x1,T_v,P_v)$$

$$r2(x1,T) := \frac{F_{LRK}(x1,T)}{F_{vRK}(x1,T)}$$

$$Q_{vRK}(x1) := \frac{V_S}{1 - y_W(x1)} \cdot R_u \cdot \frac{T_v}{P_v}$$

$$V_{vRK}(x1,T) := \frac{Q_{vRK}(x1)}{\frac{\pi}{4} \cdot (D_i - 2\delta(x1,T))^2}$$

Sample of Calculations

Step 1:

$$k1_1 := h \cdot q\left(u^{\langle 0\rangle}, T_0, P\right) \qquad k2_1 := h \cdot q\left(u^{\langle 0\rangle} + \frac{k1_1}{2}, T_0, P\right)$$

$$k3_1 := h \cdot q\left(u^{\langle 0\rangle} + \frac{k2_1}{2}, T_0, P\right) \qquad k4_1 := h \cdot q\left(u^{\langle 0\rangle} + k3_1, T_0, P\right)$$

$$u^{\langle 1\rangle} := u^{\langle 0\rangle} + \frac{k1_1}{6} + \frac{k2_1}{3} + \frac{k3_1}{3} + \frac{k4_1}{6} \qquad u^{\langle 1\rangle} = \begin{pmatrix} 0.2526 \\ 0.8962 \end{pmatrix}$$

$$T_1 := \left(T_{so} - T_{air}\right)\left(u^{\langle 1\rangle}\right)_1 + T_{air} \qquad T_1 = 321.9697\,K$$

Step 2:

$$k1_2 := h \cdot q\left(u^{\langle 1\rangle}, T_1, P\right) \qquad k2_2 := h \cdot q\left(u^{\langle 1\rangle} + \frac{k1_2}{2}, T_1, P\right)$$

$$k3_2 := h \cdot q\left(u^{\langle 1\rangle} + \frac{k2_2}{2}, T_1, P\right) \qquad k4_2 := h \cdot q\left(u^{\langle 1\rangle} + k3_2, T_1, P\right)$$

$$u^{\langle 2\rangle} := u^{\langle 1\rangle} + \frac{k1_2}{6} + \frac{k2_2}{3} + \frac{k3_2}{3} + \frac{k4_2}{6} \qquad u^{\langle 2\rangle} = \begin{pmatrix} 0.2521 \\ 0.8249 \end{pmatrix}$$

$$T_2 := \left(T_{so} - T_{air}\right)\left(u^{\langle 2\rangle}\right)_1 + T_{air} \qquad T_2 = 320.4719\,K$$

Step 3:

$$k1_3 := h \cdot q\left(u^{\langle 2\rangle}, T_2, P\right) \qquad k2_3 := h \cdot q\left(u^{\langle 2\rangle} + \frac{k1_3}{2}, T_2, P\right)$$

$$k3_3 := h \cdot q\left(u^{\langle 2\rangle} + \frac{k2_3}{2}, T_2, P\right) \qquad k4_3 := h \cdot q\left(u^{\langle 2\rangle} + k3_3, T_2, P\right)$$

$$u^{\langle 3\rangle} := u^{\langle 2\rangle} + \frac{k1_3}{6} + \frac{k2_3}{3} + \frac{k3_3}{3} + \frac{k4_3}{6} \qquad u^{\langle 3\rangle} = \begin{pmatrix} 0.2515 \\ 0.774 \end{pmatrix}$$

$$T_3 := \left(T_{so} - T_{air}\right)\left(u^{\langle 3\rangle}\right)_1 + T_{air} \qquad T_3 = 319.4049\,K$$

Sample of Results:

$u^T =$

	0	1
0	0.253	1
1	0.2526	0.8962
2	0.2521	0.8249
3	0.2515	0.774
4	0.2509	0.7366
5	0.2502	0.7082
6	0.2495	0.6856
7	0.2489	0.6669
8	0.2482	0.6507
9	0.2475	0.636
10	0.2469	0.6221
11	0.2462	0.6083
12	0.2456	0.5944
13	0.245	0.5798
14	0.2445	0.5644
15	0.244	0.5479
16	0.2435	0.53
17	0.243	0.5106
18	0.2426	0.4893
19	0.2422	0.4662
20	0.2419	0.4412

$uu =$

	0
0	0.253
1	0.2526
2	0.2521
3	0.2515
4	0.2509
5	0.2502
6	0.2495
7	0.2489
8	0.2482
9	0.2475
10	0.2469
11	0.2462
12	0.2456
13	0.245
14	0.2445
15	0.244
16	0.2435
17	0.243
18	0.2426
19	0.2422
20	0.2419

$T =$

	0
0	324.15
1	321.9697
2	320.4719
3	319.4049
4	318.6196
5	318.0213
6	317.5473
7	317.1552
8	316.8153
9	316.5065
10	316.2134
11	315.9247
12	315.6314
13	315.3262
14	315.0029
15	314.656
16	314.2805
17	313.8719
18	313.4262
19	312.9409
20	312.4152

K